

Solar Energy Desalination Analysis Tool

User Manual

January 18, 2022

**Prepared for
The Solar Energy Technologies Office (SETO)
EERE-DOE**

**Prepared by the
Center for Life Cycle Analysis (CLCA)
and
Center for International Earth Science Information Network(CIESIN)
Columbia University
New York, NY**

This report provides a User's Manual and Help Menu for the Solar Desalination Analysis Tool (SEDAT) developed at Columbia University under the auspices of the Solar Energy Technologies Office (SETO) of the United States Department of Energy (US-DOE)

To see the Help system in SDAT, click Help in the main window, or press the F1 key (command-? in MacOS) from any page in SEDAT.

Disclaimer

The Solar Energy Desalination Analysis Tool (SEDAT) or "Tool" is freely provided by Columbia University courtesy of the U.S. Department of Energy (DOE).

The names Columbia University and DOE shall not be used in any representation, advertising, publicity or other manner whatsoever to endorse or promote any entity that adopts or uses SDAT.

Columbia University is not obliged to provide any support, training or assistance of any kind with regard to the use of the Tool or any updates, revisions or new versions of the same.

You agree to indemnify Columbia University, DOE, and its affiliates, officers, agents, and employees against any claim or demand, including reasonable attorneys' fees, related to your use, reliance, or adoption of the SEDAT for any purpose whatsoever. The Tool is provided by Columbia and the DOE "as is" and any express or implied warranties, including but not limited to the implied warranties of merchantability and fitness for a particular purpose are expressly disclaimed. In no event shall DOE or Columbia be liable for any special, indirect or consequential damages or any damages whatsoever, including but not limited to claims associated with the loss of data or profits that may result from any action in contract, negligence or other tortious claim that arises out of or in connection with the use or performance of the Tool.

While every precaution has been taken in the preparation of this document, the publisher and the authors assume no responsibility for errors or omissions, or for damages resulting from the use of information contained in this document or from the use of programs and source code that may accompany it. In no event shall the publisher and the authors be liable for any loss of profit or any other commercial damage caused or alleged to have been caused directly or indirectly by this document or the Tool.

Table of Contents

User Manual	1
1. Introduction	6
1.1 Objective	6
1.2 Tool Structure	6
1.3 Databases.....	8
1.4 Techno-economic Models.....	9
1.5 Quick Analysis: Web-based Simplified Tool.....	9
1.6 Downloading and Installing SEDAT	10
1.6.1 Windows Installation	10
1.6.2 Mac and Linux Installation	12
1.7 User Support	12
2 Running SEDAT.....	13
2.1 Work Flow for Running Simulations	13
2.2 Site Selection.....	14
2.3 Select Models.....	17
2.4 Review Results	19
2.5 Parametric Simulations	20
3 File Management	22
3.1 File Menu	22
3.2 Result Reports.....	23
3.3 Case Graphs	24
3.4 Export Data and Graphs.....	24
4 Databases.....	24
4.1 Solar Resource	24
4.2 Alternative Water Resources	24
4.3 Desalination Plants.....	26
4.4 Power Plants	27
4.5 Sensitive Areas.....	27
4.6 Water Networks.....	28
4.7 Energy and Water Utility Prices	28
4.8 Regulatory/Permitting	29
4.9 County Population Growth Projections	30

5	Solar Thermal Energy Generation Models.....	30
5.1	PSA Static Solar Collector	30
5.2	SAM CSP Parabolic Trough.....	31
5.3	SAM CSP Linear Fresnel	31
5.4	SAM CSP Tower	33
5.4.1	SAM Power Cycles.....	34
5.5	SAM Industrial Process Heat.....	35
5.6	SAM Financial models	35
5.7	Integration of the SAM models into SEDAT	36
6	Thermal Desalination Models	38
6.1	Low-Temperature Multi-Effect-Distillation (LT-MED).....	38
6.1.1	Integration of the LT-MED Model	39
6.2	Multi-Effect-Distillation with Thermal-Vapor-Compression (MED-TVC)	41
6.3	Multi-Effect-Distillation with Absorption Heat Pump (MED-AHP)	44
6.4	Membrane Distillation (MD)	49
6.5	Batch Vacuum Air-Gap Membrane Distillation (V-AGMD) Models	53
6.6	Forward Osmosis (FO) Model	56
6.7	Estimation of Cooling Water Requirements for Thermal Desalination	60
7	Pressure-Driven Desalination Models.....	61
7.1	Reverse Osmosis (RO)-multiple pass model	61
7.2	Osmotically-Assisted Reverse Osmosis (OARO).....	62
8	Hybrid Desalination Models.....	63
8.1	RO + FO	63
8.2	RO + batch V-AGMD.....	65
8.3	Generic Desalination Model	65
9	Solar Collector and Desalination Cost Models.....	66
9.1	Solar Collector	66
9.2	MED Cost Estimates	67
9.3	VAGMD (Once through and Batch) Cost Estimates	68
9.4	FO Cost Estimates	70
9.5	RO Cost Estimates	71
10	Model Results Verification Analysis.....	71
10.1	Solar Static Collector Model.....	71

10.2	LT-MED Model	72
10.3	MED-TVC model.....	73
10.4	V-AGMD model	73
10.5	SAM Concentrating Solar Power Models (CSP)	75
11	Results from Sample Simulations.....	75
11.1	Industrial Process Heat and LT-MED: Application in TX, AZ and CA	75
11.2	Comparisons of Static Collector and Industrial Process Heat coupled with and LT-MED	77
11.3	Case study for a V-AGMD system operating in Phoenix, AZ.....	78
11.4	IPH LFDS and FO Parametric study	79
11.5	Comparison of LT-MED with multi-pass RO for distillate water production	80
12	Bibliography	82

1. Introduction

1.1 Objective

The Objective of this project is to develop a user-friendly and open-access software that will enable a comparative evaluation of solar thermal desalination technology options and will use geospatial data layers to identify regions of high-potential for solar thermal desalination. This is accomplished by integrating solar models with desalination models and enhancing their utility by providing GIS-based data inputs in a Solar Energy Desalination Analysis Tool (SEDAT). It is expected that the SEDAT will simplify the planning, design, and valuation of solar thermal and solar hybrid desalination systems in the U.S. and worldwide.

1.2 Tool Structure

In the SEDAT software, users can easily investigate pathways to implement solar thermal desalination technologies while identifying key locations for reaching techno-economic targets. The software development leveraged Open Source Geospatial software (OSGeo) packages and utility collections, CSP models from NREL's SAM open source, and desalination models developed by Drs. Palenzuela, Alarcon-Padilla, and Zaragoza, at the Plataforma Solar de Almeria (see Figure 1). Coding was completed in C++ and Python. The tool is made available via a user-friendly, graphical user interface (GUI) to facilitate ease-of-use. The software runs on Windows, MacOS and Linux environments. The basic structure of this tool of analysis is shown in Figure 1.

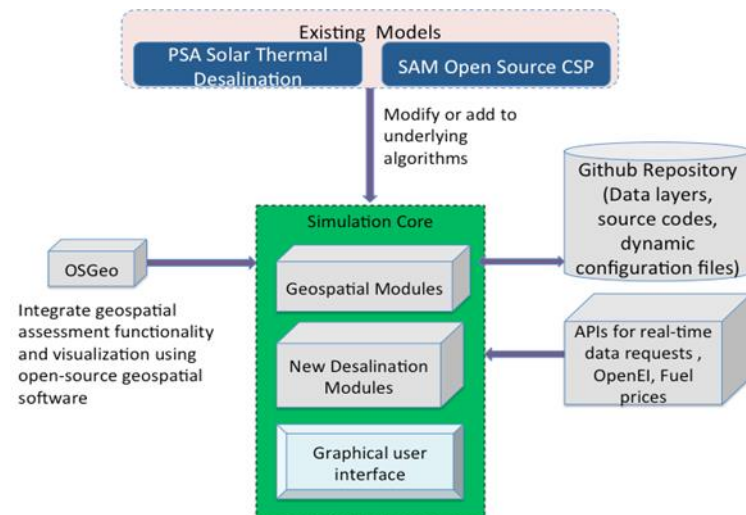


Fig. 1. Basic SEDAT architecture

The software uses a modular architecture, its design making it flexible for expansion. The techno-economic modules deliver an analytical workflow for planning and designing solar thermal desalination systems in optimal locations via a user-friendly Graphical User Interface (GUI). This interface provides default value inputs for technical design as well as capital and operating cost parameters to allow for comparative analyses between different solar thermal desalination systems as well as other competing desalination technologies.

The software quantifies the performance of user-selected desalination systems based on regional specifications and cost parameters, while listing the underlying assumptions. The user can change the assumptions and select another system of interest for evaluation. The technology suggestions are based mainly on the saline water TDS concentration, levelized cost of product water (LCOW), product purity, and target brine concentration.

The desalination techno-economic models include: Low-temperature multi-effect distillation (LT-MED), multi-effect distillation with thermal vapor compression (MED-TVC), multi-effect distillation with absorption heat pumps (MED-ABS); vacuum air gap membrane distillation (VAGMD) in continuous and batch operation modes, reverse osmosis (RO) with multiple passes, osmotically assisted reverse osmosis (OARO), forward osmosis (FO), and RO-VAGMD, and RO-FO hybridizations. The user interface goes over the subsequent steps of selecting a site of interest, selecting the technical and financial technology models, running desalination plant design and performance simulation, and showing results in terms of plant specifications and performance time-series. Figure 2 gives an overview of this architecture. The left columns list the inputs and the right one lists the outputs.

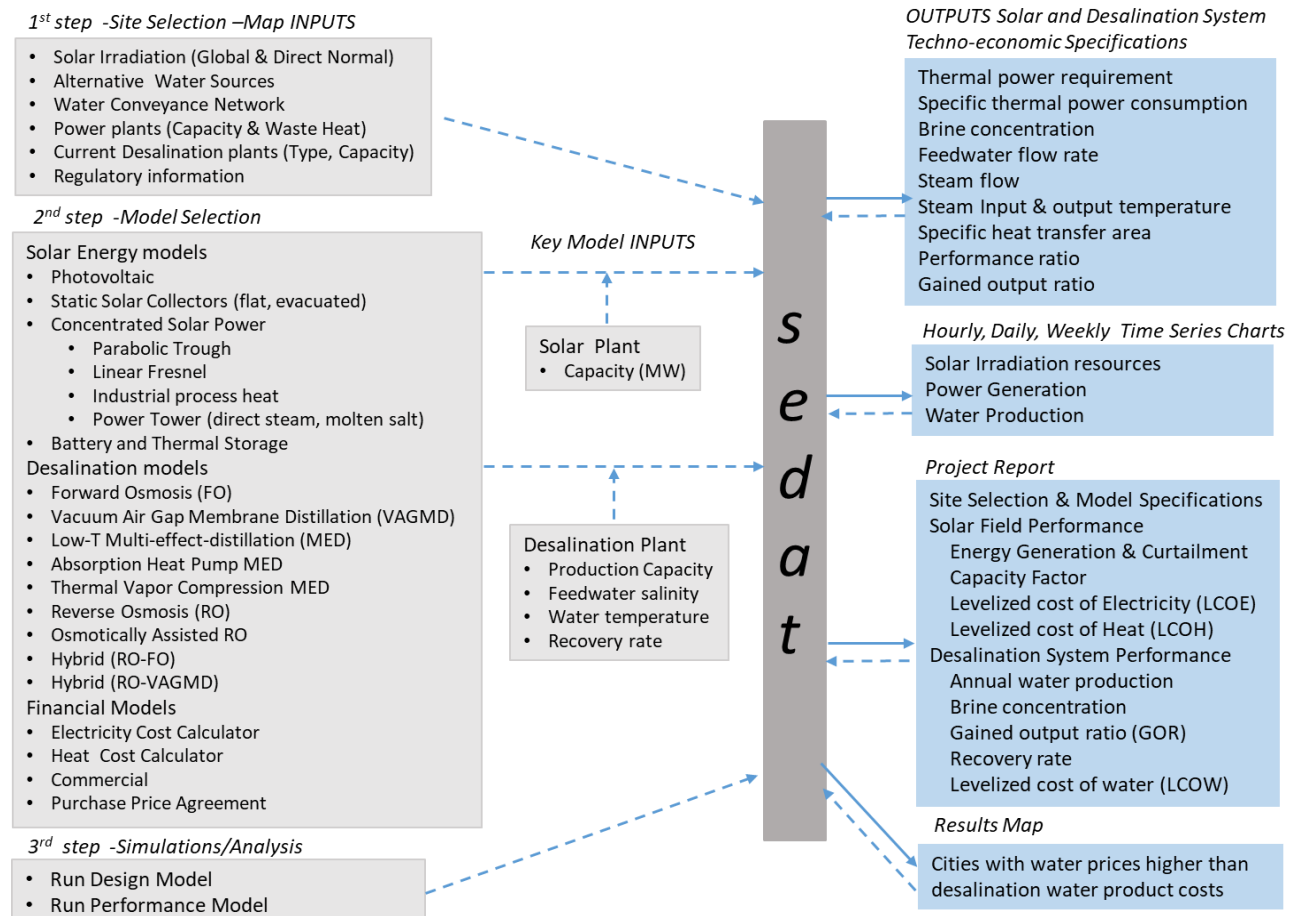


Fig. 2. Inputs and outputs of SEDAT and sequence of generating results for analysis of solar desalination technologies in considered regions.¹

¹ Fthenakis V., Yetman G., Zhang Z., Squires J., Atia A.A., Alarcon-Padilla D.-C., Palenzuela P., Vicraman V., Zaragoza G., A solar energy desalination analysis tool, sedat, with data and models for selecting technologies and regions, Nature Scientific Data, submitted 12/3/2021

Software modules based on open geographic software libraries from OSGeo² and other sources assemble, extract, transform and pass the geospatial data to techno-economic solar generation and desalination components. Logic was implemented to dynamically collect model input parameters based on user-selected location in the GUI. Once a user selects a location, the associated values for the variables needed in the solar and the desalination models are displayed to the user and stored in JavaScript Object Notation (JSON) file for use as model inputs after the model selection. This process can be repeated iteratively using different locations; once a user is satisfied with a location selection, they can select models of solar generation, desalination and financials. Variables that were derived from the geographic maps and used as input into the models are displayed together with the model results in a summary report and results map.

1.3 Databases

SEDAT is an open-source software, that integrates various layers of data describing solar and saline water resources, water and energy infrastructure, applicable regulations, costs and competitive prices. Most of these data, except for the solar irradiation and United States Geological Survey (USGS) water resources, were not available in a single database. Thus, we integrated a suite of geospatial data sources and techno-economic input parameters, shown in Table 1, for simulating integrated solar power systems and desalination technologies in one graphical user interface (GUI) that can be used and efficiently processed in desktop and laptop computers.

Table 1. List of primary GIS data source types.

Parameter	Sub-parameter	Spatial Level of Detail
Alternative water sources	Municipal and industrial wastewaters	County, local (points)
	Brackish water	Local
	Agricultural drainage water	County
	Seawater	Local
Water demand	Areas of projected population growth	County
	Sector water withdrawals (e.g., domestic, agricultural, industrial)	County and state
	Water pricing	Local, county
Energy sources	Solar Direct Normal Irradiance (DNI)	Local
	Waste heat (power plants)	Local, county
	Natural heat (geothermal)	Local
	Commercial & industrial prices for electricity and fuel (gas and diesel)	State
Site selection factors	Land cover, physical restrictions (slope, protected areas)	Local (gridded and detailed mapping units)
	Regulations and Permitting requirements	Administrative (local, state, federal)

². OpenSource Geospatial Foundation: <https://www.osgeo.org/>.

1.4 Techno-economic Models

Table 2. List of SAM models integrated in the software

CSP models	Financial models
Parabolic Trough Physical (PT)	Commercial (distributed)
Linear Fresnel Molten Salt (MSLF)	PPA single owner (utility)
Linear Fresnel Direct Steam (DSLF)	PPA partnership flip with debt (utility)
Power Tower Molten Salt (MSPT)	PPA partnership flip without debt (utility)
Power Tower Direct Steam (DSPT)	PPA sale leaseback (utility)
Integrated Solar Combined Cycle	LCOE calculator
Industrial Process Heat (IPH) Parabolic Trough	
Industrial Process Heat Linear Direct Steam	

Table 3. List of Desalination models integrated in the software

- Desalination System
- Forward Osmosis (FO)
 - Vacuum Air Gap Membrane Distillation (VAGMD-one pass)
 - Vacuum Air Gap Membrane Distillation - Batch (VAGMD-batch)
 - Low Temperature Multi-Effect Distillation (LT-MED)
 - MED with Absorption Heat Pumps (MED-ABS)
 - MED with Thermal Vapor Compression (MED-TVC)
 - Reverse Osmosis (RO) - Grid Integrated
 - Osmotically Assisted Reverse Osmosis (OARO) - Grid Integrated
 - Hybrid System (RO - FO)
 - Hybrid System (RO - VAGMD-batch)
 - Generic Model

1.5 Quick Analysis: Web-based Simplified Tool

Calculate LCOW

Capacity m3/day	SEC kWh/m3
1000	1.8
Total Capex \$	STEC kWh/m3
2755000	55
Opex \$/m3 (includes module replacement)	Plant lifetime Years
0.3	20
LCOE \$/kWh	Interest Rate %
0.05	4
LCOH \$/kWh	
0.03	

Capex: \$0.62/m3
LCOW:\$2.66/m3
[View map of prices higher than the calculated LCOW](#)

A quick analysis tool can estimate the Levelized Cost of Water (LCOW) production from a desalination plant's capacity, capital and operating costs, electricity and thermal energy requirements and costs. The tool can then display on a U.S. map all the locations where the estimated LCOW is lower than the local utility water prices.



Fig. 3. Partial scan of Quick Analysis Tool

1.6 Downloading and Installing SEDAT

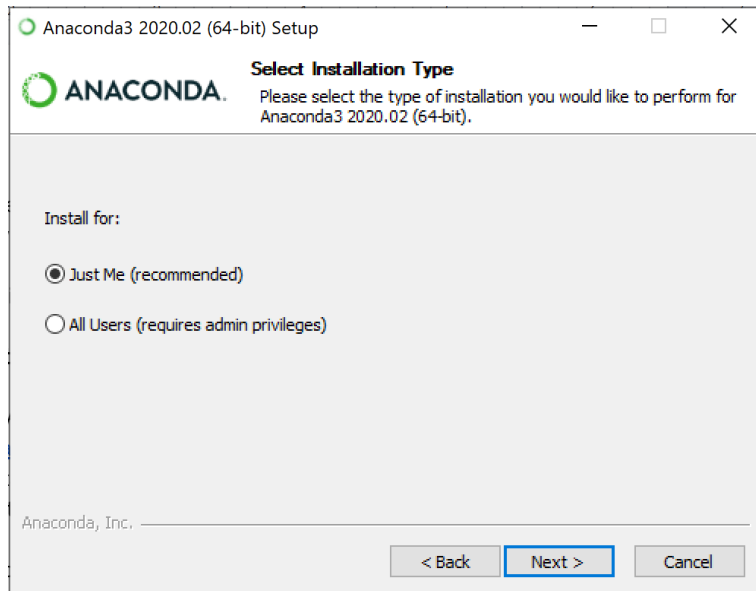
1.6.1 Windows Installation

1.1 Download and install Anaconda; if you already have a recent version of Anaconda, you can **skip** this step)

<https://www.anaconda.com/products/individual>

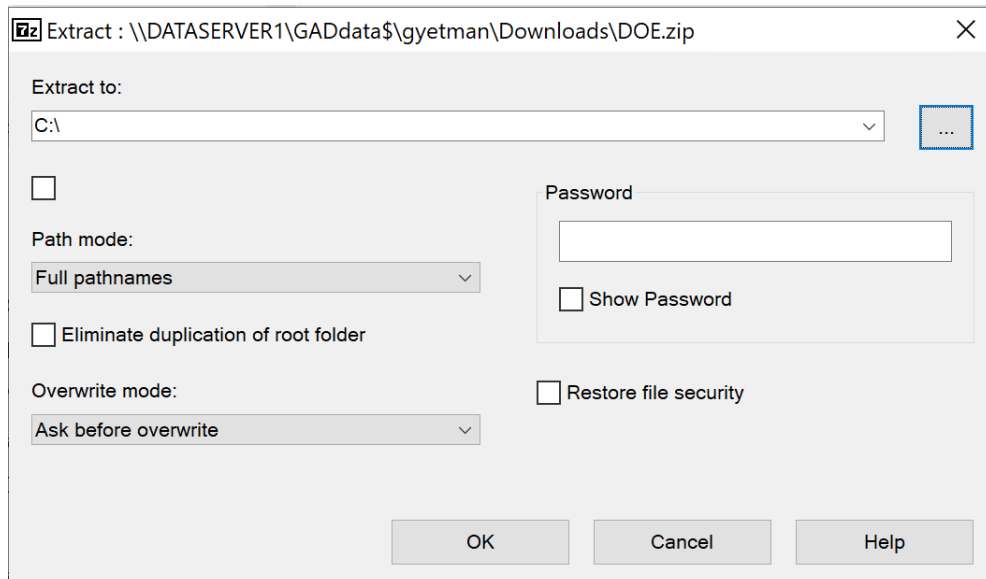
Choose the 64 bit installer.

While installing, selection the option to install it for **Just Me**



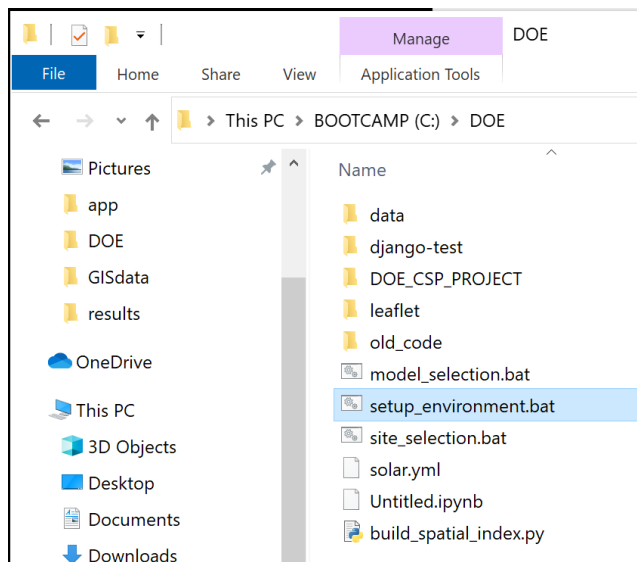
1.2 Download the bundled application and extract it to the **root** of your C:\ drive. Note that if you installed the alpha or beta version of the software, you should first **delete** the C:\DOE folder from your computer before downloading and extracting the new version from:
<https://drive.google.com/file/d/1pttB0I05JH6ebqT2YAKIQYFXtjaBDAKY/view?usp=sharing>

This should create a folder named C:\DOE that contains the application and subfolders.



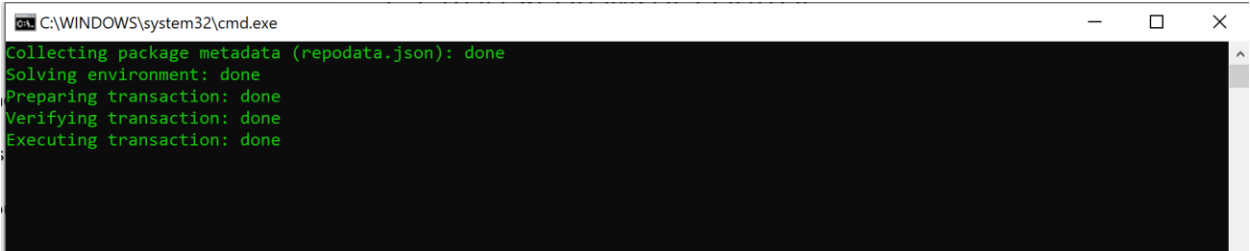
Make certain to extract to the root folder (C:\), so that you don't end up with a nested folder structure (C:\DOE\DOE), which will not work.

1.3 Open the C:\DOE folder, with Windows Explorer you should see a file named **setup_environment.bat**. Double-click the file to execute it. Some versions of Windows will give a security warning and not allow the .bat file to run. If this occurs, in the warning dialog, click "**More Info**" and then click "**Run Anyway**". This will configure the Anaconda Python environment you installed in Step 1. This may take some time (up to 10 minutes, depending on your Internet speed) to complete as it downloads files from the Internet.



Note: if a terminal window does not open and proceed to download the necessary data, you may need to override your Windows Security settings and restart your computer before trying again. To override your security settings, go to "App & Browser Control" and turn off "Check apps and

files.” From here, restart your computer and try opening **setup_environment.bat** again. A terminal window like the one shown below should open. This process takes a few minutes and depends on your internet connection.



```
C:\WINDOWS\system32\cmd.exe
Collecting package metadata (repodata.json): done
Solving environment: done
Preparing transaction: done
Verifying transaction: done
Executing transaction: done
```

Once this is done, the installation is complete!

1.6.2 Mac and Linux Installation

1. If you already have Python 3 and Anaconda installed, skip to the next step. You can test this by opening a terminal window and entering the command:
`conda list anaconda`
If the result includes a python build of 3.6 or later, you can proceed to step 2. Otherwise, download and install anaconda from <https://www.anaconda.com/products/individual>. Accept the default options for the installation.
2. Download the .zip archive from this link:
<https://drive.google.com/file/d/1MtIWCC4bU0W6WoZPMfu3CXg3iW8at0Pu/view?usp=sharing>
3. Extract the contents to your home directory (/users/<your_username>/). It should create a folder named DOE.
4. Open a terminal (shell) and change to the DOE folder (~/DOE). Run the script solar-setup.sh by entering the code:
`./solar-setup.sh`

1.7 User Support

Zhuoran Zhang, email: zz2322@columbia.edu

Greg Yetman, email: gyetman@ciesin.columbia.edu

John Squires, email: jsquires@ciesin.columbia.edu

Vasilis Fthenakis, email: vmf5@columbia.edu

2 Running SEDAT

2.1 Work Flow for Running Simulations

The data flow diagram shown in Figure 4 walks through a high-level workflow for site and model selection using the desktop application for a site-selection driven workflow. The steps shown in the data flow diagram are as follows:

1. User starts desktop application.
2. The application loads the GIS data from local files and a base map from the web, and renders selected layers over the base map. A base map provides context (highways, topography, place names, etc.). At this point, the user can zoom and pan on the map and select a site location.
3. The site details are loaded and shown to the user, including the annual DNI data, water sources (wells), waste heat sources, and existing desalination facilities within a cutoff distance.
 - a. The user can interactively choose a new site and review the site details repeatedly until satisfied with the location. This is indicated by the loop “user updates location”.
4. Once the location has been finalized, a model selection can be made by the user from the following menus:
 - a. Solar energy generation model
 - b. Desalination model
 - c. Financial model
5. The application loads the relevant parameters from the GIS data and configuration files that store parameters and default values for the selected model.
6. A subset of the parameters most commonly selected by the user are displayed in the application interface; these may be edited and revised.
7. Optionally, a user may examine and modify extended parameters (those not usually modified but perhaps of interest to some).
8. Once the user submits the parameters, the techno-economic models are run (status updates will be provided).
9. Once completed, the model outputs are displayed to the user (graphs/charts and tables). The user may also access the files generated.
10. At this point the workflow ends. The process could be started again, or the application closed.

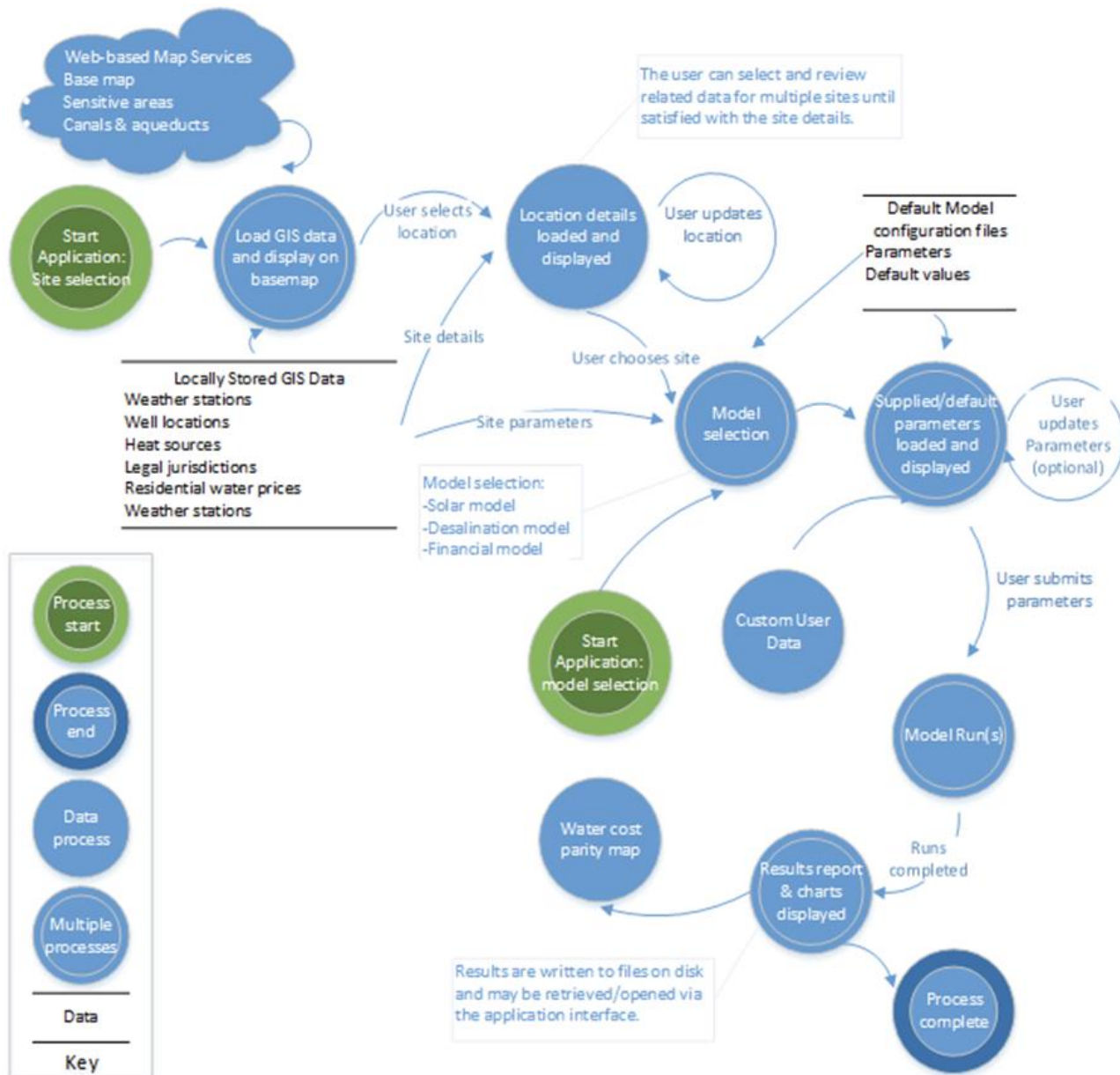


Fig. 4. Data flow diagram for a typical workflow of selecting a site, models, reviewing parameters, and model output.

2.2 Site Selection

Windows systems

Run the **solar-desalination.bat** file in the C:\DOE folder by double-clicking it. It should automatically open your web browser to the site selection page (<http://127.0.0.1:8150/>)

Mac and Linux systems

Run the run-solar.sh script in the ~/DOE folder by issuing the command “source run-solar.sh” at the command line (terminal). It should automatically open your web browser to the site selection page (<http://127.0.0.1:8150/>)

You can see maps with locations of Canals, Desalination plants, and Power plants and you can move on the map and zoom in and out to smaller or larger areas. You can select a location on either a satellite or topographic map and see, by clicking there, the nearest desalination plants, power plants, canals, associated distances and capacities, as well water prices from regional utilities.

A couple of example images are shown below; figure 5 shows desalination plants on a satellite map and Figure 6 shows power plants on a topographic map.

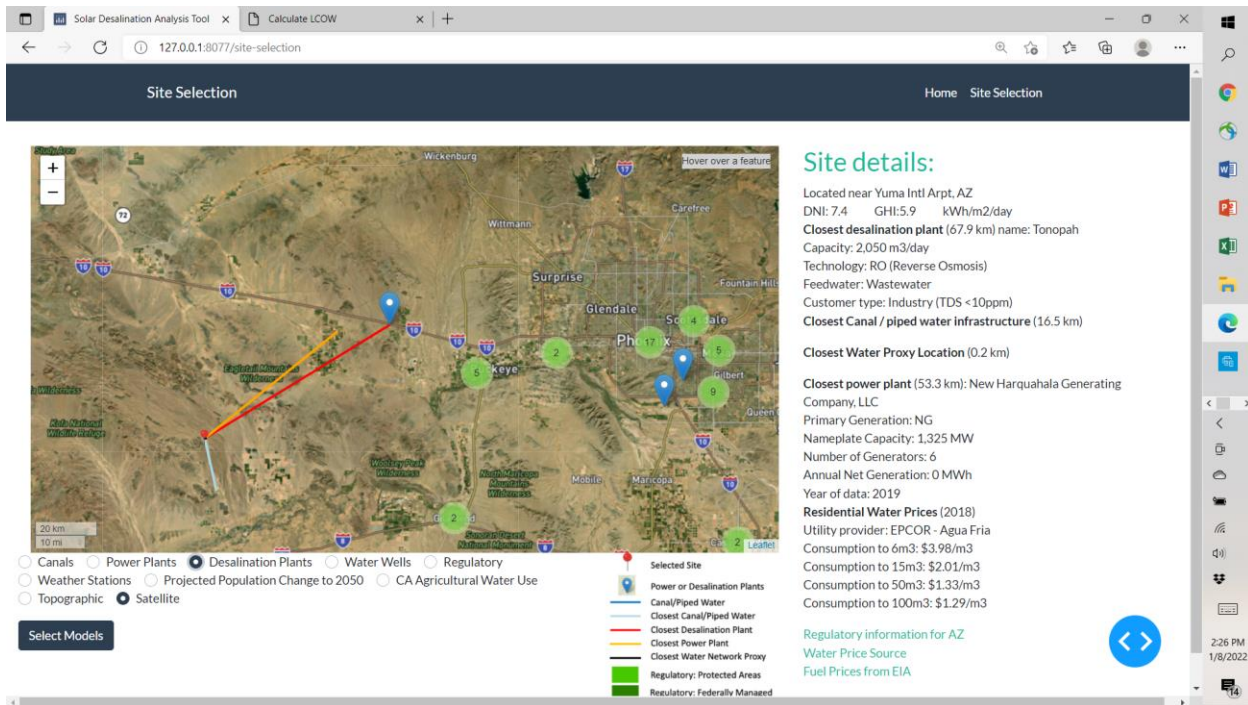


Fig. 5. Sample result of site selection –satellite map-

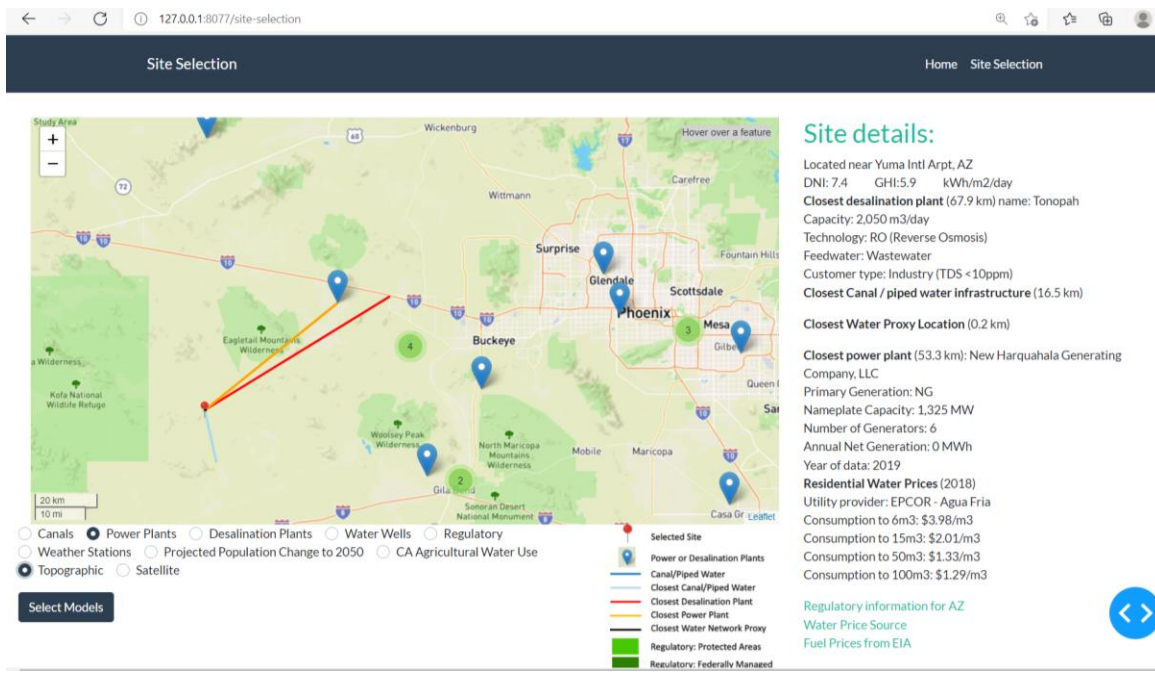


Fig. 6. Sample result of site selection –topographic map-

Then the user can proceed to techno-economic desalination modeling by clicking a “Select Models” (left bottom of the screen) to proceed to a menu listing choices of solar energy generation, desalination and financial models (Figure 7).

Model Selection

Project Name: Project_1

Solar Energy Generation

- Photovoltaic (PVWatts)
- Photovoltaic (Detailed)
- Static Collector (Flat Plate)
- Static Collector (Evacuated Tube)
- Linear Fresnel Direct Steam
- Linear Fresnel Molten Salt
- Parabolic Trough Physical
- Power Tower Direct Steam
- Power Tower Molten Salt
- Industrial Process Heat Parabolic Trough
- Industrial Process Heat Linear Fresnel Direct Steam

Desalination

- Forward Osmosis (FO)
- Vacuum Air Gap Membrane Distillation (VAGMD-one pass)
- Vacuum Air Gap Membrane Distillation - Batch (VAGMD-batch)
- Low Temperature Multi-Effect Distillation (LT-MED)
- MED with Absorption Heat Pumps (MED-ABS)
- MED with Thermal Vapor Compression (MED-TVC)
- Reverse Osmosis (RO) - Grid Integrated
- Osmotically Assisted Reverse Osmosis (OARO) - Grid Integrated
- Hybrid System (RO - FO)
- Hybrid System (RO - VAGMD-batch)
- Generic Model

Financial

- Commercial (Distributed)
- Levelized Cost of Electricity Calculator
- Levelized Cost of Heat Calculator
- PPA Partnership Flip With Debt (Utility)
- PPA Partnership Flip Without Debt (Utility)
- PPA Sale Leaseback (Utility)
- PPA Single Owner (Utility)

Parametric Study

- Enable Parametric Study Option

Next

Fig. 7. Scan of SEDAT Model Selection menu

2.3 Select Models

To run Model Selection for the last location from the last Site_Selection run (or the default supplied location in Arizona)

- Start the software as above (run solar_desalination.bat or run-solar.sh)
- In the web page that loads, choose “Model Selection”
- Choose the model combination (one model from each of the three system types, solar energy generation, desalination, and financial that you want to run using the radio buttons. Models not available in the GUI application cannot be selected.

You have the option to Enable a parametric study if you wish. However, if you enable it then you would have to introduce additional variables as described in a previous section.

Click the next button to review parameters on each of the three models. A sample of a menu that allows you to review and edit parameters is shown below.

The screenshot shows a web-based application titled "System Configuration". On the left, there are two main sections: "Desalination Design Model" and "System Performance Simulation". The "Desalination Design Model" section contains descriptive text about the model and a "Run Design Model" button. The "System Performance Simulation" section contains descriptive text and a "Run Simulation Model" button. The right side of the screen displays a detailed table of parameters for the "Vacuum Air Gap Membrane Distillation - Batch (VAGMD-batch) Desalination System". The table has columns for "Variable", "Value", and "Units". Some specific values listed include:

Variable	Value	Units
Plant capacity	1000	m ³ /day
Feed concentration (Valid range: 35 to 200)	35	g/L
'0' for ASCL1SL module and '1' for AS2GCS module	1	none
Evaporator channel inlet temperature (Valid range: 60 to 80)	80	oC
Condenser channel inlet temperature (Valid range: 20 to 30)	25	oC
Feed flow rate (Valid range: 400 to 1100)	582.7	L/h
Initial batch volume (Valid range: > 50)	50	L
Initial temperature of the saline feed (Valid range: 20 to 30 and larger than the condenser channel inlet temperature)	25	oC
Target recovery rate	30	%
Type of cooling system ('o' for open circuit, 'c' for closed circuit)	c	
Initial temperature of the cooling water (Valid range: < Feed water temperature)	15	oC
Time step for the simulation (Recommended range: 10 to 400)	60	second
Thermal storage hours	0	hour
Fossil fuel participation (fraction from 0 to 1)	0	

To review the parameters, you can expand model sections by clicking the model names. The design model recommended parameters are shown on the left, these can be updated by choosing “Run Design Model” on the left.

The screenshot shows the 'System Configuration' interface at the address 127.0.0.1:8077/model-variables. The main content area is divided into two sections: 'Desalination Design Model' and 'System Performance Simulation'.

Desalination Design Model:

- Model run complete:** A green box displays system parameters:
 - Selected module size: 25.9 m²
 - Number of modules required: 1,026
 - Maximum potential recovery rate: 88.02 %
 - Actual recovery rate: 31.15 %
 - Brine concentration: 50.00 g/L
 - Thermal power requirement: 2.49 MWth
 - Specific thermal energy consumption: 59.73 kWh/(t·m³)
 - Specific electrical energy consumption: 0.29 kWh/(t·m³)
 - Gained output ratio: 10.91 kJ/J
- Run Design Model** button.

System Performance Simulation:

- Model run complete:** A green box displays system parameters:
 - Selected module size: 25.9 m²
 - Number of modules required: 1,026
 - Maximum potential recovery rate: 88.02 %
 - Actual recovery rate: 31.15 %
 - Brine concentration: 50.00 g/L
 - Thermal power requirement: 2.49 MWth
 - Specific thermal energy consumption: 59.73 kWh/(t·m³)
 - Specific electrical energy consumption: 0.29 kWh/(t·m³)
 - Gained output ratio: 10.91 kJ/J
- Run Simulation Model** button.

At the top right of the main content area, there are three buttons labeled 'Static Collector (Evacuated Tube)', 'Levelized Cost of Heat Calculator', and 'Refresh Data'. The 'Static Collector (Evacuated Tube)' button has a blue icon with a question mark.

When you are satisfied with the inputs, scroll down to choose “Run Simulation Model”.

1. When the model run is complete, you can click “View Results to see the results charts and report.

System Performance Simulation
Simulate the hourly performance of the solar field and desalination components, and estimate the cost of the system.

Model run complete

View Results

2.4 Review Results

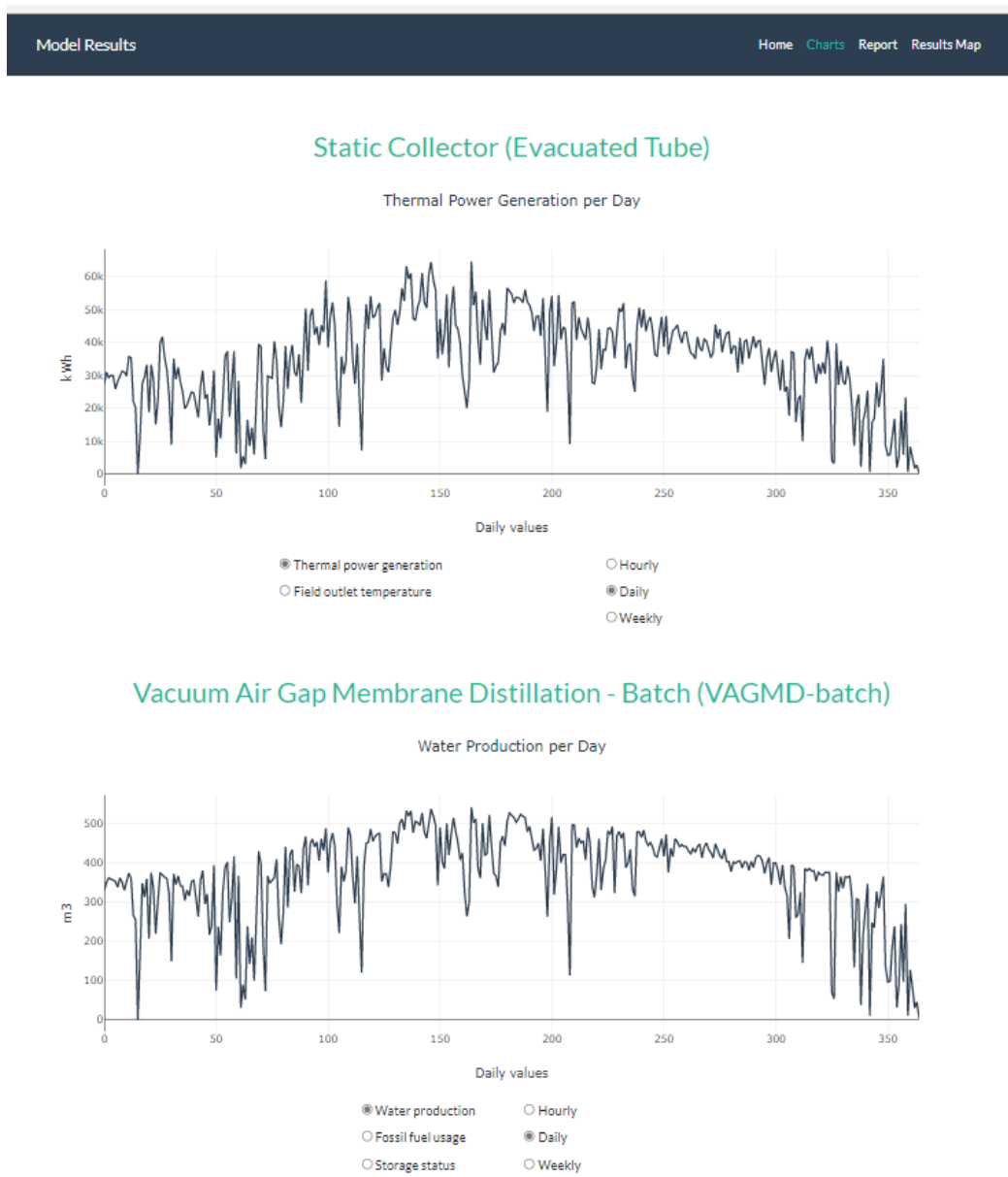


Fig. 8. Sample of Time Series results

The screenshot shows a software interface for an analysis report. At the top, there's a dark header bar with the text "Analysis Report" on the left and "Home Charts Report Results Map" on the right. Below this is a main content area divided into two main sections: "System Description" on the left and "Simulation Results" on the right.

System Description

Local Condition

- Location: Yuma Intl Arpt, AZ
- Daily average DNI: 7.4 kWh/m²/day
- Daily average GHI: 5.9 kWh/m²/day
- Feedwater salinity: 35.0 g/L
- Market water price: 1.29 \$/m³
- Distance to nearest desalination plant: 67.9 km
- Distance to nearest water network: 0.2 km
- Distance to nearest power plant: 53 km

Desalination System Configuration

- Technology: Vacuum Air Gap Membrane Distillation - Batch (VAGMD-batch)
- Design capacity: 1000 m³/day
- Thermal storage hour: 0 hrs
- Thermal storage capacity: 0 kWh
- Thermal storage cost: 26 \$/kWh
- Waste heat / fossilfuel enabled: No
- Specific thermal energy consumption: 59.73 kWh/m³
- Specific electrical energy consumption: 0.29 kWh/m³
- Thermal power consumption: 249 MW

Solar Field Configuration

- Technology: Static Collector (Evacuated Tube)
- Design thermal energy production: 5.00 MW
- Land footprint area: 30 to 40 acres

Simulation Results

Desalination System Performance

- Average daily water production: 367 m³
- Brine concentration: 50.0 g/L
- Assumed recovery rate: 31.15 %
- Total fuel usage: 0 MWh
- Percentage of energy from solar field: 100.0 %
- Percentage of energy from other sources: 0.0 %
- Number of modules required: 1026
- Module type: AS26C27L

Single module performance

Step	1	2	3	22	23	24
Operation time (min)	0	1	2	21	22	23
Batch volume (L)	59	49.3	48.6	35.8	35.1	34.4
Accumulated discharge volume (L)	0	0.7	1.4	14.2	14.9	15.6
Brine salinity (g/L)	35	35.5	36	48.9	49.9	50.8
Permeate flux (kg/hr/m ²)	1.6	1.6	1.6	1.6	1.6	1.6
Recovery rate (%)	0	1.4	2.7	28.5	29.8	31.2
Thermal energy (Wh-th)	0	40.3	40.4	40.6	40.6	40.6
Cooling energy (Wh-th)	0	5.3	9.8	32.3	32.4	32.5

Solar Field Performance

- Technology: Static Collector (Evacuated Tube)
- Annual thermal energy production: 12.57 GWh
- Capacity factor: 28.7 %
- Curtailed thermal energy: 4.57 GWh
- Percentage of curtailed thermal energy: 36.3 %
- High energy curtailment!
- Consider adding Thermal Storage hours in the Desalination Model Input and/or Reduce the Capacity of the Solar Field in Power Cycle Input

Cost Analysis

- Levelized cost of water (LCOW): 2.71 \$/m³
- Assumed cost of heat (LCOH, from other sources): 0.010 \$/kWh
- Levelized cost of heat (LCOH, from solar field): 0.019 \$/kWh
- Levelized cost of electric energy (LCOE): 0.05 \$/kWh
- Capital cost: 1.31 \$/m³
- Operational and Maintenance cost: 1.40 \$/m³
- Unit energy cost: 1.15 \$/m³

Fig. 9. Sample of Report results

2.5 Parametric Simulations

To run Model Selection while enabling parametric study, choose the model combination that you want to run using the radio buttons. Then toggle the button in the end to enable the parametric study.

- Financial Model**
- Commercial (Distributed)
 - Levelized Cost of Electricity Calculator
 - Levelized Cost of Heat Calculator
 - No Financial Model
 - PPA Partnership Flip With Debt (Utility)
 - PPA Partnership Flip Without Debt (Utility)
 - PPA Sale Leaseback (Utility)
 - PPA Single Owner (Utility)

Parametric Study Enable Parametric Study Option

Next

Select the variables you are interested in for the parametric study. Please remember to:

- Check the box on the left of the target variables
 - Input the min, max and interval values for the parametric study (No need to change the column "Value")
 - Modify the values of other variables as you see fit
- Please note that you cannot select more than 2 variables.

The screenshot displays two separate parametric study interfaces within the System Configuration software.

Desalination Design Model:

Variable	Value	Units	Min	Max	Interval
Plant capacity	1000	m³/day			
Feed concentration (Valid range: 35 to 200)	35	g/L	30	50	20
'0' for AS7C1.5L module and '1' for AS26CSL module	1	none			
Evaporator channel inlet temperature (Valid range: 60 to 80)	80	oC			
Condenser channel inlet temperature (Valid range: 20 to 30)	25	oC			
Feed flow rate (Valid range: 400 to 1100)	582.7	l/h			
Initial batch volume (Valid range: > 50)	50	L			
Initial temperature of the saline feed (Valid range: 20 to 30 and larger than the condenser channel inlet temperature)	25	oC			
Target recovery rate	30	%			
Type of cooling system ('a' for open circuit, 'c' for closed circuit)	c				
Initial temperature of the cooling water (Valid range: < Feed water temperature)	15	oC			
Time step for the simulation (Recommended range: 10 to 400)	60	second			
Thermal storage hours	0	hour			
Fossil fuel participation (fraction from 0 to 1)	0				

Static Collector (Evacuated Tube):

Variable	Value	Units	Min	Max	Interval
Plant lifetime	20	none			
System downtime	10	%			
Average interest rate	0.04				
Unit cost of electricity (LCOE)	0.05	\$/kWh			
Unit cost of heat from fossil fuel (LCOH)	0.01	\$/kWh			
Unit cost of heat from solar field (LCOH) (Input value to overwrite LCOH calculated from solar field)	0.02	\$/kWh	0.02	0.05	0.01
Heat source inlet temperature	85	oC			
Heat source outlet temperature	95	oC			
Heat exchanger efficiency	0.85				
Cost of module replacement	0.22	\$/m³			
Cost of thermal storage (from solar field)	20	\$/kWh			

Fig. 10. Sample of Inputs in Parametric Analysis

Static Collector (Evacuated Tube) / Vacuum Air Gap Membrane Distillation - Batch (VAGMD-batch)

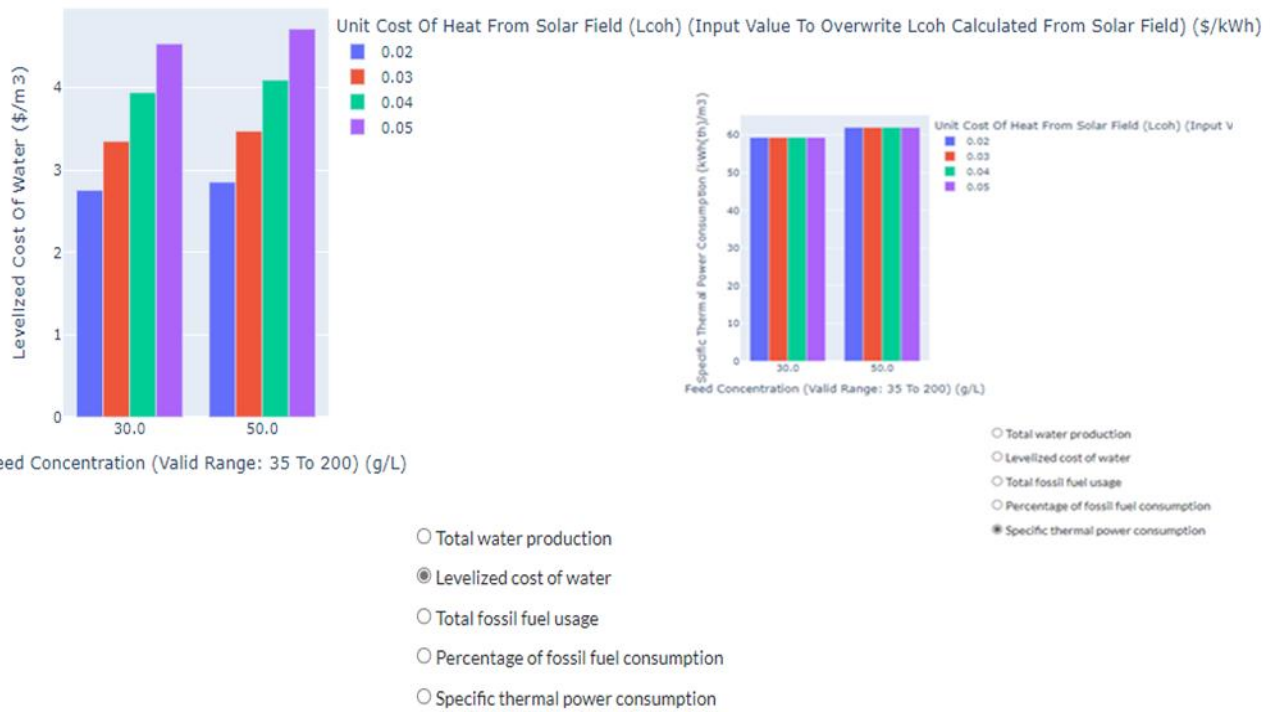


Fig. 11. Sample of Results of Parametric Analysis

3 File Management

3.1 File Menu

The users will be able to look at the detailed model results in the local drive:

(Windows) C:\DOE\DOE_CSP_PROJECT\SAM_flatJSON

(Mac and Linux) ~\DOE\DOE_CSP_PROJECT\SAM_flatJSON

“SAM_flatJSON” folder stores files and scripts that interact with SAM models and records the model results.

Name	Date modified	Type	Size
__pycache__	1/10/2022 6:48 PM	File folder	
AssociatedFiles	1/10/2022 2:23 PM	File folder	
defaults	1/10/2022 2:24 PM	File folder	
models	1/10/2022 2:24 PM	File folder	
parametric_inputs	1/10/2022 2:24 PM	File folder	
parametric_results	1/10/2022 2:24 PM	File folder	
results	1/10/2022 2:24 PM	File folder	
solar_resource	1/10/2022 2:27 PM	File folder	
XLS results	1/10/2022 2:27 PM	File folder	
init.py	12/23/2021 4:26 PM	PY File	0 KB
~\$SAM_comb.xlsx	12/23/2021 4:26 PM	Microsoft Excel W...	1 KB
PySSC.xlsx	6/28/2021 3:02 PM	PY File	8 KB
SAM_comb.xlsx	6/28/2021 3:02 PM	Microsoft Excel W...	15 KB
SamBaseClass.py	1/10/2022 2:20 PM	PY File	95 KB
ssc.dll	7/12/2021 3:18 PM	Application exten...	16,974 KB
ssc.dylib	6/28/2021 3:02 PM	DYLIB File	16,800 KB
sscapi.h	6/28/2021 3:02 PM	C/C++ Header	21 KB

Fig. 12. File menu in SAM_flatJSON folder

Table 4. Folder description in SAM_flatJSON folder

Folder	Contents	File type
models	Solar generation, desalination and financial models' input variable list	JSON
defaults	Models' default input values	JSON
results	Results in .json (each simulation generates 4 files)	JSON
parametric_inputs	Intermediate inputs for parametric analysis	JSON
parametric_results	Parametric study results in .json (each single simulation generates 4 files)	JSON
solar_resource	Weather data for all weather stations	CSV
XLS results	Results in .xls (each simulation generates 1 file, which contains 4 tabs)	XLS

* JSON files can be opened using Notepad or other text editors.

3.2 Result Reports

Each non-parametric simulation will generate a result report, which include the pieces of information listed in Table 4; a sample report page was shown in Fig. 9.

Table 5. Information in Results report

Result report	Description
Location condition	Geographic information of the selected site
Desalination System Configuration	Design point of the desalination system
Solar Field Configuration	Design point of the solar field
Desalination System Performance	Performance based on an annual simulation
Solar Field Performance	Performance based on an annual simulation
Cost Analysis	Breakdown of the LCOW

3.3 Case Graphs

For non-parametric simulations, time series will be displayed to show the annual performance as shown in Fig. 8.

For parametric simulations, bar diagrams will be generated to compare between different input combinations as shown in Fig. 11.

3.4 Export Data and Graphs

For all and detailed model results, the user can find the JSON or Excel results using the file menu shown in Figure 12.

The users can download a graph that is generated in the “Chart Results” page. In the toolbar of a certain chart, there’s a download button at the left:



Click it and a picture (by default a .png file) will be downloaded to the local download folder.

4 Databases

4.1 Solar Resource

Solar input data and weather information are necessary for generating the energy inputs into a solar desalination facility. Models for energy production from solar resources require hourly data on solar irradiation and other meteorological conditions. We integrated data of Direct Normal Irradiance (DNI) and Global Horizontal Irradiance (GHI) for visualization and query in the site selection stage and Typical Meteorological Year (TMY) weather files in the simulations stage. SEDAT embeds 1,397 TMY weather files from locations around the world. The US data (1,016 locations) were directly extracted from the NSRDB (National Solar Radiation Database). The TMY files for the locations outside the US were derived from PV-GIS dataset using PV-GIS API (Application Programming Interface) and were modified applying the NSRDB TMY format. Furthermore, since the PVGIS dataset uses UTC (Coordinated Universal Time) for all locations, the time series for each location were adjusted to the local time according to its time zone.

4.2 Alternative Water Resources

Most of the current US desalination infrastructure utilizes brackish water although seawater desalination is more common world-wide³. The prime data source for brackish groundwater is a USGS National Brackish Groundwater Assessment which provides data on occurrence and characterization of brackish groundwater resources⁴. The USGS comprises two datasets: “Dissolved Solids” and “Major Ions”. As part of the aggregation process, parametric statistics (minimum, mean, maximum, variance, standard

³. Gude, V. G., & Fthenakis, V. Energy efficiency and renewable energy utilization in desalination systems. *Progress in Energy*, 2(2), 022003 (2020).

⁴. Stanton, J. S., et al. *Brackish groundwater in the United States*. No. 1833. US Geological Survey (2017).

deviation) were calculated for the total dissolved solids, and depth attributes, water temperatures and well yields (Figure 13). The data from the brackish water wells were aggregated to county boundaries using the ArcGIS spatial join function. Also, all available data on water temperature were mapped. The aggregation to county level was found useful for statewide visualization of the brackish water characteristics.

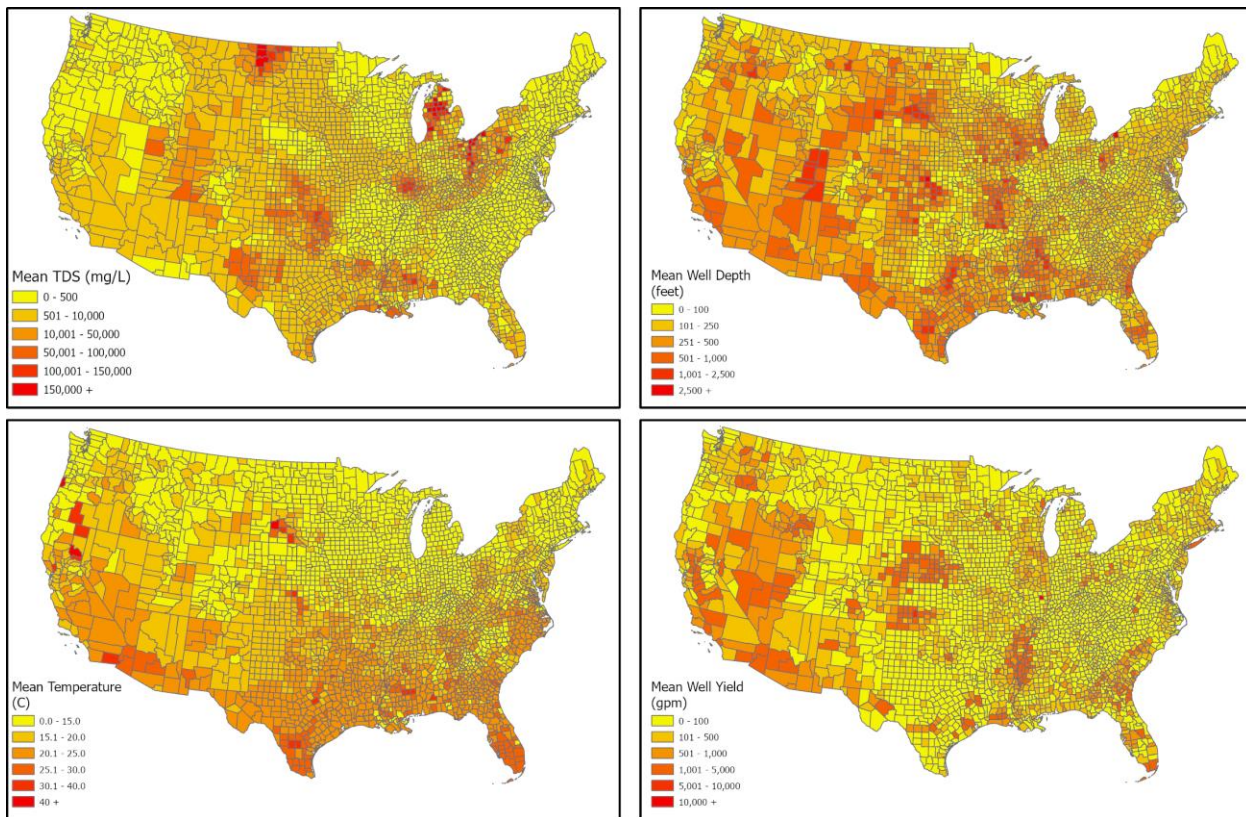


Fig. 13. Brackish water resources; a) TDS levels; b) well depth levels; c) water temperatures at well depths; d) mean well yields (data source USGS)

In addition to brackish water, we mapped the availability of other alternative water sources, such as agricultural drainage water, and produced water from oil and gas (O&G) which is more prevalent in Texas; a detail of such O&G produced water resources⁵ is shown in Figure 14. These alternative water resources are also represented by location and salinity. The feedwater salinity level, as well as the allowed brine concentration determine the appropriate desalination technology and how it impacts the cost of operating these plants⁶. Input water temperature impacts the energy requirements of the system and thus the cost of producing fresh water.

⁵. USGS Produced Waters Geochemical Database.” [Online]. Available: <https://energy.usgs.gov/EnvironmentalAspects/EnvironmentalAspectsofEnergyProductionandUse/ProducedWaters.aspx#3822349-data>. [Accessed: January 11, 2019].

⁶. Atia, A. A., Yip, N. Y., & Fthenakis, V. Pathways for minimal and zero liquid discharge with enhanced reverse osmosis technologies: Module-scale modeling and techno-economic assessment. *Desalination*, **509**, 115069 (2021).

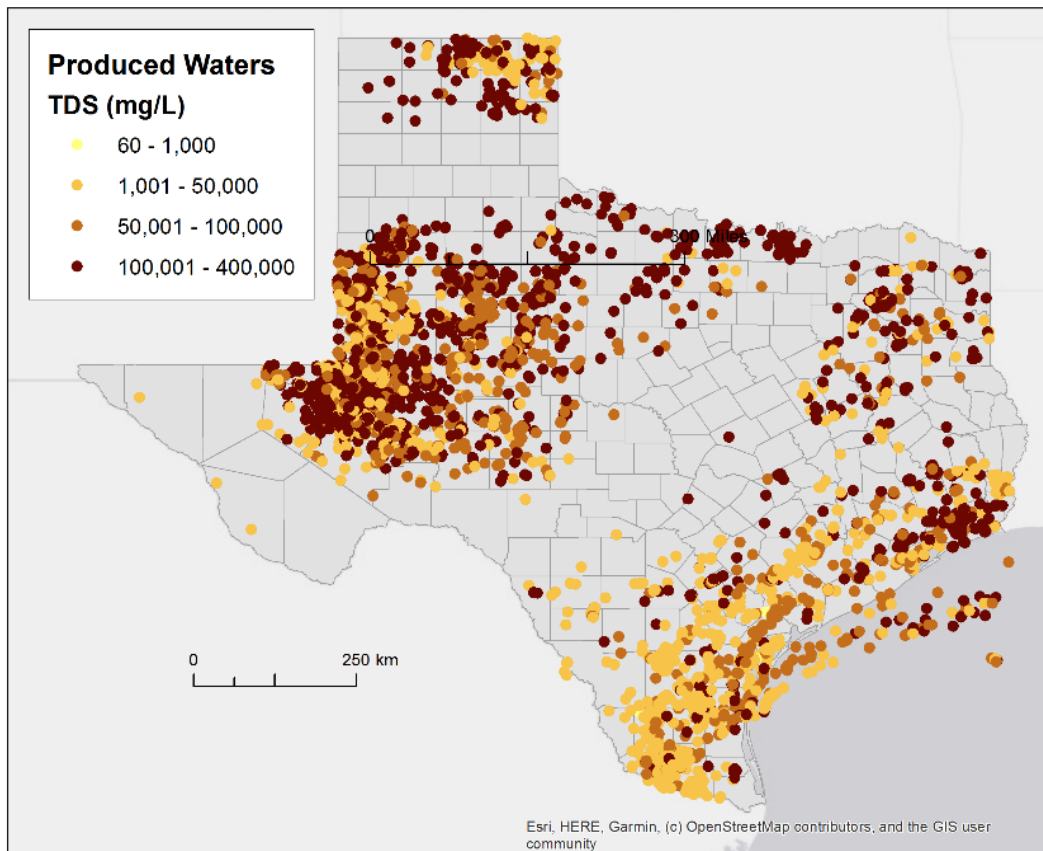


Fig. 14. Produced waters database extract for Texas (includes offshore wells). (Data source: USGS Produced Waters¹³).

4.3 Desalination Plants

Also, we included the geospatial distribution of U.S. desalination plants as of 2016, courtesy of the Global Water Intelligence (GWI)⁷; their locations are shown in Figure 15.

⁷. Email correspondence with Hugo Birch, Desalination & Reuse Editor, Global Water Intelligence, on June 16, 2021.

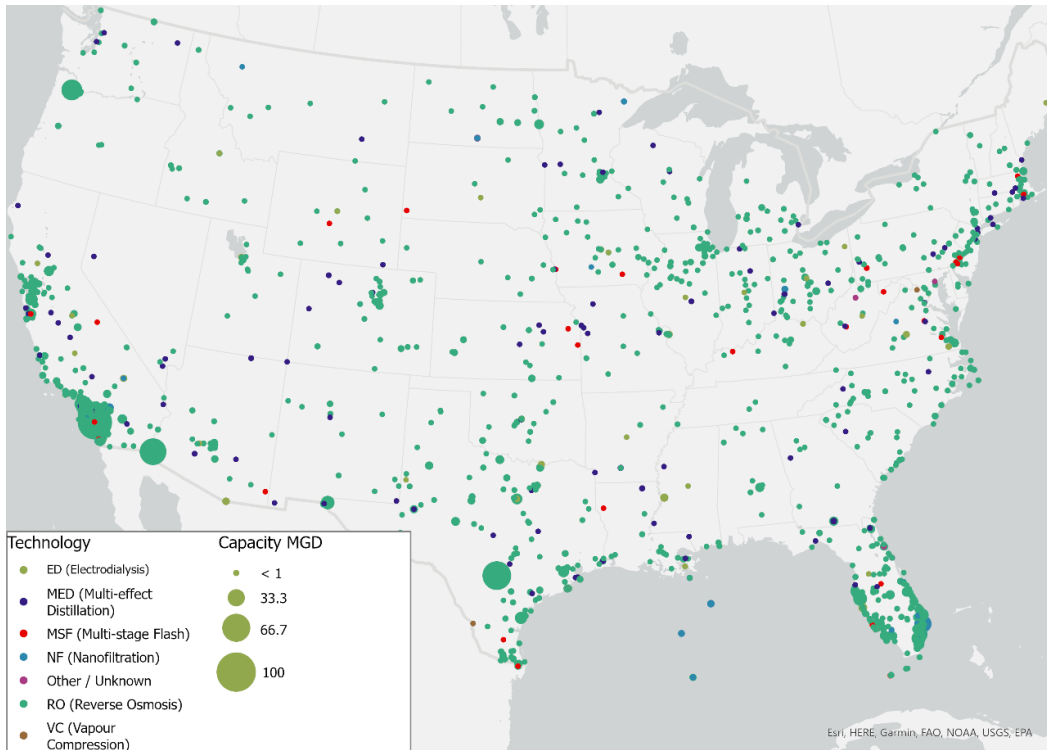


Fig. 15. Desalination Plants per desalination technology and plant capacity (GWI 2016 data³⁰).

4.4 Power Plants

We added the latest US database of power plant locations and capacities available from the Energy Information Agency (EIA) so that the user can examine the possibility of co-locating a desalination plant with a power plant, thereby sharing real estate and grid connectivity. There is also potential for solar thermal desalination to use waste heat from power plants to compliment solar resources. Gingerich and Mauter⁸ estimated that the US generated 14.6 billion GJ of electricity and 26.4 billion GJ of waste heat via coal, nuclear, and natural gas power plants. Of this waste heat, 99% is condenser heat discharged to the environment at or below 41.5 °C which under most conditions is too low to be practically recoverable. The remaining 1% of waste heat, or 155 million GJ, is discharged in exhaust streams at temperatures between 91 and 543°C which if recovered could be used in thermal desalination plants that are co-located with or are near power plants. SEDAT guides the user by showing straight-line distances between a selected site and near-by power plants.

4.5 Sensitive Areas

Two types of areas are included that may not be suitable for a site: steep areas, and protected areas (parks and ecological reserves). Switching the map type in the site-selection interface to “topographic” shows a topographic basemap that includes slope as a part of the visualization. You can zoom in to local areas to see their topography; steep slopes make siting a plant more difficult. The protected areas of the United

⁸. Gingerich, D. B. & Mauter, M. S. Quantity, quality, and availability of waste heat from United States thermal power generation. *Environmental science & technology*. **49**(14), 8297-8306 (2015).

States (Federal parks and ecological sites, state and local parks) can be seen by selecting the “Regulatory” overlay in the site selection interface. The areas shown in light green are protected areas at all levels and not suitable for development, while those in the darker green are federally managed areas that may permit development after review (federally managed lands include areas that have mixed-use provisions that vary from site to site).

4.6 Water Networks

Existing conveyance water networks can serve the delivery of desalinated water from the plant to customers; thus, the distance of the selected site to the nearest network is an important consideration given the cost of building a new water delivery system. Existing water networks are represented in SEDAT by two data sources: existing canals and aqueducts⁹ and a proxy for local municipal water systems based on road locations¹⁰. Canals and aqueducts are represented visually in the system, and the straight-line distance from a selected site is calculated and shown on the map when a user selects a location. The water network proxy locations are stored, but not displayed, in the system. The basemap in the application includes a road overlay that is separate from the water network. The road network has been subset to include types that are more likely to be residential; interstates and other road types that are mostly rural have been excluded. The network along a generalized road network are presumed to likely have water transportation networks. The distance to the nearest point is calculated based on the road network proxy.

4.7 Energy and Water Utility Prices

Electricity rates and fuel prices from the OpenEI Application Programming Interface (API) are being used for cost comparisons with solar-powered desalination. A script was developed to construct a link to the web site; it references the latest available data on the web site, which is updated regularly.

Water price data were downloaded from the free, open-access IBNET water tariff database¹¹, a joint product of the Global Water Intelligence (GWI) and the International Benchmarking Network of the World Bank (IBNET). It includes data on water utilities for 151 national jurisdictions, for a range of years up to 2017 (year range varies greatly by country and utility) on service and utility parameters (Benchmark Database), and water tariffs for 211 jurisdictions (Tariffs database). Information includes cost recovery, population served, financial performance, non-revenue water, residential and total supply, and total production. Data can be called up by utility, by group of utility, and by comparison between utilities, including the whole (global) utility database, enabling both country and global level comparison for individual utilities.

The data are multi-faceted with multiple price entries associated with fixed and consumption charges for various scales of consumption. To reduce complexity and maintain the user-friendly format of the software, only the consumption charges and the corresponding consumption levels are shown. In addition, links to local utility web-sites were added on the maps so the user can see the pricing detail and get price updates in the future.

⁹. United States Geological Survey. National Hydrography Dataset Plus High Resolution.

<https://www.usgs.gov/core-science-systems/ngp/national-hydrography/nhdplus-high-resolution>. [Accessed: August, 2021].

¹⁰. U.S. Census Bureau: 2021 TIGER/Line® Shapefiles: Roads. <https://www.census.gov/cgi-bin/geo/shapefiles/index.php?year=2021&layergroup=Roads>. [Accessed: September, 2021].

¹¹. IBNet Tariffs DB available at: <https://tariffs.ib-net.org/sites>. [Accessed: June 15, 2021].

4.8 Regulatory/Permitting

A cursory review of federal regulations as of 2020, revealed a handful of agencies with jurisdiction over desalination developments including the U.S. Environmental Protection Agency (EPA), the U.S. Army Corps of Engineers (USACE), the U.S. Bureau of Reclamation (USBR) and the U.S. Coastal Guard (USCG), among others. These federal agencies oversee the permitting associated with discharges as outlined by the National Pollution Discharge Elimination System (NPDES) permit program, alongside permitting for plant construction in the vicinity of U.S navigable waters and environmental impact on aquatic flora and fauna. The EPA empowers most states to handle the permitting, administrative and enforcement of the NPDES program while retaining oversight power.

A review of the regulatory and permitting practices abroad by the Water Environment & Reuse Foundation reveals that other countries where desalination has become a mainstay of the water supply, such as Australia and Spain, have a more streamlined process, with a key difference between the U.S. and these countries being the amount of time needed to issue the permits, with the United States being the only country where the permitting process, 3-10 years on average, can take longer than the construction time, 2 to 3 years. This discrepancy in time is not limited to international waters, however. States within the U.S have such an independent and fragmented permitting system that the permitting process for the Carlsbad Desalination Project (California) took 10 years, from project inception in 2000 to permit approval in 2010. Conversely, that of East Cherry Creek Valley Reverse Osmosis Plant (Colorado) took 2 years, from the pilot testing of brine disposal methods in 2008 to the discharge permit approval in 2010. The data show that state by state differences are significant. For example, California and Texas have fashioned different requirements for a wide range of desalination facilities within the states. In 2014, the State Water Quality Control Board of California instituted the California Ocean Plan which contains specific requirements pertaining to discharge from desalination plants. The plan covers only seawater facilities and prescribes key constraints on their development such as mandatory use of subsurface intakes for source water, a requirement for impingement and entrainment mitigation where applicable, discouragement of co-location with power plants so as to reduce open channel withdrawal and discharge, as well as a requirement that the discharge salinity at the edge of the mixing zone be lower or equal to 2 parts per thousand (ppt) above the ambient water salinity, necessitating large dilution levels. On the other hand, Texas has a pragmatic step-wise, case-by-case approach, with a permitting decision tree model for determining which existing permits apply to the user's plant specifics.

A preliminary and partial examination of regulatory and permitting requirements for desalination plants in Texas, Arizona, Nevada, Florida, California and Colorado is included in SEDAT. Available in the open literature information on the permitting requirements applicable to existing desalination plants was compiled, and the associated state and county permitting requirements were synthesized into tabular forms that will be shown to the user of the software, together with links to associated agencies and permitting forms per state and county as available and applicable. It is noted that the SEDAT database, while useful to stakeholders, is not all-encompassing and should only be used as a preliminary guideline for permitting requirements.

4.9 County Population Growth Projections

Population growth estimates for U.S. counties^{12,13} consistent with the Shared Socioeconomic Pathways (SSP) are integrated in the application to show areas of projected population growth and decline under all of the scenarios. In the GUI, the layer is available and rendered based on growth or decline; when a user selects a county, the population growth curves are shown for all five SSP scenarios along with the mean growth curve for all of the scenarios. In this way, users can see if a proposed site is within or near a county that is expected to have a growing demand for water.

The five SSP scenarios project population growth and decline based on different assumptions about economic growth, emissions, technology, and overall population growth. The scenarios and summary descriptions are shown below.

2. Scenario 1: Sustainability (taking the green road). Gradual but widespread shift to sustainability and an emphasis on human well-being.
3. Scenario 2: Middle of the road. Continuation of recent trends in social, economic and technological trends.
4. Scenario 3: Regional Rivalry (a rocky road). Focus on country and regional issues over global issues, national and regional security issues are the focus with slow economic growth and high consumption.
5. Scenario 4: Inequality (a road divided). Increased inequality globally, with more unrest and uneven growth across sectors.
6. Scenario 5: Fossil-fueled development (taking the highway). Rapid economic, technology, and population growth, with high use of fossil fuels.

The data used in the application have taken the scenario outputs for the U.S. and applied them to counties; the overall population change shown on the map is based on the first scenario (sustainability), while the graphs show all five scenarios.

5 Solar Thermal Energy Generation Models

5.1 PSA Static Solar Collector

The SAM solar collector model is limited to residential water heating; thus, we elected to code and integrate a model developed by our Plataforma Solar de Almeria (PSA) collaborators which has been verified with measurements at a pilot plant in Almeria (Figures 16 and 17). The new static collector class was created mostly by converting PSA's MATLAB functions to Python and modifying the code to be more dynamic. The class allows the user to select either flat-plate or evacuated tube collectors. The user will be able to design the collector field and simulate hourly performance.

¹². Hauer, M. & Center for International Earth Science Information Network - CIESIN - Columbia University. 2021. Georeferenced U.S. County-Level Population Projections, Total and by Sex, Race and Age, Based on the SSPs, 2020-2100. Palisades, NY: NASA Socioeconomic Data and Applications Center (SEDAC). <https://doi.org/10.7927/dv72-s254>. [Accessed: October 30, 2021].

¹³. Hauer, M. E. Population Projections for U.S. Counties by Age, Sex, and Race Controlled to Shared Socioeconomic Pathway. *Sci. Data*, 6: 190005. <https://doi.org/10.1038/sdata.2019.5> (2019).



Fig. 16. Part of the Solar Flat Plate Collector at PSA

5.2 SAM CSP Parabolic Trough

A concentrating solar power (CSP) parabolic trough (PT) system collects direct normal solar radiation and converts it to thermal energy that runs a power block to generate electricity. The components of a parabolic trough system are the solar field, power block, and in some cases, thermal energy storage and fossil backup systems. The solar field collects heat from the sun and consists of parabolic, trough-shaped solar collectors that focus direct normal solar radiation onto tubular receivers. Each collector assembly consists of mirrors and a structure that supports the mirrors and receivers, allows it to track the sun on one axis, and can withstand wind-induced forces. Each receiver consists of a metal tube with a solar radiation absorbing surface in a vacuum inside a coated glass tube. A heat transfer fluid (HTF) transports heat from the solar field to the power block and other components of the system. The power block is based on conventional power cycle technology, using a turbine to convert thermal energy from the solar field to electric energy. The optional fossil-fuel backup system delivers supplemental heat to the HTF during times when there is insufficient solar energy to drive the power block at its rated capacity. This is a summary description from the SAM User Manual; see the manual for details. Below is a figure of such a system operating in the Plataforma Solar de Almería, in Spain.



Fig. 17. Part of the Parabolic Trough CSP facility at PSA

5.3 SAM CSP Linear Fresnel

SAM includes the direct steam and molten salt CSP linear Fresnel (LF) models. Below is a summary description of these models which is extracted from the SAM User Manual; see the manual for details. The direct steam LF model utilize water/steam as the heat transfer fluid. It includes options for

recirculated (RC) and once-through (OT) steam flow in the solar field. Most steam generator designs use RC boiler designs, where water and steam exit the boiler section as a two-phase mixture. The steam mass fraction of the mixture -called the steam quality- is maintained to a desired value with a recirculation pump. At the outlet of the boiler section, dry steam is separated from the liquid and sent either to a superheater section or to the turbine, and the saturated liquid returns to the boiler. Direct steam LF system do not have thermal storage but are integrated with fossil-fired backup systems to provide heat. SAM includes options for modeling three different fossil backup scenarios. The first is “Minimum backup level”, and refers to an auxiliary boiler in parallel with the solar field that supplies additional steam flow at design temperature when the solar field isn’t able to supply the user-specified minimum operation level. The second option is “Supplemental operation” where additional flow (again, in parallel) is provided up to a user-specified maximum value to assist flow from the solar field to reach the design-point thermal requirement for the power cycle. These scenarios correspond to the plant arrangement shown in Figure 18. The final fossil backup scenario allows fossil firing up to a user-specified maximum thermal output to boost the temperature of steam entering the turbine.

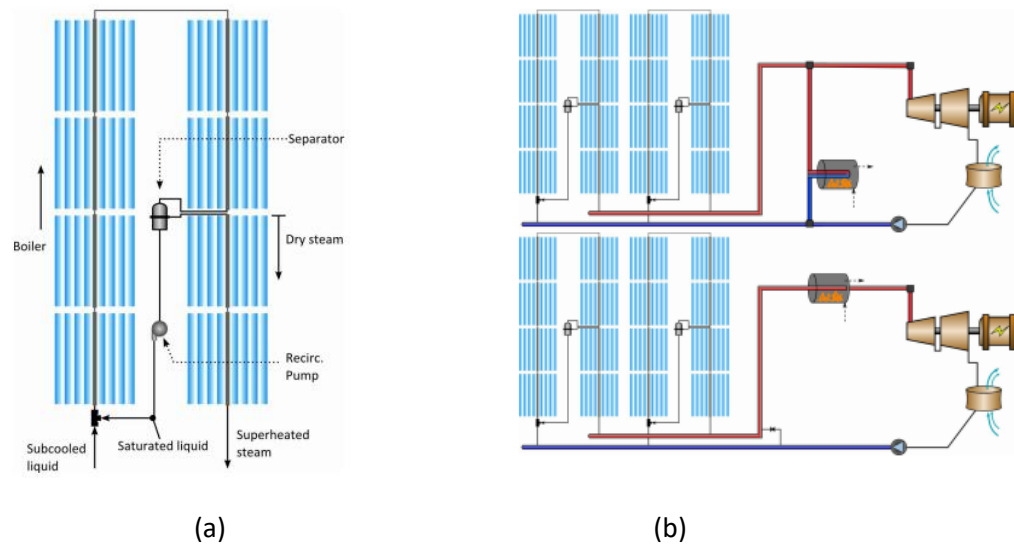


Fig 18 (a) Schematic of a recirculated boiler loop with superheating. Liquid and steam are separated partway through the loop. (b) Plant arrangements for parallel auxiliary fossil backup (top) and series back-up (bottom). (Wagner and Zhu, 2012¹⁴)

For details of the geometrical optimization implemented in this model, the user should read the source paper by Wagner and Zhu¹ and the corresponding section in SAM user manual. Figure 19, below, shows the solar angles used in this optimization.

¹⁴ Wagner M. and Zhu G., A Direct Steam Linear Fresnel Performance Model for NREL’s System Advisor Model

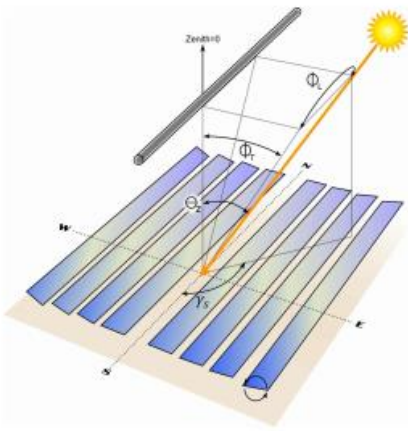


Fig. 19. Illustration of the solar-position-dependent collector angles, including the transversal plane and longitudinal plane incidence angles. By convention, SAM assumes that the solar azimuth angle is 0°–South, with negative values toward the East and positive West. (Wagner and Zhu, 2012)

The molten salt LF model simulates the performance of a linear Fresnel system that utilizes a sensible-heating liquid such as molten salt as the heat transfer fluid (HTF) in the field. The molten salt linear Fresnel model includes a thermal energy storage model, which may use either the same HTF as the solar field, or a different fluid. If the field and storage system use the same HTF, the system is modeled as a direct storage system with no heat exchanger between the field and storage system. If the field and storage fluids differ, SAM includes a heat exchanger in the storage system that impacts exergetic system performance. SAM always assumes a heat exchanger between the liquid HTF and the steam flow in the power cycle

5.4 SAM CSP Tower

A concentrating solar power tower system (also called a central receiver system) consists of a heliostat field, tower and receiver, power block, and optional storage system. SAM includes a direct steam and a molten salt power tower model. The field of flat, sun-tracking mirrors called heliostats focus direct normal solar radiation onto a receiver at the top of the tower, where a heat-transfer fluid is heated and pumped to the power block (figure 20).

The power block generates steam that drives a conventional steam turbine and generator to convert the thermal energy to electricity. The solar field optimization algorithm uses NREL's SolarPILOT™ to generate the heliostat field layout and characterize optical performance. You can design the field outside of SAM and import the layout as a table of heliostat positions with Cartesian x and y coordinates with respect to the tower at position (0,0) or you can use SAM to run SolarPILOT and automatically generate heliostat positions given a tower height, heliostat geometry and optical properties, and receiver geometry and optical properties.

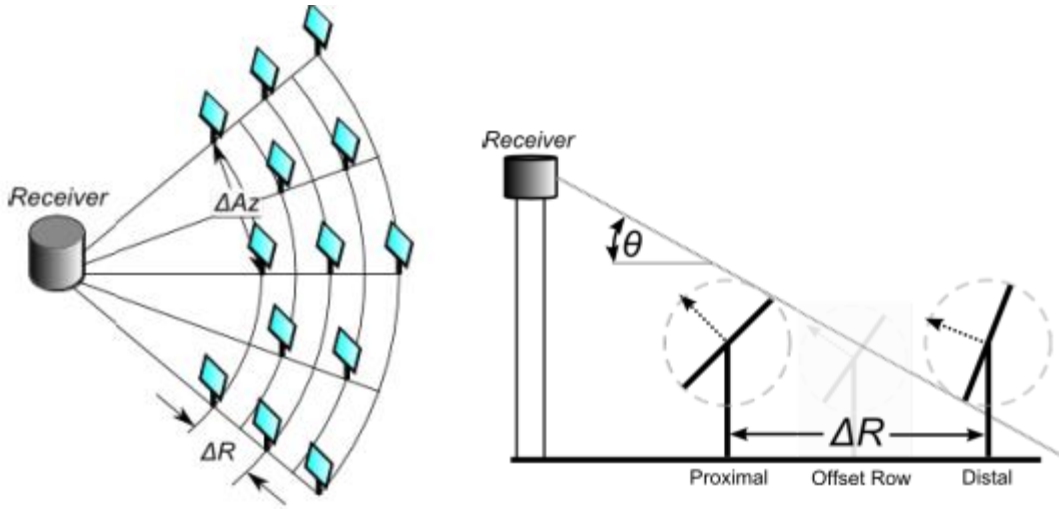


Fig. 20. The initial spacing between heliostats in a row is a distance twice the width of a heliostat. As the radial position of the rows increases, so too does the spacing between heliostats. (source: SAM User Manual)

5.4.1 SAM Power Cycles

The power cycle converts thermal energy to electric energy. The power tower model offers three options for modeling the power cycle:

- The **Rankine-cycle** model is for Rankine-cycle steam engines with two open feed-water heaters, and a pre-heater, boiler and super-heater. This regression model was developed from a detailed first-principles basis Rankine cycle model and calculates cycle performance over the expected operating range by modeling each cycle component at off-design conditions. The model assumes that deviation in cycle performance at off-design conditions is independent of cycle design and only a function of deviation from the user-specified design point. This model is fast, flexible, and accurate, and suitable for modeling most conventional CSP power cycles.

The **user-defined** power cycle model allows you to use data from your own power cycle model in SAM, and can be used to model Rankine or other types of power cycles. It requires that you provide values for general power cycle parameters along with a tables of data showing the electrical power generated over a range of HTF mass flow rates, ambient temperatures, and ambient temperatures. SAM uses this data to build a power cycle regression model that considers single variable effects and two variable interactions.

The **supercritical carbon dioxide** power cycle model allows you to model the Recompression and Partial Cooling cycle configurations. The model uses cycle and system design parameters to design a cycle that requires the smallest amount of recuperator conductance to achieve the design cycle efficiency. The off-design model assumes that all turbomachinery operates at their respective design shaft speeds. The off-design model is slow compared to SAM's annual models, so the power tower model pre-processes it over a fixed set of off-design conditions, and then interpolates this data during the annual system simulation. There is an option to pre-process before the power tower simulation and save the data so that you can run multiple power tower simulations from a single off-design pre-process simulation

5.5 SAM Industrial Process Heat

SAM includes two industrial process heat (IPH) models, a parabolic trough and a direct steam one. The industrial process heat parabolic trough model is similar to the CSP physical trough model, but assumes that heat from the solar field is used for a thermal application rather than to drive a power cycle for electricity generation. It is for a solar field of parabolic trough concentrating collectors.

The industrial process heat direct steam model is similar to the CSP linear Fresnel model, but assumes that heat from the solar field is used for a thermal application rather than to drive a power cycle for electricity generation. It is for a solar field of parabolic linear Fresnel concentrating collectors.

5.6 SAM Financial models

Levelized Cost of Heat (LCOH) calculation

In order to evaluate the economic performance of the thermal desalination system, we should determine the leveled cost of heat (LCOH) used in desalination. However, the financial models in the SAM CSP models, do not report LCOH. Thus, we made the following additions to the SAM code.

LCOH calculator (replicating the LCOE calculator in SAM)

This is a simpler calculation, where cash flow is neglected:

Starting from:

$$LCOE = \frac{FCR \times TCC + FOC}{AEP} + VOC(\$/kWh)$$

where FCR is the fixed charge rate, TCC is the capital cost (\$), FOC is the fixed annual operating cost (\$), VOC is the variable operating cost (\$/kWh), FCR is the fixed charge rate, AEP is the annual electricity production (kWh)

and LCOH is derived by replacing the electricity production with the thermal energy production:

$$LCOH = \frac{FCR \times TCC + FOC}{AHP} + \frac{AHP}{AEP} \times VOC(\$/kWh)$$

where AHP is the annual heat (thermal energy) production (kWh-t)

LCOH considering cash flow (used in most LCOE financial models)

To evaluate the leveled cost at present, the cash flow is considered:

$$LCOH = \frac{\sum_{i=0}^n \frac{C_n}{(1+d_n)^n}}{\sum_{i=1}^n \frac{Q_n}{(1+d_r)^n}}$$

where C_n is the total annual (capital+operation) cost in year n, Q_n is the thermal energy generation in year n (kWh-t), d_n is the nominal discount rate and d_r is the real discount rate.

Levelized Cost of Water (LCOW) calculation

Capital cost and O&M cost are included:

$$LCOW = CAPEX + OPEX (\$/m^3)$$

where $CAPEX$ is the unit capital cost ($\$/m^3$), to evaluate the levelized cost at present, the cash flow is considered:

$$CAPEX(\$/m^3) = \frac{C_0}{Q_p} \times \frac{r(1+r)^t}{(1+r)^t - 1}$$

where C_0 is the initial capital cost for the desalination plant (\$), Q_p is the annual water production (m^3), r is the interest rate, and t is the plant life time.

$OPEX$ is the O&M cost per unit production, including energy cost and other costs:

$$OPEX(\$/m^3) = SEC \times LCOE + STEC \times LCOH + Ope_{other}$$

SEC and $STEC$ are the specific electricity and heat consumption (kWh/m^3). $LCOE$ and $LCOH$ are the levelized cost of electricity and heat, respectively. Ope_{other} is other O&M cost such as maintenance, labor, insurance and so on.

5.7 Integration of the SAM models into SEDAT

Concentrated solar power (CSP) and photovoltaics (PV) models, from NREL's System Advisor Model (SAM) were integrated into *SEDAT* using Python wrappers. However, since these models were designed for electricity rather than heat production, the source code was modified to obtain variables needed for integration with solar thermal desalination models (e.g., condenser temperature and exhaust steam mass flow rate in the power block). In order to develop a graphical user interface (GUI) for *sedat*, the wrappers created from SAM for CSP modules and financial modules needed substantial modifications and restructuring¹. The Python wrappers for these models contain more than 300 input variables; these were initialized in the wrapper, and an interface using the DataTable function in DashPlotly was used to construct the frame of input variables and JavaScript Object Notation (JSON) was employed to structure all the variables of a given model and adapt it to our GUI.

JSON captures the structure of the input fields on the user interface along with assigning values and reading properties for each variable. JSON objects can transmit attribute-value pairs, arrays and any other serializable data objects; these were used to store and communicate data used in modeling solar and desalination plants of any type. This approach consisted of creating Python wrappers for each model from the user interface of SAM. Each variable value from the wrapper was matched with its defaulted value from SAM and added to a JSON file. The tab, section, and sub-section were added as properties of each variable initially. The functionality and simulations run by SAM are imported into the software by using the Python scripts generated by creating a SAM wrapper. The wrapper initializes all the variables used for a model within SAM, compiles the source code of SAM and executes the models.

The JSON file is used to build the GUI interface by iterating through each tab, section, and subsection in the SAM user interface and creating the corresponding menu elements in the Dash framework. This code can be reused to create menu structures that represent each of the SAM models without having to manually program the menu elements; each model can have a menu system automatically generated

from the JSON file. Logic for loading the various models was created in the Python code so that the appropriate menu system is loaded based on the user-selected model.

Our approach involved capturing the structure of the variables on the GUI inside the JSON in a non-repetitive manner along with matching default values of all the SAM variables from a sub-branch of the SAM GitHub repository¹⁵ that includes JSON files with all of the model variables and default values. The default values of different model variables in SAM are populated in from these files. The JSON file created for input variables captures the structure of the GUI by adding variables as list elements inside dictionaries. The dictionaries contain the name of the tab, section or sub-section on the GUI as a dictionary key and have the variables, sub-section or section elements as dictionary values. The different files associated in this integration are structured in folders and shown in Figure 21. SamBaseClass.py is the Python file that integrates and uses these files. The files generated from the wrapper (PySSC.py, sscapi.h, ssc.dll for Windows, and ssc.dylib for MacOS) are also placed inside the same folder. The compilation is a one-time process; once created, the files are included in SEDAT and used for all desalination models that require solar energy inputs. New versions of SAM, along with new desalination or solar thermal technologies, can be incorporated into our software by just modifying the files mentioned earlier.

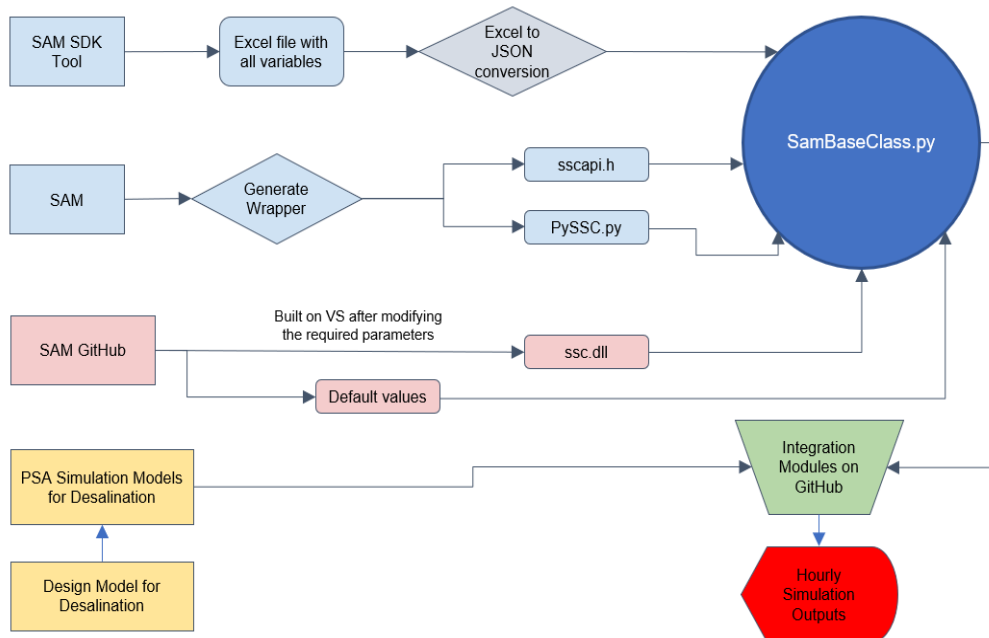


Fig. 21. Schematic of the elements and files used in the solar and desalination model integration

Each CSP or PV model can be used as a stand-alone model, or combined with one of the six financial models. All these models are integrated in a JSON structure and tested to ensure that nothing was missed

¹⁵. System Advisor Model Version 2020.2.29 (2020.2.29). SAM source code. National Renewable Energy Laboratory. Golden, CO. Accessed May 27, 2020. <https://github.com/NREL/ssc>.

in the translation. For verifying the implementation of the SAM models in our software, a number of inputs were varied to compare the outputs of the model at its source with the JSON platform¹.

6 Thermal Desalination Models

6.1 Low-Temperature Multi-Effect-Distillation (LT-MED)

Multi-effect distillation (MED) is currently the most thermodynamically efficient, commercialized thermal desalination technology. Its coupling with solar thermal energy has been intensely investigated by our partners at the Solar Desalination Unit of the Plataforma Solar de Almería (PSA). The PSA pilots include flat plate solar collectors (Fig. 16), parabolic trough concentrators (Fig. 16), and thermal storage units (Fig. 22), connected with a 14-effect MED pilot plant (Fig. 23 and 24).



Fig. 22. Solar Thermal Units at PSA



Fig. 23. Front of the MED Unit at PSA

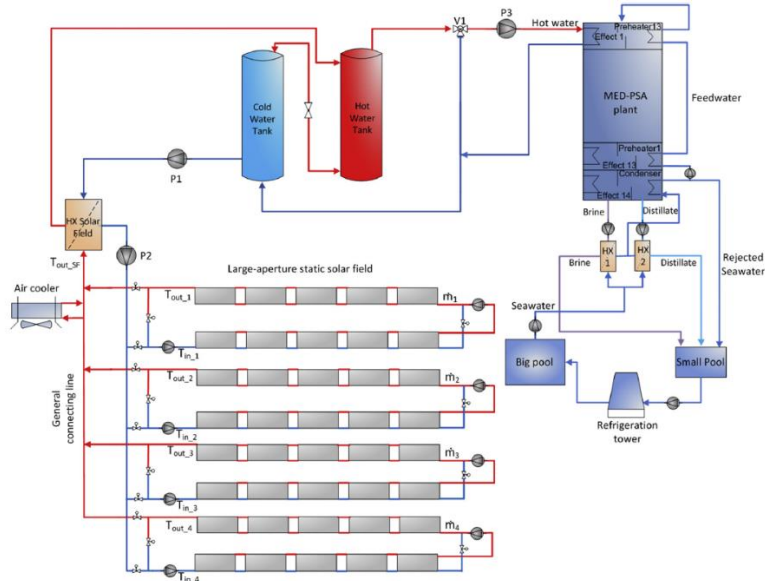


Fig. 24. Schematic diagram of the flat plate collector integrated with LT- MED system¹⁶

¹⁶ Chorak, A., Palenzuela, P., Alarcón-Padilla, D. C. and Abdellah, A. B. (2017). Experimental characterization of a multi-effect distillation system coupled to a flat plate solar collector field: Empirical correlations. *Applied Thermal Engineering*, 120, 298-313.

6.1.1 Integration of the LT-MED Model

The PSA LT-MED code model was written as a design tool using steam and feed flow rates as inputs to calculate the corresponding heat transfer area and water production. The model was changed so that steam and feed flow rates could be determined from a user-specified desalination plant capacity. This was accomplished via parametric analysis using the design model developed by PSA for a Forward-Feed Low-Temperature MED plant (FF-LT-MED). The inputs of distillate flow rate (q_D) and heating steam temperature (T_s) were changed within their ranges of applicability and polynomial equations were obtained by fitting the results from the simulation with Curve Fitting Tool in MATLAB; these were subsequently converted to Python scripts. The outputs considered are: Gain Output Ratio (GOR), the steam mass flow rate (q_s), and the feedwater mass flow rate (q_F). Different capacity and steam temperature have been considered and polynomial equations have been obtained for plants with 3,6,9,12 and 15 effects (N_{effects}).

A multivariable analysis was done by using the design model of FF-LT-MED implemented in Engineering Equation Solver, by using the MultiPolyRegress tool. The independent variables and their ranges are as follows:

- X_f (salinity of the feedwater) between 30,000 and 60,000 ppm
- RR (Recovery Ratio) between 30 and 50%
- TN (last effect vapor temperature) between 25 and 45 °C
- T_s (steam temperature entering the first effect) between 60 and 85 °C

The dependent variables are:

- GOR: Gain Output ratio
- sA : specific total area ($\text{m}^2/\text{m}^3/\text{day}$)

In all simulations, the differential temperature in the condenser and in the first preheater (the one associated to the first effect) was set as 3°C. Also, the distillate production was set at 100 m^3/day and a temperature difference between the last effect vapor temperature and the inlet seawater temperature in the final condenser was 10°C. Thus, in this model refinement, instead of using TN as a model input –as in the previous version-, we modified the equations to use the seawater temperature as the input and make the model more user-friendly.

A Normalized Root-Mean-Square Deviation (NRMSD) has been used to evaluate the fit of the regression model. Below are the polynomial equations that correlate the results of the 3-effect LT-MED model; similar correlations were developed and implemented in the SEDAT GUI for 6, 9, 12 and 15 effects.

$$GOR = a_1 X_f + a_2 RR + a_3 R R X_f + a_4 T_N + a_5 T_N X_f + a_6 T_N RR + a_7 T_s + a_8 T_s X_f + a_9 T_s RR + a_{10} T_s T_N + a_{11} + a_{12} T_s^2 + a_{13} T_N^2 + a_{14} RR^2 + a_{15} X_f^2$$

Coefficients	Value
a_1	1.60E-07
a_2	0.826895712
a_3	-2.04E-07
a_4	0.003340838
a_5	-5.56E-09
a_6	0.000666667

a_7	-0.003295958
a_8	1.17E-10
a_9	-0.000549708
a_{10}	-2.46E-06
a_{11}	2.662545127
a_{12}	-1.98E-07
a_{13}	7.41E-07
a_{14}	-0.675925926
a_{15}	-4.12E-13

The coefficients of sA are:

$$\begin{aligned}
 sA = & a_1 X_f + a_2 X_f^2 + a_3 RR + a_4 RRX_f + a_5 RRRX_f^2 + a_6 RR^2 + a_7 RR^2 X_f + a_8 T_N + a_9 T_N X_f \\
 & + a_{10} T_N X_f^2 + a_{11} T_N RR + a_{12} T_N RRRX_f + a_{13} T_N RR^2 + a_{14} T_N^2 + a_{15} T_N^2 X_f \\
 & + a_{16} T_N^2 RR + a_{17} T_s + a_{18} T_s X_f + a_{19} T_s X_f^2 + a_{20} T_s RR + a_{21} T_s RRRX_f + a_{22} T_s RR^2 \\
 & + a_{23} T_s T_N + a_{24} T_s T_N X_f + a_{25} T_s T_N RR + a_{26} T_s T_N^2 + a_{27} T_s^2 + a_{28} T_s^2 X_f + a_{29} T_s^2 RR \\
 & + a_{30} T_s^2 T_N + a_{31} + a_{32} T_s^3 + a_{33} T_N^3 + a_{34} RR^3 + a_{35} X_f^3
 \end{aligned}$$

Coefficients	Value
a_1	0.000596217
a_2	-3.66E-09
a_3	0
a_4	-2.44E-05
a_5	1.93E-09
a_6	0
a_7	5.60E-05
a_8	0
a_9	-2.95E-07
a_{10}	5.30E-11
a_{11}	0
a_{12}	7.14E-06
a_{13}	0
a_{14}	0.064807392
a_{15}	2.06E-07
a_{16}	0.00974051
a_{17}	0
a_{18}	-1.16E-05
a_{19}	-3.96E-11
a_{20}	0
a_{21}	-5.27E-06
a_{22}	0
a_{23}	-0.05718687
a_{24}	-2.61E-07
a_{25}	-0.011936049
a_{26}	-0.000702529
a_{27}	0.013464849
a_{28}	1.65E-07
a_{29}	0.003686623
a_{30}	0.000759933
a_{31}	0
a_{32}	-0.00019293
a_{33}	-0.000182949
a_{34}	0
a_{35}	3.20E-14

The NRSMD results are shown in Table 6. Since most of the errors are in the range of 0.1-3.5 % it is concluded that the regression model developed by our partners is adequately representing the results of the detailed ESS model.

Table 6. NRMSE of the outputs of the LT-MED model

Number of effects	Variable	NRMSE
3	Gain Output Ratio (<i>GOR</i>)	0.16%
	Specific area (<i>sA</i>)	1.19%
6	Gain Output Ratio (<i>GOR</i>)	0.16%
	Specific area (<i>sA</i>)	1.55%
9	Gain Output Ratio (<i>GOR</i>)	0.28%
	Specific area (<i>sA</i>)	2.25%
12	Gain Output Ratio (<i>GOR</i>)	0.45%
	Specific area (<i>sA</i>)	3.54%
15	Gain Output Ratio (<i>GOR</i>)	0.65%
	Specific area (<i>sA</i>)	6.71%

6.2 Multi-Effect-Distillation with Thermal-Vapor-Compression (MED-TVC)

A model of a TVC-MED, developed by Drs. Palenzuela, and Alarcón-Padilla, is based on the Trapani, Italy 12-effects MED desalination plant and is validated by actual performance data from this plant. The model is built in Engineering Equation Solver (EES), and it can calculate the gain output ratio (GOR) from different motive pressure and different thermo-compressor locations by operating balance equations of energy, mass, and salt of each effect (Figure 25). We converted the EES model into Python so that it will be available for public use in this open-access software and used approximations and multi-variance relationships to simplify the equations. Running of a reference case with the TVC at the last effect, produced the results with less than 1% deviation with most of the measurements from the Trapani plant, with the exception of cooling mass flow rate and number of tubes for which the results differ by 12% and 6% correspondingly. Details are shown in Section 10, Model Results Verification Analysis.

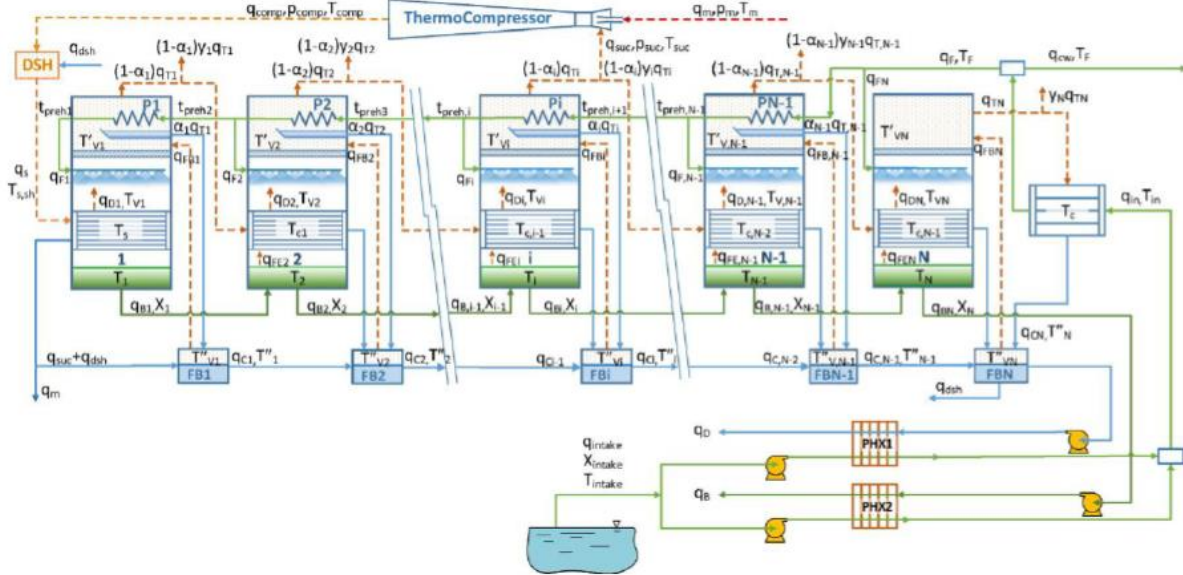


Fig. 25. Schematic of a MED-TVC plant architecture

The multivariable analysis has been done by using the design model of PC-TVC-MED implemented in Engineering Equation Solver. The tool MultiPolyRegress has been used for this analysis.

The independent variables and the range of variation are:

- X_f (salinity of the feedwater) between 30,000 and 60,000 ppm
- RR (Recovery Ratio): the highest limit of the range changes for each number of effects according to the maximum brine salinity obtained in the first effect of the MED-TVC unit for each case. Notice that for brine salinities above 120,000 ppm, the seawater properties implemented in this model are not valid. Then, the range of RR for each N is:
 - o $N=8$ effects -> RR between 30 and 40%
 - o $N=10$ effects -> RR between 30 and 40%
 - o $N=12$ effects -> RR between 30 and 40%
 - o $N=14$ effects -> RR between 30 and 38%
 - o $N=16$ effects -> RR between 30 and 37%
- T_{in} (inlet seawater temperature) between 25 and 35 °C. T_{in} lower than 25 °C are not possible due to the high Ra obtained at this case caused by the low mass flow rate of entrainment vapor that result at very low T_{in} . Higher Ra than 5-6 are not feasible because the correlation used for the thermocompressor is not valid out of this range.
- p_m (motive steam pressure entering the thermocompressor) between 4 and 45 bar (according to the steam extractions of a commercial CSP plant)
- q_D (distillate production) between 2000 and 100,000 m³/day

The dependent variables are:

- GOR: Gain Output ratio
- q_f : feedwater flow rate (m³/h)
- q_s : heating steam mass flow rate entering the first effect (kg/s)
- q_m : motive steam mass flow rate entering the thermocompressor (kg/s)

- DELTAT_effect_mean: temperature difference mean between effects (°C)

Polynomial equations have been obtained for 8, 10, 12, 14 and 16 effects:

Notice that for all simulations, the temperature of the heating steam entering the first effect (T_s) has been fixed at 70°C and the position of the thermocompressor has been established at the last effect. Also, in all simulations it has been considered that the temperature difference between T_{in} and T_N (last effect vapor temperature) is 10°C and that the temperature difference between the inlet and outlet seawater temperature in the condenser is 10°C.

The Normalized Root-Mean-Square Deviation (NRMSD) has been used to evaluate the fit of the regression models.

N= 8 effects

$$\begin{aligned} \text{Variable} = & a_1 X_f + a_2 RR + a_3 RRX_f + a_4 T_{in} + a_5 T_{in}X_f + a_6 T_{in}RR + a_7 q_D + a_8 q_D X_f + a_9 q_D RR \\ & + a_{10} q_D T_{in} + a_{11} P_m + a_{12} P_m X_f + a_{13} P_m RR + a_{14} P_m T_{in} + a_{15} P_m q_D + a_{16} + a_{17} P_m^2 \\ & + a_{18} q_D^2 + a_{19} T_{in}^2 + a_{20} RR^2 + a_{21} X_f^2 \end{aligned}$$

Variable Coefficients	GOR	q_s	q_m	ΔT_{eff_mean}
1	-1.42E-06	-7.59E-06	1.49E-05	3.44E-06
2	7.764150858	-34.3908768	-29.83707466	2.566973803
3	-1.15E-05	9.69E-06	2.86E-05	-4.53E-05
4	0.582960027	-0.131363139	-2.345398834	-0.124425745
5	1.24E-07	1.48E-07	-9.10E-07	-5.15E-08
6	0.056555556	0.200569444	0.267902778	5.52E-16
7	-2.57E-19	0.002087075	0.002171651	-3.28E-20
8	3.63E-25	-1.31E-10	4.00E-10	7.43E-25
9	3.23E-19	-0.000541286	-0.000324519	6.21E-20
10	3.04E-21	-5.70E-06	-2.78E-05	4.94E-23
11	0.104803303	-0.109758232	-0.489303064	3.99E-05
12	-2.08E-09	-3.05E-09	-7.25E-08	8.13E-10
13	0.012249322	0.000630081	0.033783875	0.000108401
14	-0.000299729	0.000228591	0.006929505	-1.90E-06
15	6.28E-22	-9.38E-08	-4.33E-06	1.32E-22
16	-5.098563697	8.029964774	43.26022001	6.962250661
17	-0.001263974	0.002098453	0.005568346	-7.49E-07
18	-3.56E-25	-2.59E-10	-1.65E-10	-1.23E-25
19	-0.005858519	0.000841111	0.035492222	-3.70E-06
20	-8.896296296	40.08888889	28.25555556	-3.014814815
21	-1.98E-11	-1.42E-12	4.56E-11	-7.42E-11

Variable Coefficients	q_f	sA
1	-0.00256597	-1.40E-05
2	-18759.69206	-1.785127142
3	0.006751389	1.65E-05
4	-0.082041658	-0.086087998
5	1.89E-06	2.85E-07
6	-0.268055556	0.027513889

7	0.240057439	1.92E-06
8	-8.51E-08	3.26E-12
9	-0.336138884	2.86E-07
10	3.40E-06	9.24E-09
11	-6.791460792	-0.011468447
12	3.61E-08	-5.61E-09
13	-0.000338753	-3.73E-05
14	0.000111789	6.36E-05
15	-6.52E-09	-6.21E-12
16	3273.041084	2.315966265
17	0.138495604	0.000180162
18	-1.79E-08	-1.92E-11
19	0.001416667	0.001250185
20	26508.05556	0.912962963
21	1.86E-09	5.25E-11

The NRSMD results are depicted in Table 7, showing that most of the errors are below 1% (just the specific area shows a higher deviation). Therefore, the regression model developed in this work shows good accuracy and concordance with the ESS model.

Table 7. NRMSE of the outputs of the MED-TVC model

Variable	NRMSE
Gain Output Ratio (GOR)	0.73%
Feedwater flow rate (q_F)	0.71%
Motive steam mass flow rate (q_m)	0.95%
Heating steam mass flow rate (q_s)	0.73%
Temperature difference mean between effects ΔT_{eff_mean}	0.00%
Specific area (sA)	11.64%

Similar correlations were derived for 10, 12, 14 and 16 effects; those are shown in the associated Python script.

6.3 Multi-Effect-Distillation with Absorption Heat Pump (MED-AHP)

Thermal vapor-compression or thermos-compression with steam ejectors classically being the heat pump configuration coupled to a MED plant. This option has been used commercially since the early seventies. A performance ratio (PR) of 16 corresponds practically to the maximum efficiency one can obtain with a MED + thermocompressor unit because a thermocompressor has a relatively low efficiency as a heat pump. Absorption heat pumps can result in higher performance ratios at the expense of the incremental cost of the heat pump.

SEDAT includes models of MED single-effect and double-effect absorption heat pumps.

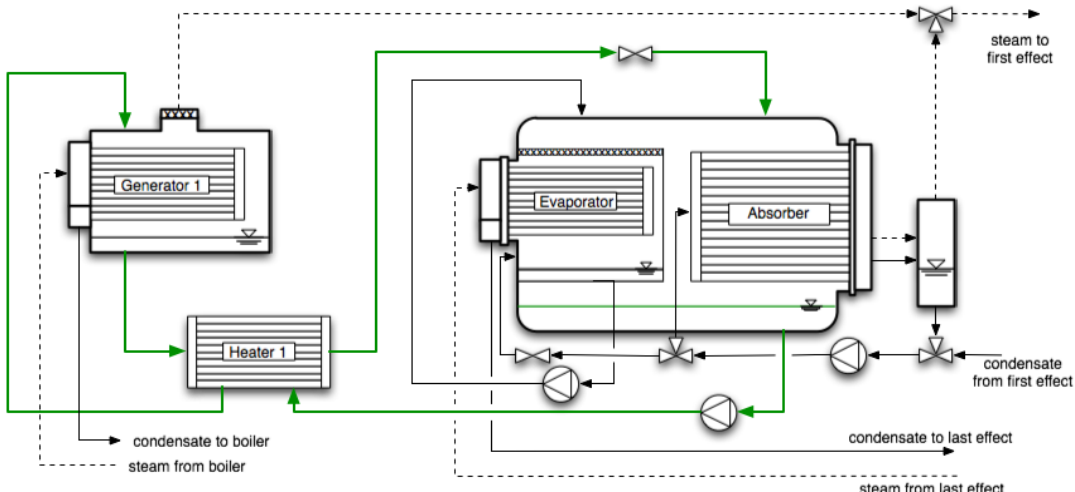


Fig. 26. Scheme of a single-effect absorption heat pump coupled to a MED unit

Figure 26 shows the scheme of coupling a single-effect absorption heat pump (SEAHP) to a MED unit. Low-pressure steam is generated in the desorption process within Generator 1, and from the exothermic absorption process that takes place within the Absorber.

In the software, the performance at the design point of an individual MED system will be calculated first, using the same algorithm as for an LT-MED system. Then we will apply the correlation equations that are described below to evaluate the effect of adding an absorption heat pump.

The thermal efficiency of a heat pump is represented by the coefficient of performance (*COP*). In air conditioning applications, the *COP* is defined as the ratio of the heat supplied at a low temperature to the Evaporator (Q_E) and the external heat supplied to the pump at Generator 1 (Q_{G1}). A typical *COP* of conventional single effect LiBr-H₂O absorption heat pumps is around 0.7.

$$COP = \frac{Q_A + Q_C}{Q_{G1}} = \frac{Q_{MED}}{Q_{G1}}$$

where Q_A is the thermal energy released in the Absorber, Q_C is the thermal energy obtained from the condensation of the steam released in Generator 1, and Q_{G1} is the thermal energy required to drive the desorption process within Generator 1. With this formulation, the typical *COP* of conventional single-effect absorption LiBr-H₂O heat pumps is around 1.7.

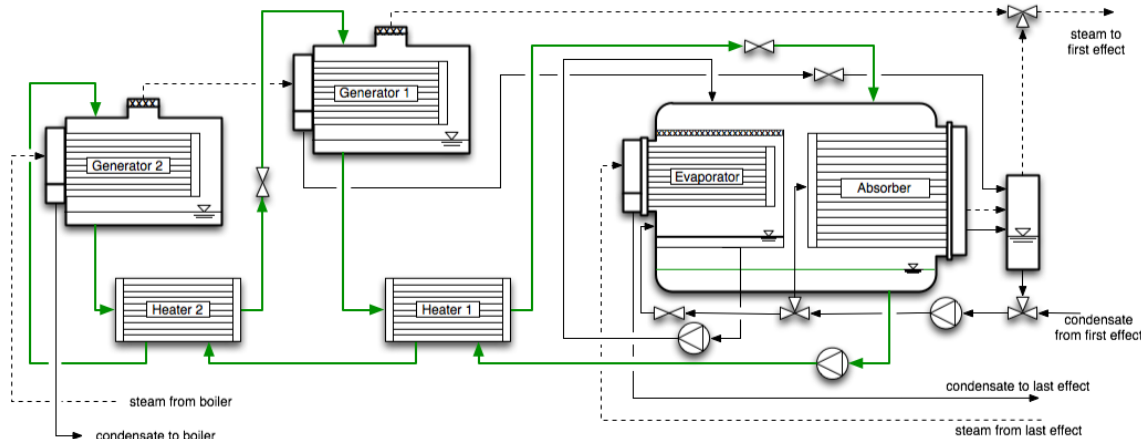


Figure 27. : Scheme of a double-effect absorption heat pump coupled to a MED unit

In a double-effect heat pump (Figure 27), the steam released in the desorption process taking place in the high-temperature generator (Generator 2), is used to drive a second desorption process within the low-temperature generator (Generator 1). Steam released from this low-temperature generator together with the steam generated from the absorption process are combined to drive the MED plant. Part of the low-pressure steam generated at the last effect of the MED is recovered by the heat pump as opposed to simply rejecting this heat to the environment as waste. The equation for the COP of a double-effect absorption heat pump for desalination applications is given by the following expression:

$$COP = \frac{Q_A + Q_{C1}}{Q_{G2}} = \frac{Q_{MED}}{Q_{G2}}$$

where Q_{C1} is the heat content of the steam released in the desorption process of the low-temperature generator. Typical COP values of conventional double-effect LiBr-H₂O absorption heat pumps are in the range of 2.2 to 2.3.

The overall thermal energy required from the solar field depends on the performance ratio (PR) of the MED plant and the COP of the absorption heat pump.

$$PR_{overall} = PR_{MED} \times COP$$

Other operational parameters can also be determined by the COP:

$$GOR_{overall} = GOR_{MED} \times COP$$

$$STEC_{overall} = \frac{STEC_{MED}}{COP}$$

GOR_{MED} : The gained output ratio of an individual MED system. It is estimated using the empirical equations derived by PSA and reported in a previous report.

$STEC_{MED}$: The specific thermal energy consumption (kWh-th/m³) of an individual MED system. It is calculated by:

$$STEC_{MED} = \frac{1}{GOR_{MED}} (h_{vsat} - h_{lsat}) \rho_{dist} \times \frac{1kWh}{3600 kJ}$$

Where h_{vsat} and h_{lsat} are the saturated steam and liquid enthalpy at the inlet steam temperature (kJ/kg), and ρ_{dist} is the density of distillate (kg/m³)

6.3.1.1 Model of single-effect MED-AHP

This section presents a set of mathematical correlations that allows estimations of the thermal performance (COP), the specific heat exchange area required for the heat pump (sA) as well as the temperature of the steam sent to the MED first effect ($T_{(s_sh)}$) together with the temperature of the external saturated steam ($T_{(s_gen)}$), required to drive the generator of the absorption heat pump (AHP).

The input parameters required for the mathematical expressions are the saturation temperature of the steam sent to the MED first effect (T_s), and the temperature of the low-pressure saturated steam coming from the end-condenser of the MED plant (T_{cond}).

The mathematical correlations were obtained from the simulation models developed and validated at PSA with the two prototypes of absorption heat pumps that were tested in STD and AQUASOL Projects. The design models include the parameters shown in the table below.

Specific solution mass flow for Generator 1 & 2	15
Heat transfer coefficient Generator 1 & 2 (kW/m ² ·°C)	0.5
Heat transfer coefficient HX 1 & 2 (kW/m ² ·°C)	0.5
Heat transfer coefficient Evaporator (kW/m ² ·°C)	2.5
Heat transfer coefficient Absorber (kW/m ² ·°C)	0.5
Min. Temp. Diff. Generator 1 – Generator 2 (°C) in DEAHP	2
Min. Temp. Diff. Absorber – Condenser 1 (°C)	2
Min. Temp. Diff. High Temp. Generator – Heat Source (°C)	10
Temp. Diff. Evaporator (°C)	2
Efficiency of solution heat exchanger 1 & 2	0.8

T_s : temperature of steam condensate at the outlet of the first effect tube bundle

T_{cond} : temperature of end condenser

Input parameters' range of validity:

$$65^{\circ}\text{C} \leq T_s \leq 85^{\circ}\text{C}$$

$$25^{\circ}\text{C} \leq T_{cond} \leq 45^{\circ}\text{C}$$

COP: Coefficient of Performance

$$\text{COP} = Q_{MED}/Q_{in}$$

where:

Q_{in} : Thermal energy input to the generator of the absorption heat pump

Q_{MED} : Thermal energy delivered from the absorber and the low temperature condenser to the MED first effect

$$COP = 0.009258 \cdot T_{cond} - 0.0082026 \cdot T_s - 0.0001356 \cdot T_{cond} \cdot T_s + 1.9532 + 5.4857 \cdot 10^{-5} \cdot T_s^2 + 7.8857 \cdot 10^{-5} \cdot T_{cond}^2$$

sA : Specific heat exchange area (m^2) of the absorption heat pump per kW of thermal energy delivered to the MED plant

$$sA = 0.1686 \cdot T_{cond} + 0.0024348 \cdot T_{cond}^2 + 4.7353 \cdot 10^{-5} \cdot T_{cond}^3 - 0.17905 \cdot T_s - 0.0085011 \cdot T_s \cdot T_{cond} - 0.00012585 \cdot T_s \cdot T_{cond}^2 - 1.4067 \cdot 10^{-6} \cdot T_s \cdot T_{cond}^3 + 0.0052416 \cdot T_s^2 + 0.00016374 \cdot T_s^2 \cdot T_{cond} + 1.7127 \cdot 10^{-6} \cdot T_s^2 \cdot T_{cond}^2 - 6.8253 \cdot 10^{-5} \cdot T_s^3 - 1.1867 \cdot 10^{-6} \cdot T_s^3 \cdot T_{cond} + 2.5029 + 3.44 \cdot 10^{-7} \cdot T_s^4 + 4.7067 \cdot 10^{-7} \cdot T_{cond}^4$$

T_{s_sh} : Outlet temperature of the superheated steam going from the absorption heat pump to the MED first effect tube bundle

$$T_{s_sh} = -0.328 \cdot T_{cond} + 1.20229 \cdot T_s - 0.008 \cdot T_{cond} \cdot T_s + 10.8171 + 0.00457143 \cdot T_s^2 + 0.00457143 \cdot T_{cond}^2$$

T_{s_gen} : Temperature of the saturated steam required to drive the absorption heat pump generator

$$T_{s_gen} = -0.736 \cdot T_{cond} + 1.808 \cdot T_s - 0.0264 \cdot T_{cond} \cdot T_s + 22.0257 + 0.012 \cdot T_s^2 + 0.0142857 \cdot T_{cond}^2$$

6.3.1.2 Model of Double-Effect MED-AHP (Serial flow)

COP : Coefficient of Performance

$$COP = Q_{MED}/Q_{in}$$

where:

Q_{in} : Thermal energy input to the generator of the absorption heat pump

Q_{MED} : Thermal energy delivered from the absorber and the low-temperature condenser to the MED first effect

$$COP = 0.002266 \cdot T_{cond} - 0.022654 \cdot T_s - 0.0003024 \cdot T_{cond} \cdot T_s + 2.8248 + 0.00014057 \cdot T_s^2 + 0.00017086 \cdot T_{cond}^2$$

sA : Specific heat exchange area (m^2) of the absorption heat pump per kW of thermal energy delivered to the MED plant

$$sA = 0.0083408 \cdot T_{cond} - 0.0097175 \cdot T_s - 0.0001152 \cdot T_{cond} \cdot T_s + 0.97403 + 5.8114 \cdot 10^{-5} \cdot T_s^2 + 7.8286 \cdot 10^{-5} \cdot T_{cond}^2$$

T_{s_sh} : Outlet temperature of the superheated steam going from the absorption heat pump to the MED first effect tube bundle

$$T_{s_sh} = -0.038 \cdot T_{cond} + 1.1574 \cdot T_s - 0.0068 \cdot T_{cond} \cdot T_s + 3.0757 + 0.0028571 \cdot T_s^2 + 0.0028571 \cdot T_{cond}^2$$

T_{s_gen} : Temperature of the saturated steam required to drive the absorption heat pump generator

$$T_{s_gen} = -0.446 \cdot T_{cond} + 1.98886 \cdot T_s - 0.0956 \cdot T_{cond} \cdot T_s + 37.9357 + 0.0417143 \cdot T_s^2 + 0.0514286 \cdot T_{cond}^2$$

6.3.1.3 Model of Double-Effect MED-AHP (Parallel Flow)

COP : Coefficient of Performance

$$COP = Q_{MED}/Q_{in}$$

where:

Q_{in} : Thermal energy input to the generator of the absorption heat pump

Q_{MED} : Thermal energy delivered from the absorber and the low temperature condenser to the MED first effect

$$COP = 0.023072 \cdot T_{cond} - 0.022487 \cdot T_s - 0.00003024 \cdot T_{cond} \cdot T_s + 2.8621 + 0.00013829 \cdot T_s^2 + 0.000168 \cdot T_{cond}^2$$

sA : Specific heat exchange area (m^2) of the absorption heat pump per kW of thermal energy delivered to the MED plant

$$sA = 0.0067028 \cdot T_{cond} - 0.0058181 \cdot T_s - 3.128 \cdot 10^{-5} \cdot T_{cond} \cdot T_s + 0.80108 + 4.5714 \cdot 10^{-6} \cdot T_s^2 + 2.7771 \cdot 10^{-5} \cdot T_{cond}^2$$

T_{s_sh} : Outlet temperature of the superheated steam going from the absorption heat pump to the MED first effect tube bundle

$$T_{s_sh} = -0.216 \cdot T_{cond} + 1.376 \cdot T_s - 0.0032 \cdot T_{cond} \cdot T_s - 1.4743 + 8.7818 \cdot 10^{-17} \cdot T_s^2 + 0.0022857 \cdot T_{cond}^2$$

T_{s_gen} : Temperature of the saturated steam required to drive the absorption heat pump generator

$$T_{s_gen} = -0.468 \cdot T_{cond} + 1.15086 \cdot T_s - 0.1136 \cdot T_{cond} \cdot T_s + 70.5714 + 0.0537143 \cdot T_s^2 + 0.0657143 \cdot T_{cond}^2$$

6.4 Membrane Distillation (MD)

MD is driven by a vapor pressure difference at two sides of a microporous hydrophobic membrane. The difference in vapor pressure is typically achieved by the temperature difference between the hot feedwater and cooler condensate sides. This technology has been thoroughly studied at the pilot scale at the Plataforma Solar de Almeria and we have implemented the latest advances as they are reported by Zaragoza and co-workers at PSA. In addition, we implemented

a model of a solar flat plate collector developed by Alarcon-Padilla, PSA in simulations of MD powered by low temperature heat from a solar collector (Figure 28).

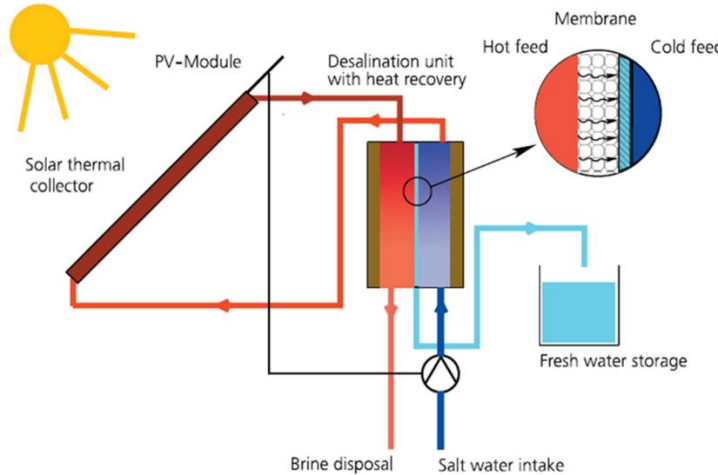


Fig. 28. Schematic diagram of the flat plate collector and MD system

The distillate water production is estimated from the thermal energy provided by the solar field. For LT-MED system, the nominal required thermal energy (P_{req} , kW) is calculated from the gained output ratio (GOR), which is assumed to be 10 in this case.

$$P_{req} = \frac{1}{GOR} \times Capacity \times (h_{vsat} - h_{lsat}) \times \rho_{dist} \times \frac{1}{24 \times 60 \times 60}$$

$$M_{d_rel} = -0.23064P_{rel}^2 + 1.4384P_{rel} - 0.184$$

M_{d_rel} : Distillate water production relative to nominal production rate (%)

P_{rel} : Thermal load relative to nominal thermal energy consumption (%)

For AGMD system, two types of modules (AS26C7.2L and AS7C1.5L) from Aquastill were selected for our modeling. The following equations were derived from PSA's experimental data to estimate the permeate flux (P_{flux} , $l/h \cdot m^2$) and the specific thermal energy consumption (STEC, kWh/m^3):

AS7C1.5L:

$$P_{flux} = 1.487 + 1.348 \cdot TEI + 1.969 \cdot F - 0.477 \cdot TCI - 0.235 \cdot FeedC + 0.519 \cdot TEI \cdot F - 0.515 \cdot F^2$$

AS26C7.2L:

$$P_{flux} = 5.155 + 0.398 \cdot TEI + 0.696 \cdot F - 0.168 \cdot TCI - 0.214 \cdot FeedC + 0.139 \cdot TEI \cdot F - 0.105 \cdot TCI \cdot F - 0.129 \cdot F^2$$

TEI : Evaporator inlet temperature ($^{\circ}C$), the nominal value is 80 $^{\circ}C$

TCI : Condenser outlet temperature ($^{\circ}C$), the nominal value is 25 $^{\circ}C$

F : Feed flow rate (l/h), the value is optimized to 582.7 l/h to maximize P_{flux} while minimizing STEC

Zaragoza et al. developed empirical equations for simulating the performance of the Aquastill V-AGMD (vacuum air-gap membrane distillation) pilot plant, their best performing MD system so far. A schematic of this pilot is shown in Fig. 29. Its performance was compared with AGMD system with the same modules, which include AS7C1.5L and AS26C2.7L, with an effective membrane area of 7.2 m^2 and 25.9 m^2 respectively. Both modules have spiral-wound geometry, and the membrane material is the same for both, made of low-density polyethylene. AS7 has 6 spiral envelopes, while AS26 has 12 envelopes. The

differences in the number of channels and their lengths lead to different residence times, which in AS26 module is 3.6 times longer than that in AS7 module.

The Zaragoza et al. model is based on their actual testing at PSA¹⁷; the fit of the model results to the field measurements is shown in Section 10, Verification of Model Results. The model is based on empirical equations applicable for a feed salinity range of 35 g/L to 105 g/L, while the pilot-plant investigation of the AGMD and V-AGMD systems took place at an extended feed salinity range i.e., 35 g/L to 292 g/L. Fig. 30a and 30b show the advantages of V-AGMD and AGMD in terms of water production and thermal energy consumption over a large range of feed salinity.

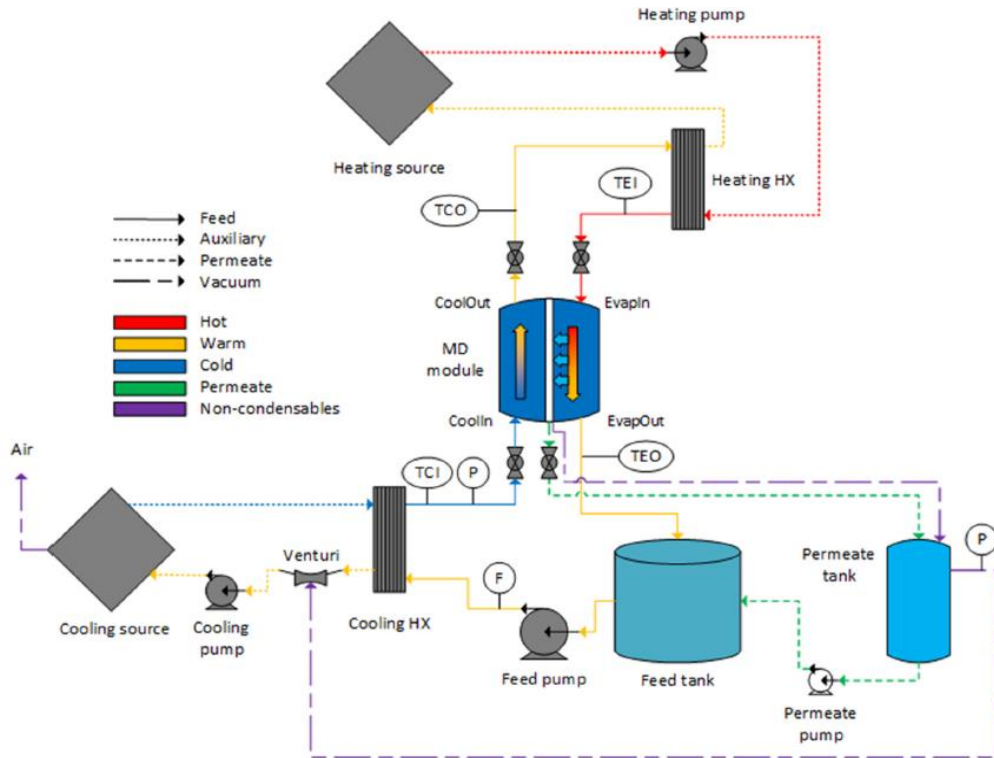


Fig. 29. Layout of the Aquastill V-AGMD system¹

¹⁷ Andrés-Mañas, J. A., Ruiz-Aguirre, A., Acién, F. G., & Zaragoza, G. (2020). Performance increase of membrane distillation pilot scale modules operating in vacuum-enhanced air-gap configuration. *Desalination*, 475, 114202.

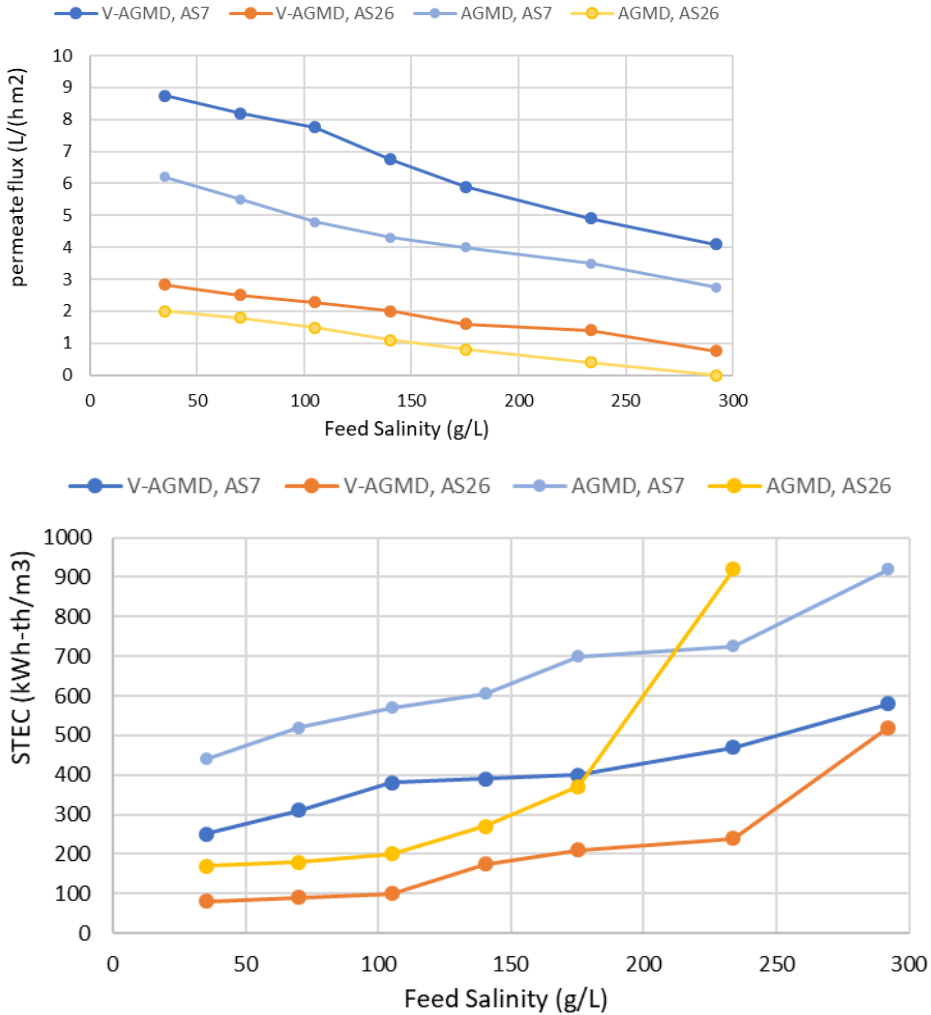


Fig. 30. Comparative results of (a) permeate flux and (b) STEC in experiments of AGMD and V-AGMD. (Feed flow rate = 1100 l/h, inlet evaporator temperature=80 °C, inlet condenser temperature = 25 °C)

As shown in these figures, the shorter residence time VAGMD, AS7 module exhibits the highest permeable flux (PF) whereas the VAGMD, AS26 module shows the best (lowest) STEC. It appears that the reason for this is that for the same driving force (vapor pressure), it's harder for a vapor flux to take place through the membrane with larger residence time.

For the thermal energy consumption, theoretically the $\text{STEC} = Q_{\text{th}}/V$ water, is proportional to the evaporator inlet temp (TEI) minus the condenser outlet temp (TCO), where TEI is fixed at 80 deg C (parameters shown in Fig. 29). As shown, TCO for AS26 would be larger than that for AS7, when TCI (condenser inlet temp) is the same, considering a longer heat exchange delta T. So the total thermal energy consumption is actually 3 times larger in AS7 than AS26. Even with a higher Pflux, the STEC for AS7 is still larger.

6.5 Batch Vacuum Air-Gap Membrane Distillation (V-AGMD) Models

Batch MD pilot experiments at Plataforma Solar de Almería (PSA) by the Zaragoza team, employed the Aquastill modules AS7C1.5L and AS26C2.7L. Models of those systems were developed applying a Box-Behnken design of experiments and were tested and validated under multiple stationary operating conditions.

The system shown in Figure 31 works in recirculation. There is a permeate tank that releases intermittently (every 3,22 litres); this was used as discretization interval for the batch model, since it would be more physically adequate than employing equal time increments.

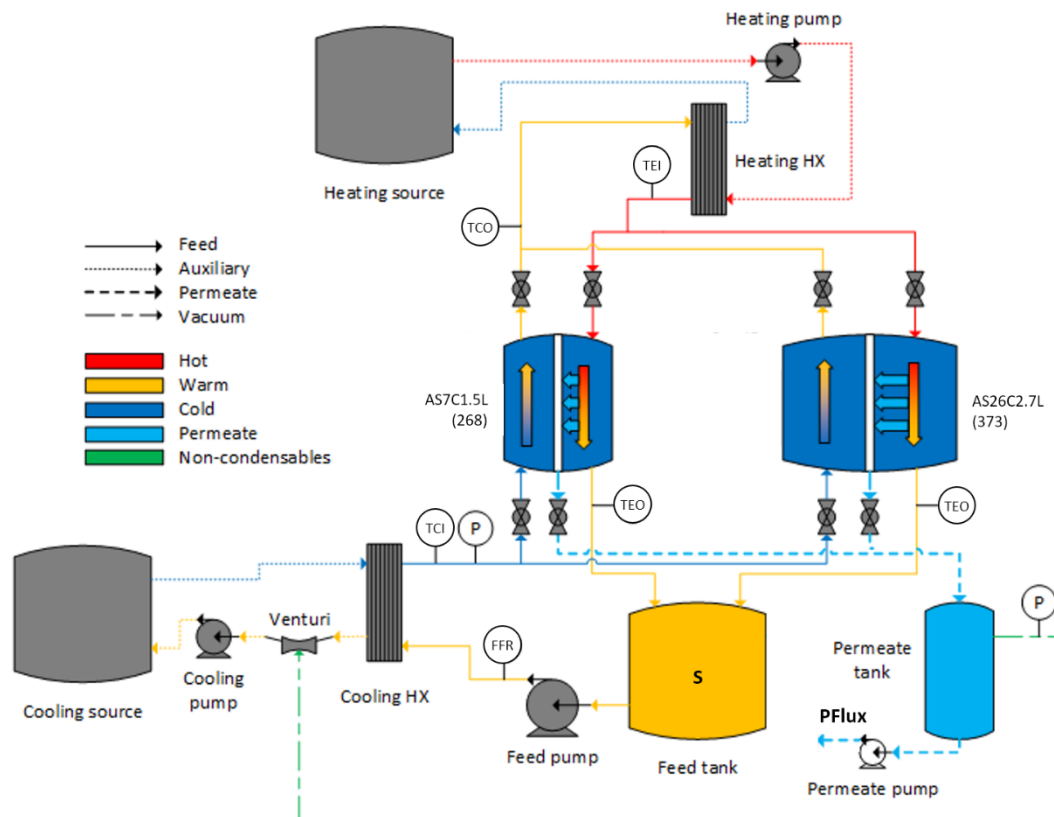


Fig. 31. Schematic of the MD-Batch-MD pilot plant at the PSA field-test facility.

The experiments allow to simulate the permeate productivity (PFlux), the outlet temperature of the feed stream that circulates through the evaporation channels (TEO), and the outlet temperature of the feed stream that circulates through the cooling channels of the module (TCO), which is used to calculate the thermal energy consumption. Batch MD operation is performed in a single recirculation step from an initial feed volume, taking as inputs the inlet temperature of the feed into the evaporation channels (TEI), the feed flow rate (FFR), the inlet temperature of the feed into the cooling channels (TCI), and the initial feed salinity (S). Based on the TCO, the model estimates the thermal power (ThPower) and the thermal efficiency, that is given commonly in thermal desalination by the specific thermal energy consumption (STEC) and, alternatively, by the gained output ratio (GOR). Valid ranges of operating conditions are $60 \text{ }^{\circ}\text{C} \leq \text{TEI} \leq 80 \text{ }^{\circ}\text{C}$; $20 \text{ }^{\circ}\text{C} \leq \text{TCI} \leq 30 \text{ }^{\circ}\text{C}$; $400 \text{ l/h} \leq \text{FFR} \leq 1100 \text{ l/h}$. The allowed range of feed salinity (S) is $35 \text{ g/l} \leq S \leq 175.3 \text{ g/l}$ for module AS7C1.5L(268) and $35 \text{ g/l} \leq S \leq 105 \text{ g/l}$ for module AS26C2.7L(373).

To develop the models, TEI, FFR and TCI are considered constant throughout the duration of the treatment. In addition, full mixing in the feed tank is considered, without temperature or concentration gradients, and feed losses through the permeate channels are supposed negligible. When the code is executed, the user is asked for the required inputs to carry out the simulation. The module to be simulated, the initial feed salinity, and the recovery ratio (RR) to be achieved will be specified. The software asks subsequently for the initial batch volume and the operating conditions, i.e., TEI, FFR and TCI. With all the required inputs, the simulation begins automatically, taking a constant permeate volume of 3.22 litres as the discretization interval of the process. This corresponds to the volume that the permeate tank discharges from the Aquastill unit during the operation. Permeate discharge is carried out discontinuously by means of a system that allows to maintain the vacuum level within the modules, even when the permeate tank is opened to the outside. By choosing this volume, the discretization is done in more physically similar intervals regarding the operation than if a constant time was chosen.

First of all, PFlux is calculated, and then the treatment time (t), the permeate flow rate (PFR) and the current RR, using the membrane area (A) of the simulated module. Subsequently, TEO and TCO are calculated for the current iteration with the model equations, and from them the mean logarithmic temperature difference (ATml), the thermal power (ThPower), the temperature in the feed tank (T_{tank}), the thermal energy per iteration (ThEnergy) and accumulated (AccThEnergy), the cooling power (CPower), the cooling energy per iteration (CEnergy) and accumulated (AccCEnergy), and the typical thermal performance indicators in thermal desalination: Gained Output Ratio (GOR) and Specific Thermal Energy Consumption (STEC). The equations of the model are solved iteratively until the target Recovery Rate given by the user at the beginning of the execution is reached, and a table with the results of each iteration is presented to the user.

Below are the equations describing the results of the Batch-VAGMD pilot with Aquastill modules in the PSA testing site.

Equation 1 is used to calculate the responses PFlux and TCO for S ≤ 157.6 g kg⁻¹ for module AS7, and S ≤ 128.4 g kg⁻¹ for module AS26.

$$R = a_0 + a_1 \cdot TEI_n + a_2 \cdot FFR_n + a_3 \cdot TCI_n + a_4 \cdot S_n + a_5 \cdot TEI_n \cdot FFR_n + a_6 \cdot TEI_n \cdot TCI_n + a_7 \cdot TEI_n \cdot S_n + a_8 \cdot FFR_n \cdot TCI_n + a_9 \cdot FFR_n \cdot S_n + a_{10} \cdot TCI_n \cdot S_n + a_{11} \cdot TEI_n^2 + a_{12} \cdot FFR_n^2 + a_{13} \cdot TCI_n^2 + a_{14} \cdot S_n^2 + a_{15} \cdot FFR_n^3 \quad (1)$$

where the response "R" can be either PFlux (permeate flux) or TCO (condenser channels outlet temperature). Operating variables "V" are TEI (evaporation channels inlet temperature), FFR (feed flow rate), TCI (condenser channels inlet temperature), and S (feed salinity). Subindex "n" means normalized variable, being -1 the minimum value of those variables and 1 the maximum. Normalizing coefficients for each operating variable "V" are calculated with Equation 2; coefficients "n_i" are given in Table 2.

$$V_n = n_0 + n_1 \cdot V + n_2 \cdot V^2 \quad (2)$$

Table 2. Variables of the batch-MD model

Variable	TEI	FFR	TCI	S
n ₀	-5.6849	-1.5846	-4.2770	-1.4933
n ₁	0.0706	0.0010	0.1755	0.0147
n ₂	0.0002	1.1967·10 ⁻⁶	-0.0002	5.6151·10 ⁻⁶

The coefficients “ a_i ” used in Equation 1 within the aforementioned salinity range are shown in **Error! Reference source not found.7**.

Table 7. Parameters corresponding to the Coefficients of Eqn. 1

Term	Coefficient	AS7		AS26	
		PFlux [$\text{I h}^{-1} \text{m}^{-2}$]	TCO [$^{\circ}\text{C}$]	PFlux [$\text{I h}^{-1} \text{m}^{-2}$]	TCO [$^{\circ}\text{C}$]
Intercept	a_0	4.83	58.82	1.49	66.33
TEI _n	a_1	1.37	8.80	0.40	9.52
FFR _n	a_2	1.92	-2.07	0.70	-0.73
TCl _n	a_3	-0.57	1.63	-0.18	0.48
S _n	a_4	-0.64	-0.91	-0.22	-0.43
TEI _n · FFR _n	a_5	0.40	-0.54	0.14	-0.24
TEI _n · TCl _n	a_6	0	0	0	0
TEI _n · S _n	a_7	0	-0.25	0	0
FFR _n · TCl _n	a_8	0	0.40	-0.11	0
FFR _n · S _n	a_9	0	-0.15	0	0
TCl _n · S _n	a_{10}	0	0.10	0	0
TEI _n ²	a_{11}	0	0	0	-0.52
FFR _n ²	a_{12}	-0.59	0.70	-0.13	0
TCl _n ²	a_{13}	0	0	0	0
S _n ²	a_{14}	0	-0.30	0	0
FFR _n ³	a_{15}	0	-0.56	0	0
AdjR ²		0.9943	0.9985	0.9979	0.9975

If $S > 157.6 \text{ g kg}^{-1}$ in the case of module AS7, or $S > 128.4 \text{ g kg}^{-1}$ in the case of module AS26, Equation 3 must be applied, and no normalization of variable S is necessary. In this salinity range, TEI, FFR and TCI are fixed to 80 °C, 1100 l h^{-1} , and 25 °C, respectively.

$$R = b_0 + b_1 \cdot S \quad (3)$$

where “R” can be either PFlux or TCO. Coefficients “ b_i ” used in Equation 3 are given in **Error! Reference source not found.8**.

Table 8. Parameters corresponding to the Coefficients of Eqn. 3

Term	Coefficient	AS7		AS26	
		PFlux [$\text{I h}^{-1} \text{m}^{-2}$]	TCO [$^{\circ}\text{C}$]	PFlux [$\text{I h}^{-1} \text{m}^{-2}$]	TCO [$^{\circ}\text{C}$]
Intercept	b_0	9.66	67.16	3.20	76.13
S	b_1	-0.02	-0.02	-0.01	-0.02
AdjR ²		0.9923	0.9952	0.9926	0.9935

The empirical results from Table 7 and 8 are imported to the equations listed in Table 9 to determine the system performance.

Table 9. Parameters calculated in the model execution and their initial values.

	Unit	Initial value
$PFR(t) = PFlux(t) \cdot A$	l/h	$PFR(t = 0)$
$PermV(t) = PFR(t - 1) \cdot \Delta t$		0
$AccPermV(t) = PermV(t) + AccPermV(t - 1)$	m^3	0
$FeedV(t) = FeedV(t - 1) - PermV(t)$	m^3	$FeedV(t = 0)$
$S(t) = \frac{S(t - 1) \cdot FeedV(t - 1)}{FeedV(t)}$		$S(t = 0)$
$RR(t) = 100 \cdot \left(1 - \frac{S(t)}{S(t = 0)}\right)$	%	0
$T_{tank}(t) = \frac{FFR \cdot \Delta t \cdot TEO(t - 1) + FeedV(t - 1) \cdot TCI}{FeedV(t - 1) + FFR \cdot \Delta t}$	$^{\circ}C$	TCI
$\Delta T_{ml}(t) = \frac{(TEI - TCO(t)) - (TEO(t) - TCI)}{\ln \left(\frac{TEI - TCO(t)}{TEO(t) - TCI} \right)}$	$^{\circ}C$	$\Delta T_{ml}(t = 0)$
$ThPower(t) = FFR \cdot \rho_f(t) \cdot C_{pf}(t) \cdot (TEI - TCO(t))$	kW_{th}	$ThPower(t = 0)$
$ThEnergy(t) = ThPower(t - 1) \cdot \Delta t$	kWh_{th}	0
$AccThEnergy(t) = ThEnergy(t) + AccThEnergy(t - 1)$	kWh_{th}	0
$CPower(t) = FFR \cdot \rho_f(t) \cdot C_{pf}(t) \cdot (T_{tank}(t) - TCI)$	kW_{th}	$CPower(t = 0)$
$CEnergy(t) = CPower(t - 1) \cdot \Delta t$	kWh_{th}	0
$AccCEnergy(t) = CEnergy(t) + AccCEnergy(t - 1)$	kWh_{th}	0
$GOR(t) = \frac{AccPermV(t) \cdot \rho_p(t) \cdot \Delta H_V(t)}{AccThEnergy(t)}$	-	Undefined
$STEC(t) = \frac{AccThEnergy(t)}{AccPermV(t)}$	kWh_{th}/m^3	Undefined

6.6 Forward Osmosis (FO) Model

The forward osmosis (FO) model implemented in SEDAT was provided by Trevi Systems Inc. one of the DOE desalination award recipients that majorly contributed in the SEDAT development. The Trevi System's FO system relies on a bi-phasic synthetic polymer draw agent that is either a hydrophilic liquid or a

hydrophobic liquid depending on temperature. In its' hydrophilic state, this agent draws water across a semi-permeable membrane by osmotic pressure. Once the draw has been diluted by the fresh water crossing the FO membrane, the draw mixture is heated, causing it to become hydrophobic and release water. The water and draw polymer are separated in a traditional "oil/water" coalescer, and a polishing nano-filtration (NF) membrane further purifies the product stream by removing stray polymer. At the technical heart of the system, two counter-flow heat exchangers recover process heat from both the draw and purified water streams – transferring heat directly to the dilute draw as it exits the osmosis membrane cartridges.

Trevi also provided us with an Excel-based model of their prototype that includes details of the heat exchanges. A schematic of this model is shown in Figure 32.

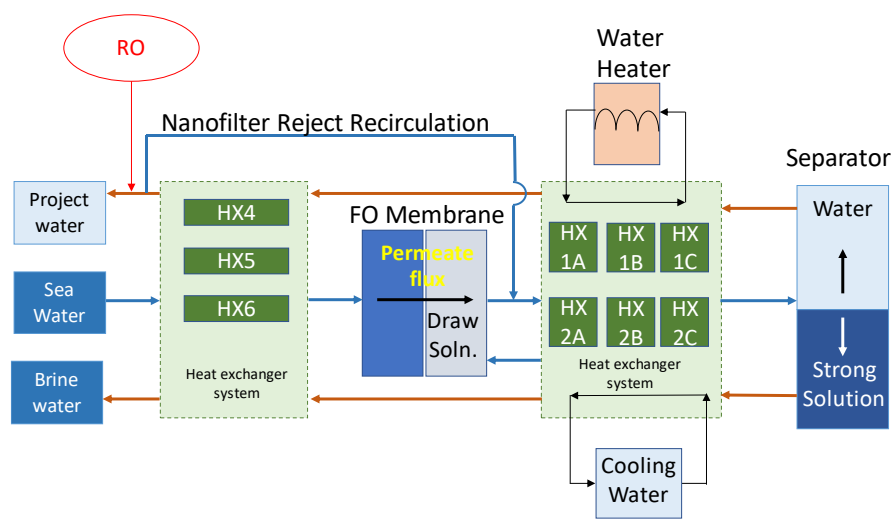


Fig 32. Simplified schematic of mass flows in the Trevi Systems FO prototype

hot coalesce concentrate and product streams, and finally heated to regeneration temperature by passing through a waste heat exchanger. NF permeate is the desalination unit product water. The NF brine stream is a warm stream containing the NF-rejected draw solution polymer. It is recirculated and combined with cold dilute draw solution downstream of the FO membrane. In case that FO is coupled with RO, the RO permeable can be treated with the NF system to remove boron. The inputs and outputs to this system are summarized in Table 10.

Table 10. Trevi FO model inputs/outputs

Inputs			Outputs
Water/draw properties	Operational parameters	System size	
Seawater temperature	NF recirculation rate	Product water flowrate	Flow temperature
Seawater salinity	RO reject rate		Flowrate
Draw Properties	Operation temperature, purity		Heat load in HXs

The FO membrane separates the feed seawater using the concentrated draw solution. FO brine exits the FO membrane module and is discharged after heat recovery and chemical neutralization. The diluted draw solution is circulated through heat exchangers to the coalesce and the draw solution polymer is separated. In detail, the diluted draw solution is first pre-heated with

Trevi reported costs of their 500 m³/day demonstration pilot project in Hawaii and based on those they estimated that a scaled-up 10,000 m³/day plant could offer a LCOH of 0.96 cents/kWh, and a LCOW of 0.52 \$/m³. In their Masdar pilot Trevi measured thermal energy consumption in the range of 135-180 MJ/m³ (37.5-50 kWh/m³) and 1.5-1.9 kWh/m³ for electricity. In their proposed 10,000 m³/day plant - scaling up from a pilot in Hawaii, they estimate the thermal energy consumption to be 30 kWh/m³, and the electrical energy consumption is 1 kWh/m³. An Excel-based mathematical model of the pilot plants was provided by Trevi Systems and we converted it to Python. Table 11 and 12 show that the results from running the model in our platform were identical to those of the source models.

Table 11. Verification of the results of the Trevi FO model (based on a 1 m³/day pilot)

Variables	Excel model	Python model	Difference
Hot side heat load in draw/seawater HX4 (kW)	0.1663	0.1663	0.0%
Cold side heat load in draw/seawater HX4 (kW)	-0.171	-0.171	0.0%
Approach temperature in draw/seawater HX4 (°C)	5.3608	5.3608	0.0%
Hot side heat load in draw/hotwater HX2C (kW)	0.8843	0.8843	0.0%
Cold side heat load in draw/hotwater HX2C (kW)	-0.9728	-0.9728	0.0%
Approach temperature in draw/hotwater HX2C (°C)	5.2811	5.2811	0.0%
Hot side heat load in draw/draw HX1B (kW)	3.6589	3.6589	0.0%
Cold side heat load in draw/draw HX1B (kW)	-3.0271	-3.027	0.0%
Approach temperature in draw/draw HX1B (°C)	4.996	4.996	0.0%

Table 12. Verification of the results of the Trevi FO model (for the 500 m³/day pilot in Hawaii)

Variables	Excel model	Python model	Difference
Hot side heat load in draw/seawater HX4 (kW)	83.16	83.16	0.0%
Cold side heat load in draw/seawater HX4 (kW)	-85.49	-85.49	0.0%
Approach temperature in draw/seawater HX4 (°C)	5.3608	5.3608	0.0%
Hot side heat load in draw/hotwater HX2C (kW)	442.13	442.13	0.0%
Cold side heat load in draw/hotwater HX2C (kW)	-486.38	-486.38	0.0%
Approach temperature in draw/hotwater HX2C (°C)	5.2811	5.2811	0.0%
Hot side heat load in draw/draw HX1B (kW)	1829.44	1829.44	0.0%
Cold side heat load in draw/draw HX1B (kW)	-1790.12	-1790.12	0.0%
Approach temperature in draw/draw HX1B (°C)	4.996	4.996	0.0%

Generalization of Trevi's FO model: We converted from Excel to Python and generalized a Trevi FO desalination model designed for seawater desalination at constant temperature and specific draw solution; a schematic of the revised model is shown in Fig. 33. The model's functionality was enhanced to

simulating different feed salinities, feed water temperatures, system capacities and draw solution properties.

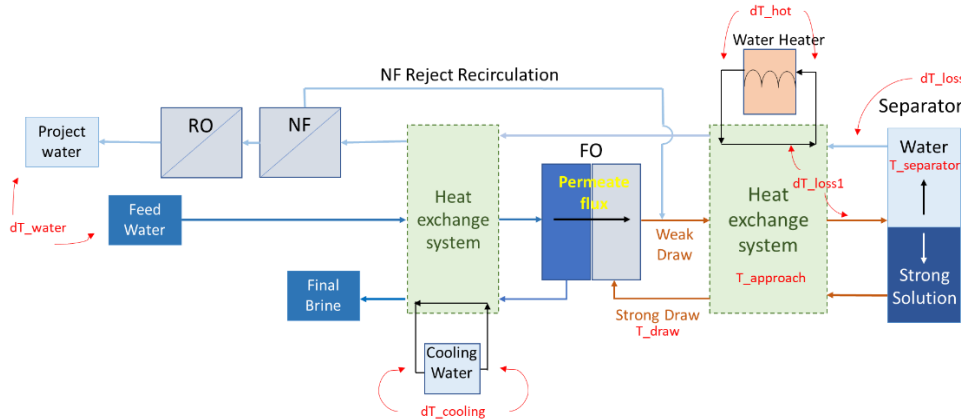


Fig. 33. Schematic of the Trevi FO desalination prototype

Our enhancements of the model included the following:

Generalizing design inputs: Introduced design parameters to significantly reduce the number of operational parameters and make the model friendlier to the user and more dynamic with fewer input variables. These parameters are shown in Table 13.

Table 13. New Operational Parameters in the FO Model

New operational parameters	Default values
Temp. of the draw solution entering the membrane system (T_{draw})	20 °C
Temp. difference between the inlet/outlet supplemental seawater ($dT_{cooling}$)	6 °C
Temp. difference between the feed and produced water (dT_{water})	10 °C
Operational temperature of separator ($T_{separator}$)	90 °C
Temp. loss in the separator (dT_{loss2})	1 °C
Temp. difference between hot water and solution entering the separator (dT_{loss1})	3 °C
Temp. difference between inlet and outlet hot water (dT_{hot})	10 °C
Approach temperature at HX 1C and 2C ($T_{approach}$)	5.28 °C

These variables should be determined by the user demand and the properties of draw solution, and they help to determine the solution temperature within the heat exchangers.

Coding Variable Dependencies: We also identified dependencies among variables and created solvers to further reduce the number of model variables. These solvers include:

- Membrane temperature solver (function `T_memb_solver` in the Python code):

This solver optimizes the strong draw solution flowrate and the brine temperature, so that the heat balance in the membrane system and HX 4&5 converge. It helps determine the solution properties entering HXs downstream.

- Membrane delta_T solver (function `find_deltaT` in the Python code):

It's a solver embedded in the first solver that estimates the heat transferred to weak draw and outgoing brine at the membrane, and thus determine the delta_T.

- Approach temperature solver (function `T_app_solver` in the Python code):

This solver is designed to determine the solution temperature within a certain HX, given the designed approach temperature.

Fig. 34 shows the simulated STEC (specific thermal energy consumption) of the system with different seawater temperature, feed salinity and recovery rate. We noticed that STEC increases as the seawater temperature increases. The reason is that the brine osmotic pressure increases as its temperature increases (a function of inlet seawater temperature). It results in a higher minimum osmotic pressure for the draw solution, and the draw solution cannot be diluted as much. As a consequence, more draw solution needs to be circulated for a certain amount of water production, thus the STEC increases.

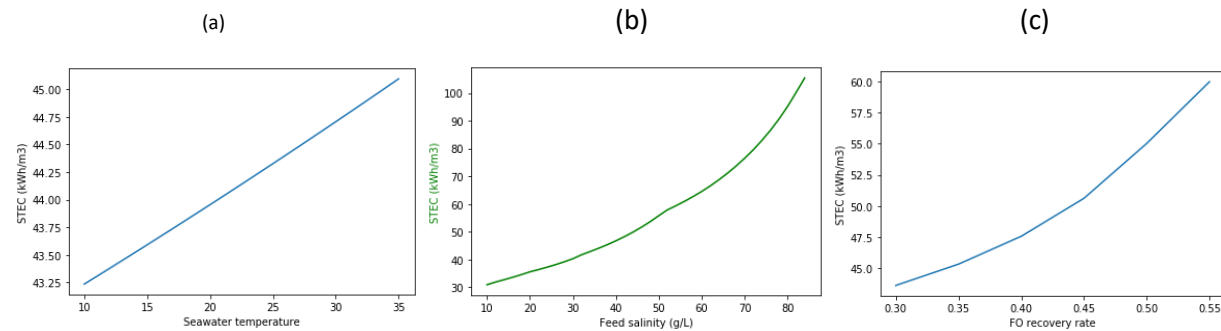


Fig. 34. System STEC varies with temperature (a) -salinity fixed as 35g/L-, (b)feed salinity feedwater temperature fixed as 15 °C and recovery rate at 30% and (c) recovery rate –at constant temperature and salinity

6.7 Estimation of Cooling Water Requirements for Thermal Desalination

We established the algorithm of estimating the required cooling water flow rate of MED-based desalination technology.

Assuming a 15% loss of the thermal energy, we have the following energy balance in the system:

$$85\%Q_{MED} = m_b h_b + m_d h_d + m_{cool} h_{cool} - m_{sw} h_{sw}$$

Also, we have the mass balance:

$$m_{sw} = m_f + m_{cool}$$

$$m_f \times RR = m_d$$

Where,

Q_{MED} : Required thermal energy for the MED system (kJ)

m_b : Brine mass flow rate (kg/hr)

m_d : Distillate mass flow rate (kg/hr)

$m_{cooling}$: Cooling water mass flow rate (kg/hr)

m_{sw} : Seawater mass flow rate (kg/hr)

m_f : Feed water mass flow rate (kg/hr)

RR: Recovery rate

h : Specific enthalpy of the corresponding fluid (kJ/kg)

The temperature relationship established for the configuration implemented in the system is:

$$T_d = T_{cond} = T_{sw} + 10$$

The mass flow rate will be calculated and reported in the design results of the software.

7 Pressure-Driven Desalination Models

7.1 Reverse Osmosis (RO)-multiple pass model

In most applications, seawater reverse osmosis (RO) can produce potable water at costs lower than thermal desalination such as MED. However, the product water from RO would contain total dissolved solids (TDS) in the range of 200-500 mg/L, whereas MED produces distilled water which is needed for emerging electrolytic hydrogen generation. RO may also produce high purity water if additional passes are implemented and/or the desalination unit is complimented with ion-exchange units in series. Thus, for enhancing the applicability of our software, we modelled RO systems with multiple passes of RO and compared those, based on LCOW, with thermal technologies. Fig. 35 shows the configuration of multi-pass RO, where the permeate water from the first pass will be fed to the following passes. The final permeate can reach a concentration less than 1 mg/L.

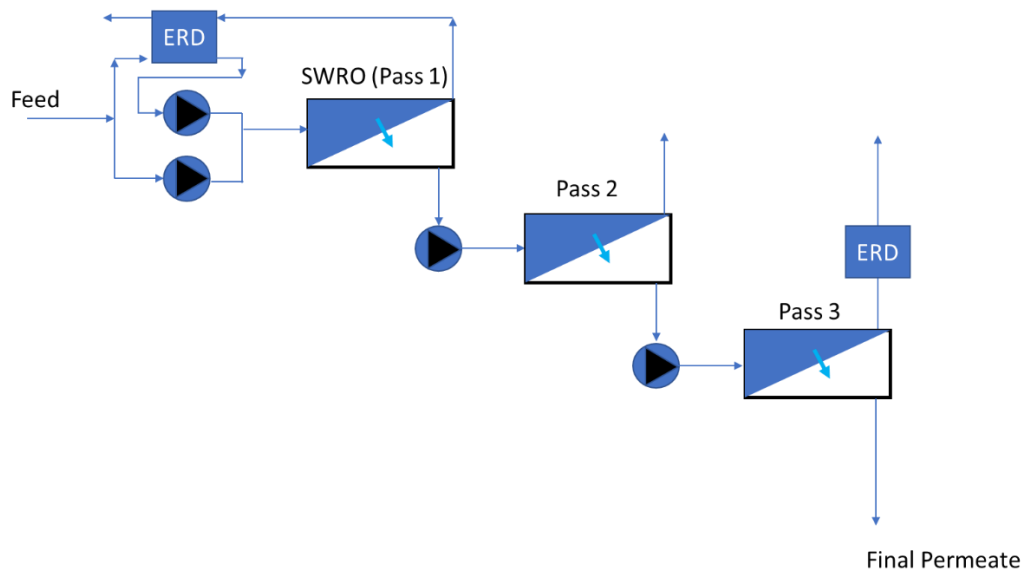


Fig. 35. Multiple-pass RO configuration implemented in the GUI

To estimate the RO system cost with multi-passes, we analyzed the EPC costs of 329 SWRO plants of various capacities from the GWI dataset (Global Water Intelligence, 2019). Subsequently, we developed the following correlations between EPC cost and system capacity, for the first pass RO (SWRO) and the following passes RO.

$$SWRO_EPC(\$/m^3/day) = 3726.1 \times Capacity^{-0.071}$$

$$Additional_RO_EPC(\$/m^3/day) = 808.39 \times Capacity^{-0.017}$$

The user also has the option to add an IX (Ion exchanger) component if needed for further permeable water purification. A fixed operational cost of 0.145 \$/m³ is applied for IX.¹⁸

7.2 Osmotically-Assisted Reverse Osmosis (OARO)

As reported in the previous quarterly report, we developed three models of new, enhanced RO technologies, which are likely to compete for brine concentration and ZLD applications. With thermal desalination technologies. This work is described in a paper in press in the journal *Desalination Pathways for minimal and zero liquid discharge with enhanced reverse osmosis technologies: module-scale modeling and techno-economic assessment*¹⁹. It was determined that osmotically assisted RO (OARO), which is the most tested among the three technologies, is also the best among the three in terms of performance for treating brines and high salinity waters, and therefore, we implemented an optimization code that we developed for this technology into our GUI.

Figure 36 shows a simplified schematic of the OARO model.

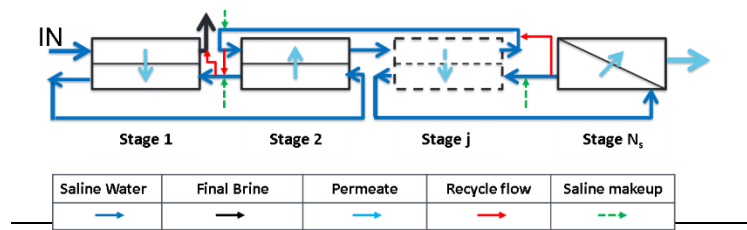


Fig. 36. Configuration of an OARO system. Modules with dashed lines indicate a repeating unit, denoted as stage *j*. The final stage is denoted as *N_s*.

Figure 36 shows the total specific energy consumption (SEC) and breakdown for each stage in OARO. The total SEC for desalinating a 70 g/L feed at 75% recovery rate, is 10.3 kWh/m³; the energy consumption is related to the feed pressure and mass flow rates throughout the system. The high-pressure pump for the conventional RO stage is the highest contributor to the SEC for OARO.

¹⁸ <https://frtr.gov/matrix2/section4/4-49.html>

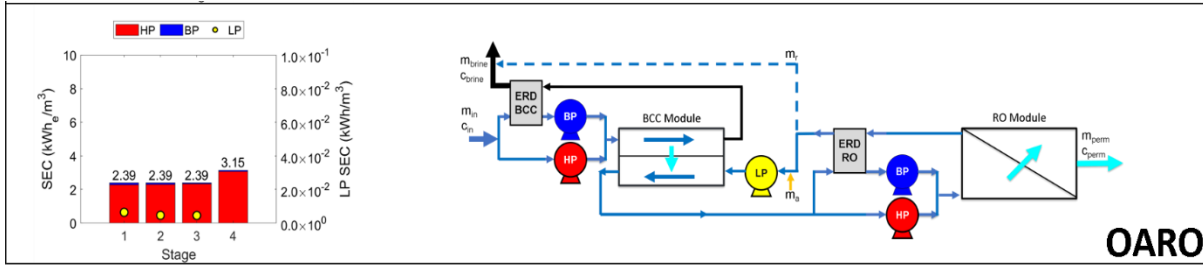


Fig. 37. Breakdown of specific energy consumption per stage OARO for a feed concentration and recovery rate of 70 g/L and 75%, respectively. Total SEC per stage is labeled over each bar. Truncated system diagrams are shown to the right, color-coded by pump type. HP= high pressure pump, BP= booster pump, LP= low pressure pump, BCC= bilateral countercurrent, RO= reverse osmosis.

8 Hybrid Desalination Models

8.1 RO + FO

We developed an RO-FO model connecting in series the Columbia RO model and the Trevi FO and implemented the new hybrid model in the GUI. Regarding costs, we assumed synergies in use of chemicals and labor. Specifically, we assumed a reduction by 50% of the chemicals and labor cost in the technology where the associated costs are lower.

Below are default parameters of an RO-FO desalination system powered by PV and static flat collector.

Table 14 shows the energy consumption for RO, FO and crystallization process and Table 12 gives the size of PV and flat collector fields.

Table 14. Energy consumption for each process

	RO	FO	Crystallizer	Total
Specific electricity energy (kWh/m³) *	3.16	2.60	0.77	-
Specific thermal energy (kWh/m³) *		29.5	178	-
Nominal electricity consumption (kW)	754	187	6	947
Nominal thermal energy consumption (kW)		2121	1335	3456

* The specific energy consumption regards to 1 m³ of permeate flow for RO and FO process or 1 m³ of brine fed into the crystallizer.

Table 15. Size of the solar field

	Module	Nameplate capacity	Total module area (m²)	Capacity factor (%)
PV (tilt-fixed)	SunPower SPR-E19-310-COM	1132 (kWdc)	5948	20.9
Flat collector	Wagner Solar LBM HTF10	3457 (kWth)	6444	21.9

Figure 38 shows an overall performance of the system located in Phoenix, AZ, where the annual DNI is 2,520 kWh/m². With solar multiple of 1 and 0-hour storage system, the capacity factor of desalination is around 20%. Figures 39 and 40 give a detailed hourly simulation of the system at the same location, over a course of a week in May. The load rate indicates the percentage of energy provided from the solar field.

It is shown that at different hours either electricity or thermal energy may limit the performance of the system. In most days, thermal energy generation is limiting the water production in the morning and evening (with lower load rates), while electricity generation is the limiting factor in the middle of the day. We plan to develop an algorithm for optimizing the sizing of the PV-static collector combination.

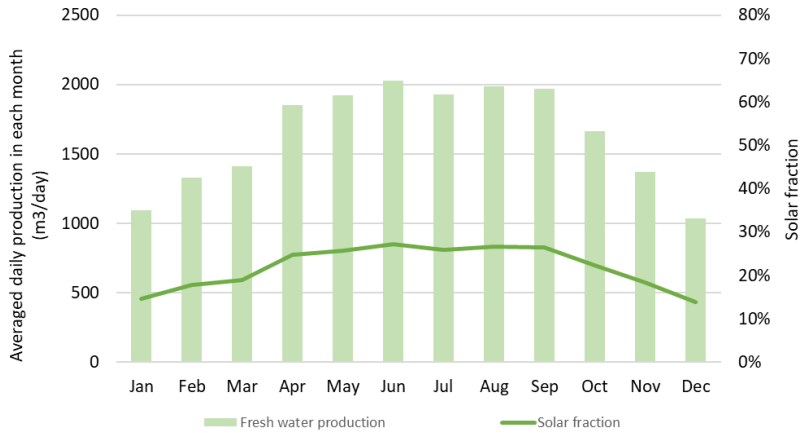


Fig. 38. Monthly water production (m^3/day) and averaged solar fraction (energy contribution from solar field) for a RO-FO-crystallizer system (Production capacity: $310 m^3/h$) in Phoenix, AZ

Future implementations include the logic of partial load operation in cases of hybrid desalination system. A proper sizing strategy between PV, solar thermal and storage can be developed to maximize the load rate while minimizing the solar field area.

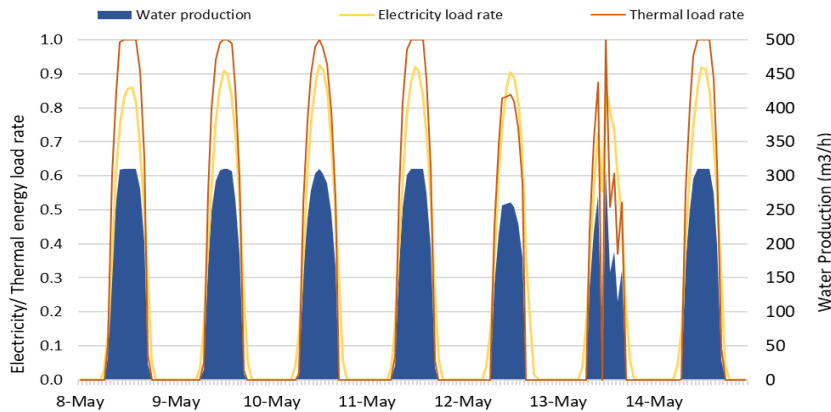


Fig. 39. System performance during a week in May in terms of power load rate (powered by with a 1,123-kW PV field and a 3,456-kW thermal flat-plate collector field)

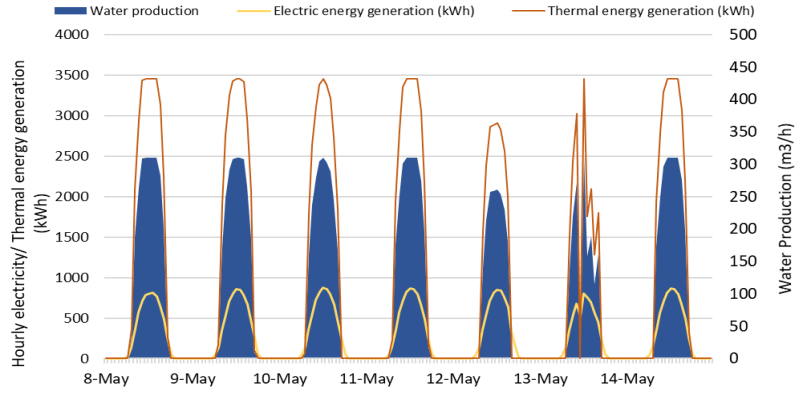


Fig. 40. System performance during a week showing hourly electricity and thermal energy demand of a RO-FO system powered by 1,123-kW PV field and a 3,456-kW flat-plate collector field.

8.2 RO + batch V-AGMD

We also developed a model for RO-MD hybrid, utilizing the PSA batch-VAGMD model which is based on performance data from a pilot plant at the PSA testing facility in Almeria, Spain.

8.3 Generic Desalination Model

We developed a simplified algorithm to represent any desalination model, for the users with less desalination expertise or for the purpose of testing new desalination systems. This model includes the basic balance of mass and energy and calculates the major design parameters. The core idea is to build a simple connection between the water production and the solar field generation.

The input parameters for the design model are shown in Table 16 below:

Table 16. Inputs in the generic desalination model

Variable	Default value	Unit
System capacity	2000	m ³ /day
Feed concentration	35	g/L
Recovery rate	50	%
Specific thermal energy consumption (STEC)	50	kWh(th)/ m ³
Specific electric energy consumption (SEEC)	1.5	kWh(e)/ m ³

The following design parameters are calculated:

$$\text{Thermal energy requirement (kW)} = \frac{\text{System Capacity} \times \text{STEC}}{24}$$

$$\text{Electric energy requirement (kW)} = \frac{\text{System Capacity} \times \text{SEEC}}{24}$$

$$\text{Brine salinity (g/L)} = \frac{\text{Feed salinity}}{1 - \text{Recovery rate}}$$

The energy requirement will be used with the generation data from solar field to simulate the hourly performance. The user may use this model to represent either thermal desalination technologies or RO based technologies, by adjusting the value of STEC and SEEC accordingly.

9 Solar Collector and Desalination Cost Models

9.1 Solar Collector

We built the following algorithm for estimating the cost of static collectors.

The total capital cost is composed of the solar field and the boiler:

$$C_{TOTAL} = C_{SOLAR} + C_{BOILER}$$

The solar field includes the thermal storage system and collectors.

$$C_{TES} = c_{TES} \cdot TES_CAP_h \cdot P_{req}$$

$$C_{SOLAR} = A_{solar_field} \cdot c_{solar} + C_{TES}$$

$$C_{BOILER} = 102.36 \cdot P_{req}$$

c_{TES} : Specific cost of thermal storage (USD/kWh) (Typical values around 45 USD/kWh using hot water tanks)

A_{solar_field} : Total area of solar collectors (m²) (Design area x Solar Multiple)

P_{req} : Thermal energy required by desalination unit (kW)

TES_CAP_h : Thermal storage capacity (in hours)

A_{land} : Land area required (Ha)

CAP_{DESAL} : Desalination plant capacity (m³/day)

c_{solar} : Specific cost of the solar thermal field (USD/m²)

c_{solar} : Specific cost of the solar thermal field (USD/m²)

Based on cost data collected by PSA, we picked 372 \$/m² as the default input of the cost of collector.

9.2 MED Cost Estimates

The capital cost for MED plants, designed for seawater desalination, is estimated by an empirical equation reported by Kosmadakis et al.¹⁹ (Eqn. 1). This equation takes the plant capacity (D) and the heat exchanger area (HEX area) as inputs; it was verified by 6 MED seawater desalination plants in the Middle East and 1 plant in Italy. The capacity of these plants varies from 9,000 to 270,000 m³/day. This cost relationship is applicable to both LT-MED and MED-TVC systems, with the HEX area being the major difference between the two types of plants.

$$C_{MED} = 6291D^{-0.135} \left[1 - f_{HEX} + f_{HEX} \left(\frac{HEXarea}{HEXarea, ref} \right)^{0.8} \right] \quad (1)$$

The O&M cost was broken down into major components including chemicals, labor, maintenance, brine discharge and miscellaneous cost based on the study from Papapetrou et al.²⁰

An example of input parameters for the LT-MED cost model is shown in Table 17.

Table 17. Input parameters for a reference LT-MED costing model

Capital cost			Output from simulation model
Design Capacity	1000	m ³ /day	
Annual water production	328500	m ³	Yes
HEX area	4157	m ²	Yes
Expected plant lifetime	20	yr	
Average interest rate	0.04		
Cost fraction of the evaporator	0.4		
Thermal storage tank	30	\$/kWh	
Energy expenses			
Specific thermal energy consumption	58.3	kWh/m ³	Yes
Specific electricity consumption	1.5	kWh/m ³	
Cost of heat	0.01	\$/kWh	Yes
Cost of electricity	0.04	\$/kWh	
Other O&M costs			
Chemicals	0.04	\$/m ³	
Labor	0.033	\$/m ³	
Maintenance	2%	% to CAPEX	
Brine disposal/discharge	0.02	\$/m ³	

Figure 41 shows the unit capital cost of MED as a function of capacity, based on the Global Water Intelligence (GWI) dataset. While the data agree with the prediction curve by Kosmadakis et al. for large plants, the Kosmadakis curve seems to underestimate costs for smaller plants under 10,000 m³/d.

¹⁹ Correlations between MED capital costs and design parameters. "Kosmadakis, G., Papapetrou, M., Ortega-Delgado, B., Cipollina, A., & Alarcón-Padilla, D. C. (2018). Correlations for estimating the specific capital cost of multi-effect distillation plants considering the main design trends and operating conditions. Desalination, 447, 74-83."

²⁰ Summary of "Papapetrou, M., Cipollina, A., La Compare, U., Micale, G., Zaragoza, G., & Kosmadakis, G. (2017). Assessment of methodologies and data used to calculate desalination costs. Desalination, 419, 8-19."

Assuming a LCOH of \$0.01/kWh, the LCOW for a relatively small (1000 m³/d) plant is 1.28 \$/m³, comprising an annualized specific CAPEX of 0.53 \$/m³ and 0.85 \$/m³ OPEX. For large plants the LCOW goes down to \$1.10/m³; the water production cost is a strong function of the LCOH; when the LCOH is essentially zero (waste heat available on site), then the LCOW can be down to \$0.50/m³.

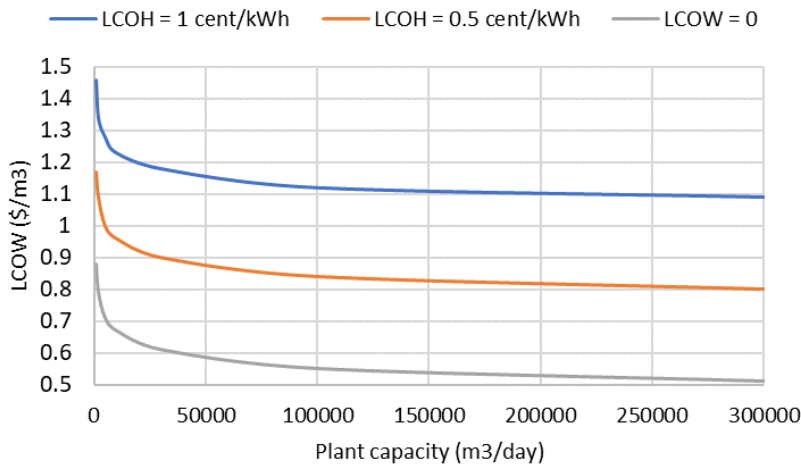


Fig. 41. The dependence of leveled cost of water on MED plant size

For ABS-MED configuration, additional cost is added for the absorption heat pump. Based on the ENTROPIE ("Aqasol Model (2005)") data, PSA developed the following correlations for the capital cost of the additional heat pump, as a function of system capacity.

Single effect:

$$CAPEX = 0.9168 \times Capacity^{-0.255}$$

Double effects:

$$CAPEX = 1.5602 \times Capacity^{-0.255}$$

9.3 VAGMD (Once through and Batch) Cost Estimates

Based on the performance of the pilots at PSA, we developed a model of costing-AGMD systems the results of which are summarized below.

To determine the CAPEX of each component, the following equation is applied to consider the scale-up effect:

$$CostA = CostB \left(\frac{CapA}{CapB} \right)^X$$

CostA and CostB are the unknown and known cost, CapA and CapB are the unknown and known capacity, and X is the scale-up factor.

The associated parameters for each component are listed in Table 18.

Table 18. Parameters of the MD Cost Model

Equipment	Base price, k Euro	Base capacity	Scale-up factor
Housing Rack	5	3 modules	0.6

Price of tank (with plumbing)	5	3 modules	0.5
Price of each pump	3	5 m ³ / h	0.6
Controller, cabling, programming	15	3 modules	0.3
Price per sensor	0.25		
AGMD membrane, Euro / m ²	0.075		
Heat exchanger, endplates	0.85 / unit	10 m ²	0.6
Heat exchanger Euro / m ²	0.35		
Heating installation	5	10 m ³ / h	0.6
Cooling installation	5	10 m ³ / h	0.6

Our cost modeling yields the cost curves shown in Fig. 42 for two V-AGMD modules that were studied at PSA; AS7C1.5L stands for the smaller module with channel length of 1.5 m and effective module area of 7.2 m² and AS26C2.7L stands for the larger module with channel length of 2.7 m and effective module area of 25.9 m². Under the conditions listed above, the larger module gives the lowest LCOW.

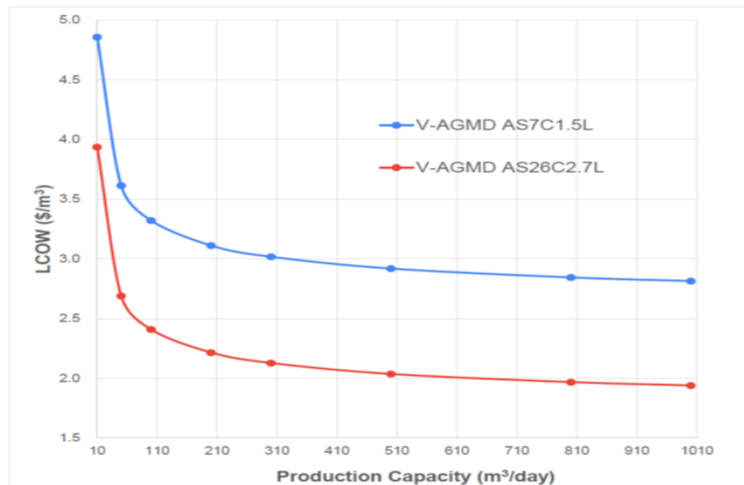


Fig. 42. Cost comparison between two V-AGMD systems

Assumptions:

Evaporator Channel Inlet Temperature = 80 oC

Condenser Channel Inlet Temperature = 25 oC

Feed Flow Rate = 582.7 L/(h*module)

Feed Concentration = 35 g/L

It is noted that these operation conditions were used at PSA V-AGMD pilot plant testing to maximize the energy efficiency of the larger V-AGMD module (25.9 m²), under which the lowest specific thermal energy consumption of 49 kWh/m³, equivalent to the highest GOR of 13.5, is achieved. However, the operating conditions can greatly affect the cost-based selection of one or the other module. For example, when assuming the following conditions, the smaller module gives the lowest LCOW (Fig. 42):

- a) Evaporator Channel Inlet Temperature = 80 °C (normally maximized at 80 °C to ensure the highest possible energy efficiency for each operation).
- b) Condenser Channel Inlet Temperature = 20 °C (which is the lowest allowed temperature in PSA V-AGMD performance modeling)
- c) Feed Flow Rate = 400 L/(h*module) (which is the lowest allowed feed flow rate in PSA V-AGMD performance modeling)
- d) Feed Concentration = 105 g/L (which is the highest allowed seawater salinity in PSA V-AGMD)

performance modeling)

This result shows that not only designated daily production capacity, but also the operational parameters play a major role in affecting the final fresh water production costs. In this case, the high-salinity feed source seawater reduces the vapor pressure across the V-AGMD module, resulting in an even lower permeate flux at a rather low feed flow rate for the larger module. Even if it has a larger module area, the resultant low permeate flow rate requires a higher number of V-AGMD modules in parallel operation to reach the nominal fresh water production capacity. A sharp increase on capital expenditures is caused correspondingly, for which the advantage on its operational expenditures due to low thermal energy consumption is not able to compensate. All in all, there is no guarantee regarding which module works the best in terms of costs. In principle, the operational parameters will change the extent to relative advantage and disadvantage of CAPEX and OPEX between two modules at any time, thereby altering the LCOW advantage of one versus the other.

In our cost model, operational parameters include evaporator channel inlet temperature, condenser channel inlet temperature, feed flow rate per module and feed concentration. Additionally, there are V-AGMD plant design parameters which are part of user's inputs and will be listed in detail in the user's manual. Since those design parameters are specific to each project location and condition, there is no way to generalize their ranges accurately. As was the case with the LT-MED, the biggest parameter among all the operational and design parameters that is affecting the costs of fresh water production turns out to be the unit cost of heat (\$/kWh_{th}). As of now, it is left as 0.01 \$/kWh_{th} in our model, and the modeling results show that thermal energy cost accounts for over 80% of OPEX. If the user is able to implement free waste heat or low-price low-temperature geothermal energy as thermal energy source for MD system, where the unit cost of heat could be even lower than 0.002 \$/kWh_{th}, then the percentage of thermal energy cost can be lower than 50% and OPEX can be largely reduced by over 70%. Eventually, LCOW is reduced by more than 60%.

9.4 FO Cost Estimates

We gathered and implemented the costing numbers on the FO system from Trevi Systems Inc. Empirical equations were derived from Trevi Co. to estimate the system capital cost and labor cost:

$$CAPEX(\$) = 26,784 \cdot CAP^{-0.426}$$

$$OPEX_{Labor} \left(\frac{\$}{m^3} \right) = 0.4757 \cdot CAP^{-0.178}$$

The breakdown of the CAPEX is shown in Table 19.

Table 19. FO Cost breakdown (source Trevi Systems)

CAPEX breakdown	CAPEX Percentage
FO membranes	11.6%
Heat exchangers	13.9%
Construction	22.5%
Draw solution	9.0%
Coalescers	4.9%
Structural	4.5%
Polishing	8.3%

Pipes and plumbing	5.3%
Pre-filtration	4.9%
Controls/Electrical	3.4%
Pumps	4.7%
Instrumentation	2.6%
Valves	2.4%
CIP	1.1%
Tanks	1.1%

9.5 RO Cost Estimates

For the RO cost model, the reference case is described in Table 21. The system SEC is determined by the design model, for seawater desalination it is likely in the range of 3-4 kWh/m³.

Table 21. Cost parameters for a reference RO model

	User Inputs	Model Estimates	
Capital Costs			
Design Capacity	m ³ /day	1000	
Annual water production	m ³		328500
Unit Capital Cost	\$/ m ³ /day	2500	
Expected plant lifetime	yrs	20	
Average interest rate		0.04	
Membrane area	m ²		2284.8
Membrane cost	\$/m ²	50	
Energy Use			
Specific electricity consumption (SEC)	kWh/ m ³		2
Cost of electricity	\$/kWh		0.05
O&M			
Chemicals	\$/ m ³	0.05	
Labor	\$/ m ³	0.1	
Membrane replacement	\$/ m ³	0.05	
Brine disposal/discharge	\$/ m ³	0.03	
Other maintenance	\$/ m ³	0.03	

10 Model Results Verification Analysis

10.1 Solar Static Collector Model

The SAM solar collector model is limited to residential water heating; thus, we elected to code and integrate a solar static collector model developed by Alarcon-Padilla and co-workers in PSA which has been verified with measurements at a PSA pilot plant in Almeria. A new static collector class of flat-plate and evacuated tube collectors was created by converting PSA's MATLAB functions to Python and modifying the code to be more dynamic. We replaced some of PSA's customized MATLAB functions related to solar geometry with functions from the PVLIB library so that the calculations of solar zenith and azimuth angles were consistent with those in SAM. We then

compared the modeling results to the original model using the specifications of the Wagner Solar LBM HTF module comprising 10 collectors each of 10 m^2 area and design flow rate of 0.02 kg/s . As shown in Table 22, the energy generation estimates from the two versions of the model agree within 0.8% or better.

Table 22. Hourly comparison between the PSA source and the Python model (for a June 18th day)

DNI (W/m ²)	Energy generation (kWh) from original model	Energy generation (kWh) from Python based model	Deviation
0	0.00	0.00	0.0%
11	0.00	0.00	0.0%
235	0.00	0.00	0.0%
478	83.06	83.04	-0.0%
695	287.20	286.45	-0.3%
861	446.45	445.54	-0.2%
961	544.90	544.78	0.0%
993	579.84	580.40	0.1%
945	540.30	541.08	0.1%
825	433.71	435.12	0.3%
633	262.04	263.83	0.7%
403	55.86	57.32	0.8%
170	0.00	0.00	0.0%
3	0.00	0.00	0.0%
0	0.00	0.00	0.0%

10.2 LT-MED Model

Then we compared the results from the regression equations with those from the original EES simulations; the differences are shown in Table 23.

Table 23. Comparisons of source and adopted LT-MED models for a 12-effect system;
% deviations for main model outputs

Capacity (m ³ /day)	GOR	Steam flow rate	Feed flow rate	Delta_T
2000	0.1%	10.5%	0.1%	0.7%
50000	0.1%	0.4%	0.1%	1.6%
100000	0.2%	0.2%	0.1%	1.6%

As shown in this table, the multivariable equations can generally predict GOR and the temperature difference with small biases. However, the prediction on the steam flow rate is not ideal for small capacity systems, although a maximum of 10% deviation is still acceptable.

10.3 MED-TVC model

A model of a TVC-MED, developed by Palenzuela, and Alarcón-Padilla, is based on the Trapani, Italy 12-effects MED desalination plant and is validated by actual performance data from this plant. The model is built in Engineering Equation Solver (EES), and it can calculate the gain output ratio (GOR) from different motive pressure and different thermo-compressor locations by operating balance equations of energy, mass, and salt of each effect. Comparison of the MED-TVC Python Model Results and the Trapani plant measurements is shown in Table 24.

Table 24. Comparison between actual plant data and modeling results in EES

Variable	Trapani plant	Model	Error (%)
Vapor temperature in the 1 st effect °C	62.2	62.67	0.76%
Vapor temperature in the 5th effect °C	53	52.6	-0.75%
Vapor temperature in the 11th effect °C	39.3	39.45	0.38%
Intake seawater mass flowrate (T/h)	1280	1273	-0.55%
Feed seawater mass flowrate (T/h)	1130.4	1127	-0.30%
Brine blowdown mass flowrate (T/h)	755	753.1	-0.25%
Brine blowdown salinity (g/kg)	59.9	59.8	-0.17%
Cooling steam flow rate (T/h)	149.6	147.9	-1.14%
Motive steam flow rate (T/h)	22.5	22.8	1.33%
GOR	16.7	16.3	-2.40%
Number of tubes in evaporators	11,000	11,697	6.34

Table 25. Comparison of the MED-TVC EES Model Results and the empirical equations

Variable	NRMSD
Gain Output Ratio (<i>GOR</i>)	1.54%
Feedwater flow rate (<i>q_F</i>)	0.82%
Motive steam mass flow rate (<i>q_m</i>)	1.17%
Heating steam mass flow rate (<i>q_s</i>)	0.80%
Temperature difference mean between effects (ΔT_{eff_mean})	1.62%
Specific area (<i>sA</i>)	5.30%

The average NRSMD results for 5 different number of effects (8, 10, 12, 14 and 16) are depicted in Table 25, showing that most of the errors are below 5% (just the specific area shows a higher deviation).

Therefore, the regression model developed in this work shows good accuracy and concordance with the ESS model.

10.4 V-AGMD model

The V-AGMD model developed by the Zaragoza team was validated with measurements at PSA pilots. The agreement of the model with the data is shown in Figures 43a and 43b.

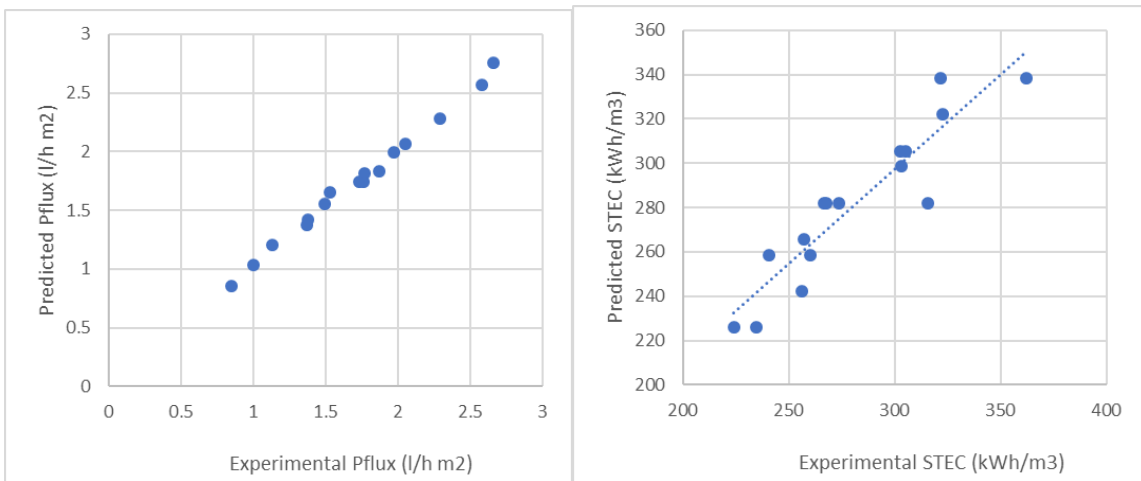


Fig 43. Experimental versus predicted results; a) Pflux comparisons, b) STEC comparisons

The PSA model was in Matlab and we converted it to Python. We tested the two versions under various input data scenarios and we obtained the same results as those reported by Zaragoza et al. Figure 44 shows the results we obtained by running these models.

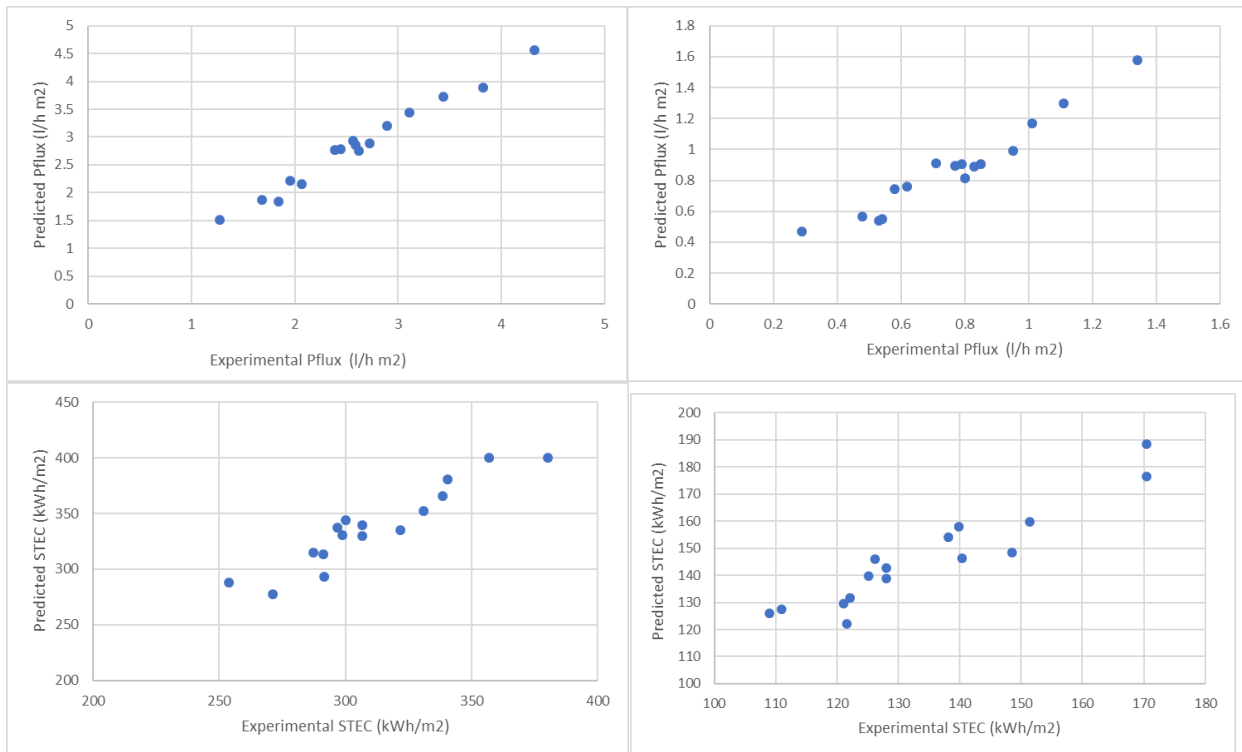


Fig. 44. Experimental and predicted values from Python models (left: AS7C1.5L, right:AS24C5L)

The curves show the same accuracy as described in PSA's documents; a good fit is obtained for P_{flux} in both modules, and less for the STEC. Values of STEC have more deviation because the STEC calculation involves

several parameters measured experimentally and may entail measurement errors. With a maximum deviation of 7.69% for P_{flux} and 11.34% for STEC, the modeling values are considered acceptable and the equations can be used to predict the AGMD system performance.

10.5 SAM Concentrating Solar Power Models (CSP)

For the SAM CSP models, for the purpose of testing the implemented structure of SAM inputs, one variable is selected from each data type and increased by 10% to verify that the new structure is able to capture user's inputs for different data types. As shown in Table 26 there is a good agreement in the three model combinations we tested. We also conducted numerous tests to check accuracy when variables are updated by the users.

Table 26. Model's results comparison between SAM software and implemented Json structure

Model	Case	Data type	Capacity Factor (%)			Annual energy (kWh)			LCOE/LCOH (¢/kWh)		
			SAM	Json	Δ	SAM	Json	Δ	SAM	Json	Δ
DSLF + PPA partnership flip with debt	Defaulted	-	27.3	27.27	0.1%	240285600	240285744	0.0%	12.40	12.39	0.1%
	Constant loss	Number	26.7	26.70	0.0%	235279648	235279792	0.0%	12.65	12.65	0.0%
	Fossil fill fraction	Array	51.4	51.44	0.1%	453190656	453191072	0.0%	6.76	6.76	0.0%
	Tracking error	Matrix	27.3	27.28	0.1%	240407872	240406736	0.0%	12.39	12.39	0.0%
PT Physical + PPA Single owner	Defaulted	-	41.4	41.47	0.2%	362558848	362927104	0.1%	11.51	11.50	0.1%
	TES capacity	Number	29.6	29.67	0.2%	259456688	259685376	0.1%	15.92	15.92	0.0%
	Fossil fill fraction	Array	93.8	93.83	0.0%	820860992	821085568	0.0%	5.31	5.31	0.0%
	IAM_matrix	Matrix	40.3	40.59	0.7%	354905088	355199936	0.1%	11.75	11.74	0.1%
IPH Parabolic Trough + LCOH calculator	Defaulted	-	-	-		24504810	24504810	0.0%	3.76	3.76	0.0%
	Initial HTF%	Number	-	-		24445904	24445904	0.0%	3.77	3.77	0.0%
	Aperture area	Array	-	-		23963456	23963456	0.0%	3.84	3.84	0.0%
	IAM_matrix	Matrix	-	-		24174192	24174192	0.0%	3.81	3.81	0.0%

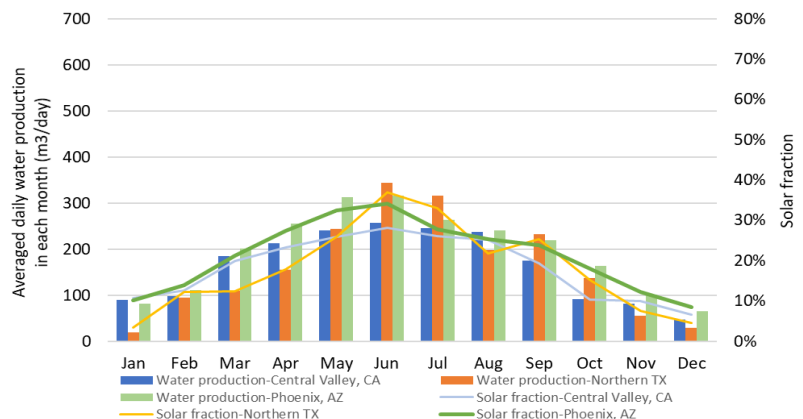
11 Results from Sample Simulations

11.1 Industrial Process Heat and LT-MED: Application in TX, AZ and CA

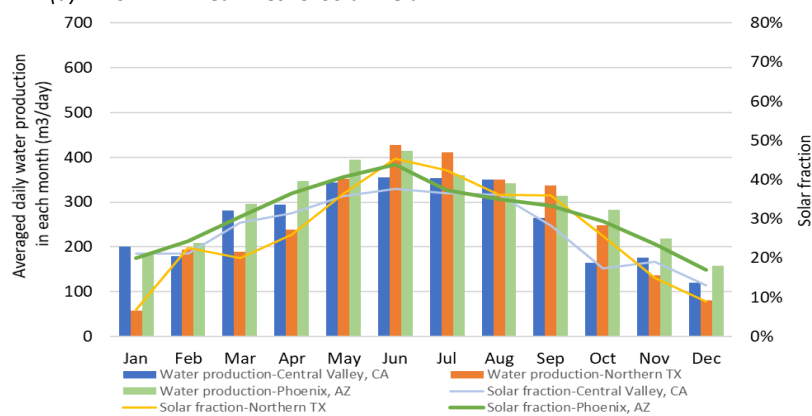
The SAM industrial process heat (IPH) model simulates the thermal energy collected from the solar field that can be used for thermal applications. We simulated a case study of coupling an IPH (Linear Fresnel process heat) system with a LT- MED plant in three locations, namely Central Valley, CA, Phoenix, AZ and near Dallas, TX.

The LT-MED system was specified as 1000 m³/day capacity with a GOR of 12 for 35 g/L feed water. The nominal thermal power required for this system is 2.24 MWth. The solar field was sized at 2 times of the nameplate power demand of the MED (solar multiple =2). The actual field output is 4.98 MWth with a field area of 1.52 acres. Scenarios with and without thermal storage were simulated.

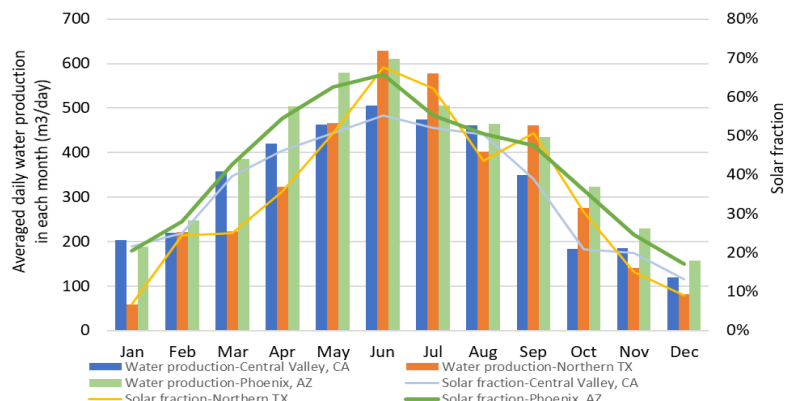
Figure 45 shows the monthly performance of the system in each of the three locations. It is noted that a 6-hr storage system could almost double the annual water production. Its benefit is dependent on the seasons; in the winter (November, December and January) the monthly product volume is increased, with storage, by about 5%, while the increment can reach 48% during each of the summer months. However, even in the best case (June with storage) the solar system alone cannot enable more than 70% of the desalination plant. Our software will allow the user to compliment the solar system with auxiliary power and/or waste or geothermal heat, if available near the selected site.



(a) 2.5 MW Linear Fresnel Solar Field



(b) 5.0 MW Linear Fresnel Solar Field with no storage



(c) 5.0 MW Linear Fresnel Solar Field Coupled with a 6-hr storage system

Fig. 45. Averaged daily water production (m^3/day) of a 1,000 m^3/day LT-MED system powered by Linear Fresnel solar field and the corresponding solar fraction (energy contribution from solar field) for locations in Central Valley, CA, Northern TX and Phoenix, AZ

11.2 Comparisons of Static Collector and Industrial Process Heat coupled with and LT-MED

This MED model has been integrated with both the static collector and SAM industrial process heat (Linear Fresnel) models. A quick comparison is made between these two combinations. For a 1000 m^3/day LT-MED plant located in Phoenix, AZ, the thermal energy consumption is 2.24 MW. With a solar multiple of 1.8, the solar design models result in a flat-plate static collector capacity of 4.03 MW, whereas SAM gives a Linear Fresnel (LF) solar field capacity of 4.27 MW. Both configurations include a 6-hr thermal storage system. The annual water production is estimated to be 157,571 m^3 for flat-plate collectors, and 158,248 m^3 for SAM's LF collectors; the annual thermal power production is 9.8 GWh and 10.5 GWh respectively. Fig.46 shows the results of hourly simulations of these systems for 5 days in January and June of a typical meteorological year.

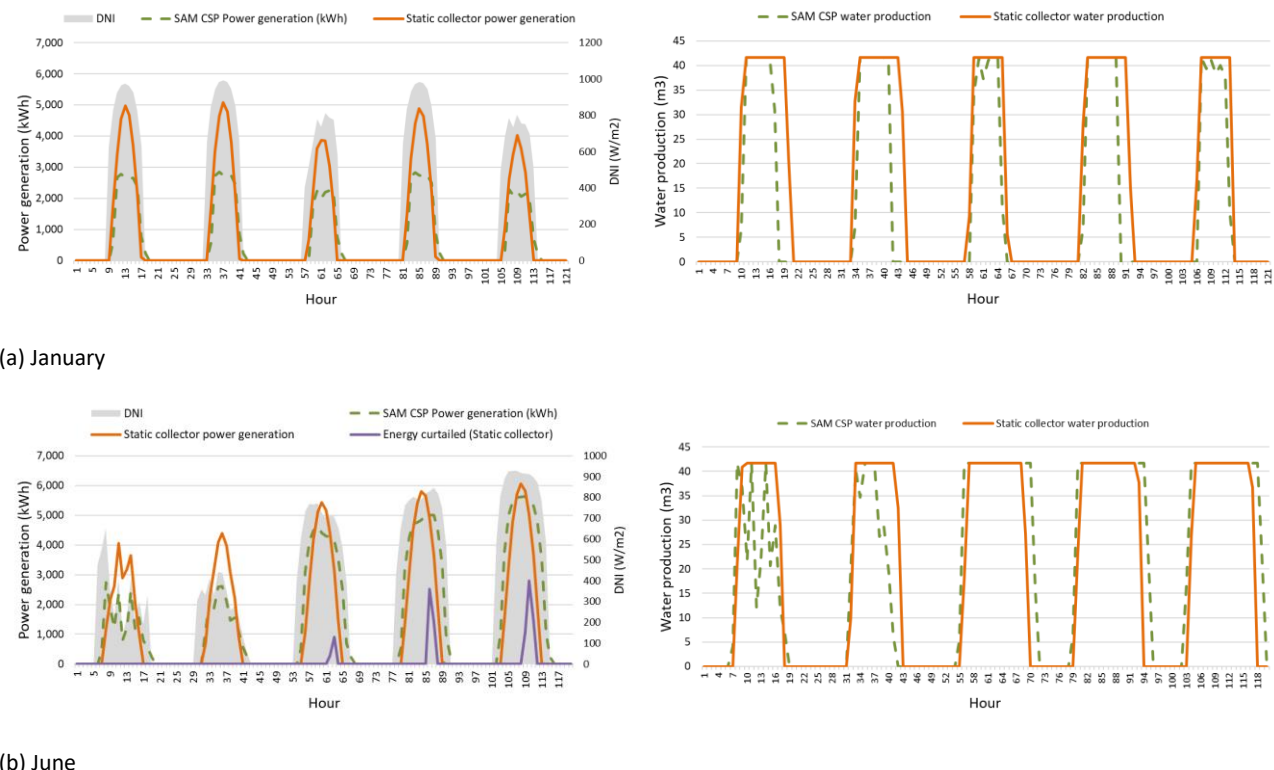


Fig. 46. Thermal power generation and water production for 4.27 MW SAM CSP-LF and 4.03 MW PSA flat-plate static collector systems, combined with a 1000 m^3/day LT-MED plant in Phoenix, AZ

The results suggest the annual performance of the two systems are similar (7% difference in annual thermal power generation and 0.5% difference in annual water production), considering the actual capacity for the two solar fields are different (6% difference). It is also worthy to note that the linear

Fresnel system tends to perform better than the flat-plate collector system during the summer since it operates longer during the morning and evening. On the other hand, the flat-plate collector system outperforms the linear Fresnel system during the winter as it utilizes global irradiation on tilted plane, whereas the LF system uses only DNI. The thermal storage system stores the excess energy from the oversized solar field and provide it to the desalination system. The overall energy loss (curtailment) during a year is 5.4% for the static collector and 0% for the LF system, which is a very small component considering a solar multiple of 1.8. The capital cost of the storage tank is compensated by the increased energy utilization and water production, so that the LCOW is reduced comparing to a non-storage system.

11.3 Case study for a V-AGMD system operating in Phoenix, AZ.

In this case study we compared the efficiency and associated LCOW of systems using two different VAGMD modules operating in Phoenix, AZ. The solar field is sized as 224 kW, the nominal power required for a 100 m³/day LT-MED desalination system. The feed salinity is a constant 35 g/L. Figure 47 shows comparisons of the performance of the two VAGMD systems with the previously described MED system model, given the same thermal energy input. Figure 48 shows hourly water production for MED and the VAGMD systems during a week in the spring. It can be seen that MED has in overall a higher thermal efficiency than VAGMD systems. As discussed before, AS26 module has a lower STEC and thus can produce more water than AS7 does with the same solar field area. On the other side, it would need more modules as the permeate flux is lower. In this case, 38 modules are needed for AS26 while 13 modules are enough for AS7.

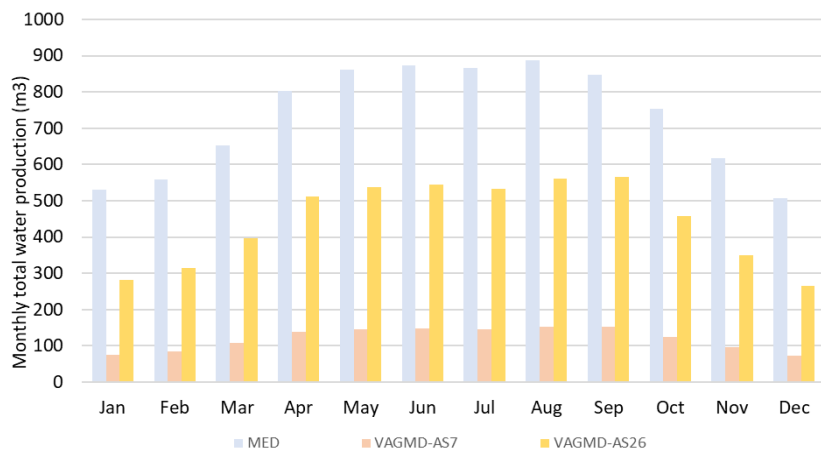


Fig. 47. Monthly water production for MED and VAGMD powered by 224 kW flat collector in Phoenix, AZ (38 modules for AS26 and 13 modules for AS7)

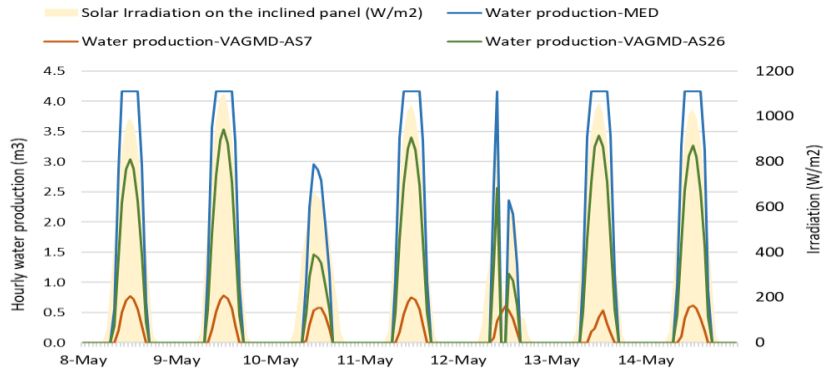


Fig. 48. Hourly water production for MED and VAGMD during a week

11.4 IPH LFDS and FO Parametric study

Seawater temperature (10, 15 and 20 °C) and FO recovery rate (30%, 40% and 50%) are selected for parametric study; this combination results in nine cases. Enacting this parametric option, results in nine simulations with results stored separately. The bar graphs in Figure 49 provide a summary comparison of the nine cases.



Industrial Process Heat Linear Direct Steam / Forward Osmosis

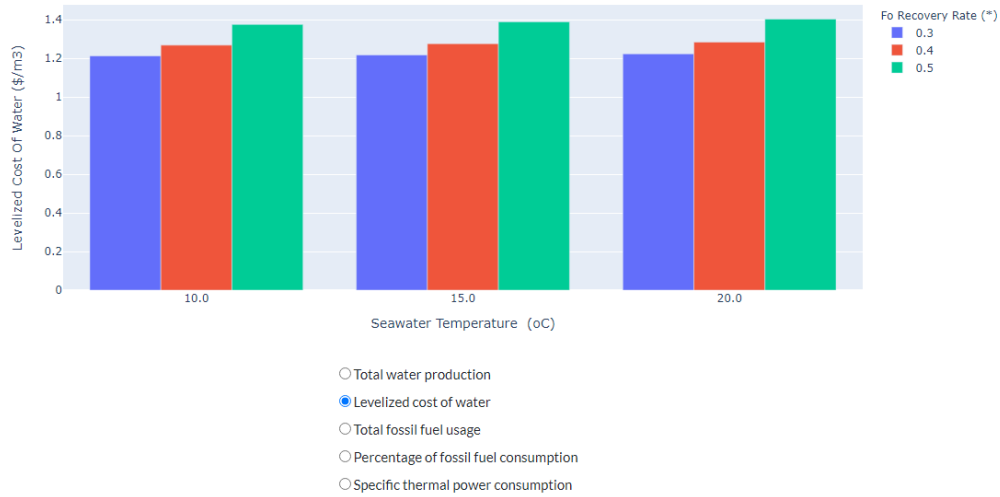


Fig. 49. Sample outputs from parametric study. Bar graphs of total water production (top) and LCOW (bottom) of a 10,000 m³/day FO plant coupled with a 20 MW industrial process heat linear Fresnel solar field

11.5 Comparison of LT-MED with multi-pass RO for distillate water production

As discussed in section 7.1, electrolytic production of hydrogen from seawater creates a new market opportunity for solar thermal desalination technologies that produce higher purity water than reverse osmosis. The conventional RO-single pass typically creates permeate with TDS concentration in the 250-500 mg/L, whereas thermal technologies can produce distillate with less than 1 mg/L TDS. RO may also produce high purity water if additional passes are implemented and/or the desalination unit is complimented with ion-exchange units in series. Thus, for enhancing the applicability of our software, we modelled RO systems with multiple passes of RO and compared those, based on LCOW, with thermal technologies such as MD-batch and LT-MED. The cost breakdowns are shown in Fig. 50.

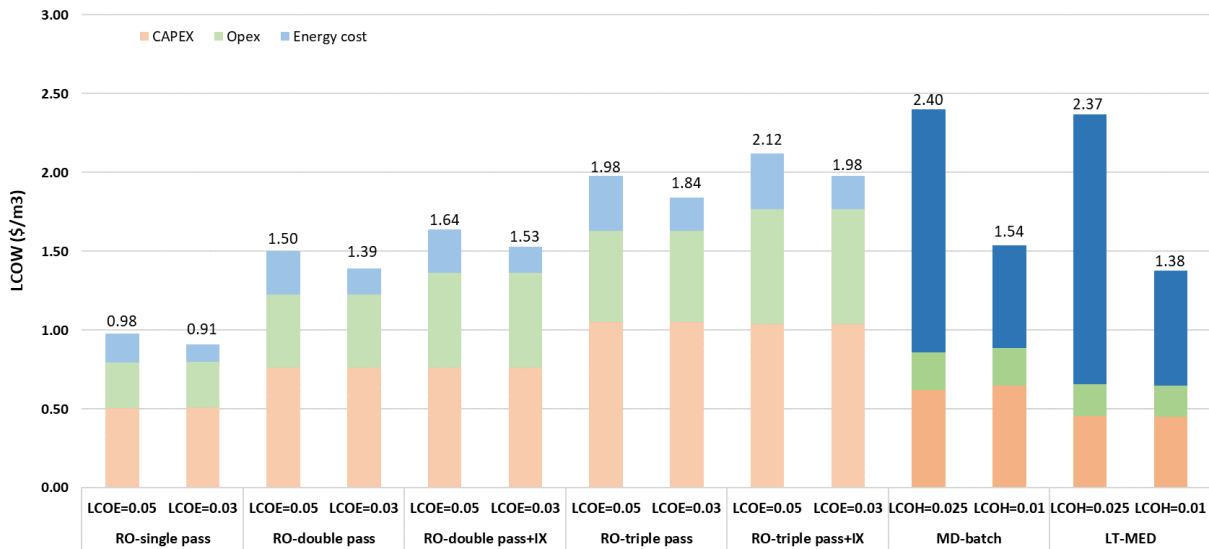


Fig. 50. LCOW of potable water production from RO and of high-purity water production from multi-pass RO, batch-MD-batch and LT-MED desalination plants; assumed 2000 m³/day capacity and feedwater salinity of 35 g/L. Assumed LCOE=\$0.05/kWh and LCOH=\$0.025/kWh and \$0.01/kWh

As shown in Fig. 50, although conventional RO can produce potable water at leveled costs of water (LCOW) much lower than that of thermal desalination plants, the addition of passes and/or ion-exchange systems to further de-mineralize the RO permeate water adds a significant cost. The thermal desalination technologies reach a lower LCOW than multi-pass RO when the leveled cost of heat (LCOH) falls to \$0.01/kWh (assuming waste heat).

Acknowledgements

Support for this study was provided by the U.S. Department of Energy's Office of Energy Efficiency and Renewable Energy (DOE-EERE) under the Solar Energy Technologies Office (SETO) Award Number DE00008401. This User Manual was prepared as an account of work sponsored by an agency of the United States Government. Neither the United States Government nor any agency thereof, nor any of their employees, makes any warranty, express or implied, or assumes any legal liability or responsibility for the accuracy, completeness, or usefulness of any information, apparatus, product, or process disclosed, or represents that its use would not infringe privately owned rights. Any opinions, findings, and conclusions or recommendations expressed in this material are those of the authors and do not necessarily reflect the views of the Department of Energy. The authors thank the DOE project manager Andru Prescod and the project Advisory Board members Leon Awerbuch, Bernie Mack, Aaron Mandel, Paul Choules, Hassan Arafat, James Golden, Raed Bkayrat, Yuliana Porras-Mendoza, Michael Greene, and John Webley for fruitful discussions. Also, Columbia U. students Boris Lin, Jianson Zhao and Somto Uyanna contributed in the data collection.

12 Bibliography

1. Atia, A. A., & Fthenakis, V. Active-salinity-control reverse osmosis desalination as a flexible load resource. *Desalination*, **468**, 114062 (2019).
2. Atia, A. A., Yip, N. Y., & Fthenakis, V. Pathways for minimal and zero liquid discharge with enhanced reverse osmosis technologies: Module-scale modeling and techno-economic assessment. *Desalination*, **509**, 115069 (2021).
3. Bartholomew, T. V., Siefert, N. S. & Mauter, M. S. Cost optimization of osmotically assisted reverse osmosis. *Environmental science & technology*. **52(20)**, 11813-11821 (2018).
4. Bindels, M., Carvalho, J., Gonzalez, C. B., Brand, N. & Nelemans, B. Techno-economic assessment of seawater reverse osmosis (SWRO) brine treatment with air gap membrane distillation (AGMD). *Desalination*, **489**, 114532 (2020).
5. Calle de laA., Roca L., Bonilla J., P. Palenzuela P., Dynamic modeling and simulation of a double-effect absorption heat pump. *International Journal of Refrigeration* 72:171-191 (2016)
6. Chorak A., Palenzuela P., Alarcon-Padilla D-C, Abdellah A.B., Experimental characterization of a multi-effect distillation system coupled to a flat plate collector: Empirical correlations, *Applied Thermal Engineering*, **120**, 298-313, (2017).
7. Desalination Projects - Innovative Water Technologies | Texas Water Development Board. [Online]. Available: <https://www.twdb.texas.gov/innovativewater/desal/projects.asp>. [Accessed: January 12, 2019].
8. EIA API available at <https://www.eia.gov/petroleum/gasdiesel/>. [First Accessed: May 1, 2020].
9. EIA data from <https://www.eia.gov/electricity/data/eia923/>. [Accessed: June 15, 2021].
10. Fthenakis V., Atia A., Morin O., Bkayrat R., and Sinha P., New Prospects for PV Powered Water Desalination Plants: A case study in Saudi Arabia, *Progress in Photovoltaics: Research and Applications*, **4**, 543–550, 2016
11. Gingerich, D. B. & Mauter, M. S. Quantity, quality, and availability of waste heat from United States thermal power generation. *Environmental science & technology*. **49(14)**, 8297-8306 (2015).
12. Ginsberg, M., Zhang, Z., Atia, A. A., Venkatraman, M., Esposito, D., & Fthenakis, V. M. Integrating Solar Energy, Desalination and Electrolysis. *Solar RRL*. In press.
13. Global Water Intelligence- Desal Data Database." [Online]. Available: <https://www.desaldata.com/>. [Accessed: November 14, 2018].
14. Gregorzewski A., K. Gentner, E. Zarza, J. Leon, J. de Gunzbourg, G. Alefeld, J. Scharfe. The Solar Thermal Desalination research project at the Plataforma Solar de Almería. *Desalination* 82:145-152, (1991).
15. Gude, V. G., & Fthenakis, V. Energy efficiency and renewable energy utilization in desalination systems. *Progress in Energy*, **2(2)**, 022003 (2020).
16. Hauer, M. & Center for International Earth Science Information Network - CIESIN - Columbia University. 2021. Georeferenced U.S. County-Level Population Projections, Total and by Sex, Race and Age, Based on the SSPs, 2020-2100. Palisades, NY: NASA Socioeconomic Data and Applications Center (SEDAC).
<https://doi.org/10.7927/dv72-s254>. [Accessed: October 30, 2021].
17. Hauer, M. E. Population Projections for U.S. Counties by Age, Sex, and Race Controlled to Shared Socioeconomic Pathway. *Sci. Data*, **6**: 190005. <https://doi.org/10.1038/sdata.2019.5> (2019).
18. Hitsov, I., De Sitter, K., Dotremont, C. & Nopens, I. Economic modelling and model-based process optimization of membrane distillation. *Desalination*. **436**, 125-143 (2018).
19. IBNet Tariffs DB available at: <https://tariffs.ib-net.org/sites>. [Accessed: June 15, 2021].
20. Koschikowski, J., Wieghaus, M., Rommel, M., Ortín, V. S., Suárez, B. P., & Rodríguez, J. R. B. Experimental investigations on solar driven stand-alone membrane distillation systems for remote areas. *Desalination*, **248(1-3)**, 125-131 (2009).
21. Kosmadakis G., Papaperou M., Ortega-Delgado B., Cipollina A., D-C., Desalination, **447**, 74-83, (2018)
22. OpenEI API available at: <https://openei.org/services/>. [Accessed: June 15, 2021].
23. Ortega-Delgado B., Palenzuela P.,
24. Palenzuela P., Hassan A.S., Zaragoza G.,
25. Palenzuela P., Zaragoza G.,
26. Papapetrou, M., Cipollina, A., La Commare, U., Micale, G., Zaragoza, G. & Kosmadakis, G. Assessment of methodologies and data used to calculate desalination costs. *Desalination*. **419**, 8-19 (2017).

27. Ruiz-Aguirre A., Andrés-Mañas J., , J. Fernández-Sevilla, and G. Zaragoza Z., Experimental characterization and optimization of multi-channel spiral wound air gap membrane distillation modules for seawater desalination, *Separation and Purification Technology*, vol. 205, pp. 212-22, (2018).
28. Qi., S. L. & Harris, A. C., Geochemical Database for the National Brackish Groundwater Assessment of the United States. U.S. Geological Survey (2017).
29. Service documented at: <https://docs.mapbox.com/vector-tiles/reference/mapbox-terrain-v2/>. [First Accessed: 09-01-2019, current application accesses latest version].
30. Stanton, J. S., et al. *Brackish groundwater in the United States*. No. 1833. US Geological Survey (2017).
31. System Advisor Model Version 2020.2.29 (2020.2.29). SAM source code. National Renewable Energy Laboratory. Golden, CO. Accessed May 27, 2020. <https://github.com/NREL/ssc>.
32. Trevi Systems Desalination Plant Operation Report, Pilot Testing Results of a 50 m3/d FO for Desalination of Seawater, February 6 (2018).
33. U.S. Census Bureau: 2021 TIGER/Line® Shapefiles: Roads. <https://www.census.gov/cgi-bin/geo/shapefiles/index.php?year=2021&layergroup=Roads>. [Accessed: September, 2021].
34. U.S. Geological Survey (USGS) Gap Analysis Project (GAP). Protected Areas Database of the United States (PAD-US) 2.1: U.S. Geological Survey data release. <https://doi.org/10.5066/P92QM3NT> (2020).
35. United States Geological Survey. National Hydrography Dataset Plus High Resolution. <https://www.usgs.gov/core-science-systems/ngp/national-hydrography/nhdplus-high-resolution>. [Accessed: August, 2021].
36. USGS –National Hydrography Datasets, https://www.usgs.gov/core-science-systems/ngp/national-hydrography/national-hydrography-dataset?qt-science_support_page_related_con=0#qt-science_support_page_related_con [Accessed: November 30, 2020]
37. USGS Produced Waters Geochemical Database.” [Online]. Available: <https://energy.usgs.gov/EnvironmentalAspects/EnvironmentalAspectsofEnergyProductionandUse/ProducedWaters.aspx#3822349-data>. [Accessed: January 11, 2019].
38. World Bank. White paper on cost of desalination for domestic water supply in the MENA region (2016).